DEVELOPMENT AND OPTIMIZATION OF CATALYTIC MEMBRANE APPLIED IN WASTEWATER TREATMENTS

Verónica Patricia Pinos Vélez

Universitat Rovira I Virgili
Department of Chemical Engineering

Doctoral Thesis

DEVELOPMENT AND OPTIMIZATION OF CATALYTIC MEMBRANE REACTORS FOR WASTEWATER TREATMENTS

Supervised by

Prof. Dr. Francisco Medina
Dr. Anton Dafinov

Verónica Patricia Pinos Vélez

Tarragona, 2016

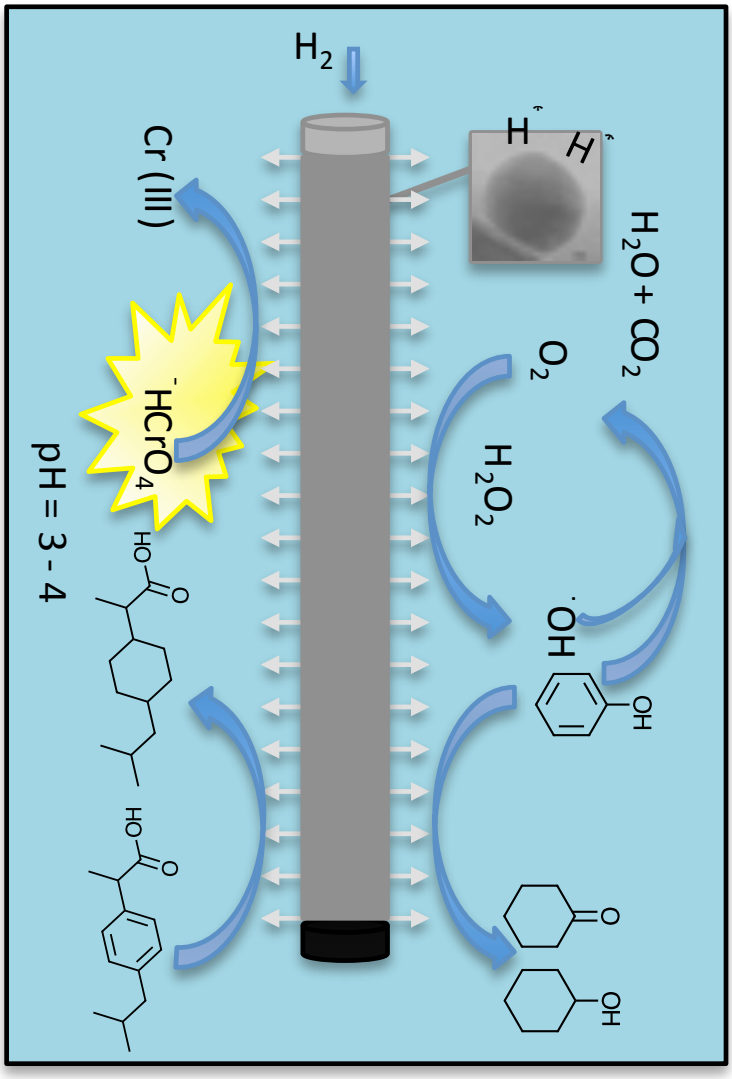
H2
Cr (III)
HCrO4-
pH = 3 - 4
H2O + CO2
O2
H2O2
OH
OH
O
OH
HO
O
HO
O

ACKNOWLEDGMENT

En primer lugar quisiera agradecer a mis directores de tesis al Dr. Anton Dafinov por su guía, apoyo y dedicación durante todo el proceso de ejecución de la tesis y al Dr. Francesc Medina por darme la oportunidad de realizar mis estudios doctorales dentro del grupo y por el apoyo recibido en el transcurso del doctorado. Extiendo mis agradecimientos a mis compañeros de laboratorio y al personal de Catheter-Amic-Aplicat: Oscar, Luis, Pallavi, Shailesh, Biniam, Dana, Dragos, Yurani, Llorenç, Mayra, Abel, Susana, Sandra, Vanessa, Carla, Bárbara y Ana. Agradezco además a Nuria Juanpere, al Dr. Alex Fragoso y en general al personal de la Escola Tècnica Superior d'Enginyeria Química y del Servei de Recursos Científics i Técnics por la ayuda prestada. Quiero agradecer al Dr. Jordi Llorca, al Dr. Javier García y a Rita Marimon por su ayuda en el área de microscopía.

Agradezco también al SENESCYT (convocatoria abierta 2012, I fase) y a la Universidad de Cuenca por el apoyo económico recibido para realizar mis estudios de doctorado. Quisiera agradecer además al Dr. Jaime Bojorque, a los investigadores titulares de la UC y a todo el equipo de la DIUC por el respaldo recibido desde el inicio de esta etapa.

No puedo dejar de agradecer a los amig@s que han hecho especial mi estancia en Tarragona. Mis compañer@s de cafés, almuerzos, pp3 y de los momentos deportivos, musicales, informativos, políticos, multiculturales, etc.

Y al final pero no por eso menos importante, gracias totales a mis padres y hermanas que en la distancia siempre se han encontrado presentes.

UNIVERSITAT
ROVIRA I VIRGILI
ESCOLA TÈCNICA SUPERIOR D'ENGINYERIA QUÍMICA
DEPARTAMENT D'ENGINYERIA QUÍMICA

Avinguda Països Catalans, 26
Campus Sescelades
43007 Tarragona (Spain)
Tels.: 977 55 96 03 - 977 55 86 75
Fax: 977 55 96 21
e-mail:secdeq@urv.cat
http://www.etseq.urv.cat/DEQ

Prof. Dr. Francisco Medina Cabello and Dr. Anton Dafinov,

CERTIFY THAT:

I STATE that the present study, entitled "Development and optimization of catalytic membrane reactors for wastewater treatments", presented by Verónica Patricia Pinos Vélez for the award of the degree of Doctor, has been carried out under our supervision at the Department the chemical engineering department of this university, and that it fulfils all the requirements to obtain the degree of Doctor in Chemical, Environmental, and Process Engineering.

Tarragona, 11th of January, 2016

Doctoral Thesis Supervisor/s

Dr. Professor Francisco Medina

Dr. Anton Dafinov

RESUMEN

Los reactores catalíticos de membrana (RCM) nos dan la posibilidad de optimizar diversos procesos industriales debido a su versatilidad. Esta versatilidad reside en la posibilidad de ejecutar varias funciones con un mismo dispositivo, p. ej. filtración, dosificación y catálisis. Con respecto a esto, los reactores catalíticos de membrana pueden actuar: 1) Como extractores: donde un producto de la reacción es removido de la zona de reacción por la membrana. 2) Como distribuidores: en este modo la membrana controla la cantidad introducida de uno de los reactantes en la zona de reacción. 3) Como contactores: en este modo la membrana facilita el contacto entre los reactantes y el catalizador. La membrana usada en los RCM puede ser catalítica por si misma o ser el soporte del catalizador. El reactor catalítico de membrana actúa en modo interfacial cuando los reactivos ingresan desde lados opuestos de la membrana para ponerse en contacto entre ellos y el catalizador en la superficie de ésta. En el modo por contacto en flujo libre, ambos reactivos entran juntos y fluyen a través de la membrana donde se ponen en contacto con el catalizador.

Las ventajas de los reactores catalíticos de membrana por contacto interfacial son: 1) En lo económico, son dispositivos poco costosos pues se puede emplear en ellos membranas inertes y porosas que tendrán el único propósito de soportar al catalizador y hacer de interfaz de la reacción. Por otro lado, el requerimiento de catalizador, generalmente un metal noble soportado, es menor en comparación a los otros modos. 2) Hacen posible reacciones entre reactivos en distintas fases o inmiscibles entre ellos debido a que la alimentación de los reactivos se hace desde lados opuestos de la membrana. Por ejemplo, la membrana hace de interfaz de contacto entre un catalizador sólido, un reactivo en fase gaseosa y otro en fase líquida.

Considerando las diversas ventajas de los reactores catalíticos de membrana en modo de contacto interfacial; esta tesis se ha enfocado en el desarrollo de reactores catalíticos de membrana en este modo para ser probados en el tratamiento de aguas contaminadas.

Para la realización de los reactores catalíticos de membrana, se emplearon membranas comerciales de fibra hueca de corindón. Como principal fase activa se empleó paladio depositado por diferentes métodos tales como impregnación, sputtering (pulverización catódica) y microemulsión; o nanopartículas de paladio-cobre obtenido por el método del poliol. El paladio se eligió por su capacidad de catalizar tanto reacciones de hidrogenación como la formación de peróxido de hidrógeno.

Los reactores obtenidos fueron probados en las siguientes reacciones: Generación in situ de peróxido de hidrógeno, oxidación de fenol, hidrogenación de fenol, reducción de cromo (VI) e hidrogenación de ibuprofeno. Las reacciones se realizaron a presión atmosférica y a temperatura ambiente o 60 ^{o}C. Todas las pruebas fueron ejecutadas con soluciones acuosas de los contaminantes indicados.

El montaje consistió en un reactor de vidrio que contenía la solución del contaminante modelo o agua Milli-Q. Dentro de este líquido, se sumergía completamente al reactor catalítico de membrana. El hidrógeno era alimentado desde un extremo del reactor catalítico de membrana mientras su otro extremo permanecía cerrado. Para obtener oxígeno, se hacía burbujear aire u oxígeno dentro del líquido.

De modo general, en cada reacción se espera que el hidrógeno que atraviesa el reactor catalítico de membrana sea activado por el paladio para que a su vez reaccione con el oxígeno o con el compuesto contaminante sobre el RCM que hace cada vez de interfaz catalítico.

Con el mismo montaje se pueden propiciar dos reacciones. La primera es una reacción de oxidación donde el paladio activa al hidrógeno para que reaccione con el oxígeno disuelto en el agua. En la reacción se forma peróxido de hidrógeno que a su vez genera radicales hidróxido. Estos radicales son aprovechados en la oxidación de la materia orgánica. Por otro lado se puede dar una reacción de hidrogenación o de reducción donde el hidrógeno activado por el paladio actúa directamente sobre la materia inorgánica para reducirla o sobre la materia orgánica para hidrogenarla.

Con respecto a las pruebas realizadas se obtuvieron los siguientes resultados:

En el test de reducción de cromo (VI) en forma de cromato, se encontró que es indispensable emplear un pH ácido para conseguir $HCrO_4^-$, que tiene un mayor potencial de reducción. Se estableció en las pruebas un pH de 3 y condiciones ambientales. El seguimiento de la reacción se hizo con un espectrofotómetro. Se usó 1,2 difenilcarbazida como indicador para la identificación del cromo hexavalente. Los reactores catalíticos de membrana con paladio, como única fase y aquel que incorporaban además óxidos de hierro y cerio, fueron los más efectivos en la reducción de cromo (VI) a cromo (III) hasta los niveles requeridos, es decir, por debajo de 50 ppb de Cr (VI). El cromo (III) fue removido de la solución final tras ser precipitado a pH 8 y filtrado.

Se encontró que todos los reactores que contenían paladio por impregnación fueron activos en la generación in situ de agua oxigenada; a diferencia de los reactores catalíticos de membrana que incluían paladio por sputtering, microemulsion o paladio cobre por la ruta del poliol que presentaron una rápida desactivación durante la reacción.

En referencia a la oxidación y reducción de fenol, una vez más, los reactores de paladio por impregnación presentaron actividad superior al resto de los reactores. Las reacciones se realizaron a presión ambiental y a 60 ^oC. En general se demostró que los RCM realizados con una membrana de menor tamaño de poro (4 nm) son más efectivos en comparación a los preparados con una membrana de mayor tamaño de poro (1400 nm). Todas las reacciones fueron monitorizadas con el HPLC-DAD y TOC. Las soluciones finales fueron extraídas con etanoato de etilo y analizadas con el GC-FID. En las reacciones de oxidación con aire, se llegó a una conversión de fenol entre el 34 % y el 60 %. Además, se encontró que simultáneamente se producía oxidación e hidrogenación del fenol. En las reacciones de oxidación con oxígeno se consumió entre el 34 % y el 39 % de fenol. De esta cantidad, alrededor de un 60 % fue mineralizado. En estas condiciones, no se encontraron productos de hidrogenación.

Finalmente, en las reacciones de hidrogenación, se eliminó entre un 26 % y un 39 % de fenol. Como productos de hidrogenación se encontraron el ciclohexanol y la ciclohexanona. De esto se deduce, que de acuerdo a la prevalencia de oxígeno disuelto en el agua puede producirse oxidación, hidrogenación o ambas reacciones. Es decir, en una solución saturada de oxígeno, únicamente se produce oxidación, mientras que en presencia no predominante de oxígeno, la oxidación compite con la hidrogenación. En ausencia de oxígeno, el hidrógeno activado por el paladio reacciona directamente con el fenol para su hidrogenación.

Para la prueba de hidrogenación del ibuprofeno, únicamente se usó el RCM con paladio como única fase y de 4 nm de tamaño de poro. Los resultados fueron seguidos mediante HPLC-DAD. Se encontró que para esta prueba es indispensable establecer un pH por debajo del valor pKa del ibuprofeno. Las pruebas se realizaron a pH 4 y a temperatura ambiente. En 8 horas de prueba, alrededor del 90 % de ibuprofeno fue consumido. El producto de hidrogenación del ibuprofeno fue detectado por el HPLC-QTOF.

Con el propósito de determinar las alteraciones de las nanopartículas de paladio durante las diferentes aplicaciones en las que fueron testados los RCM, se sintetizaron nanopartículas de paladio por diferentes métodos tales como impregnación, sputtering y microemulsion; además de las nanopartículas paladio-cobre obtenidos por la ruta del poliol. Todas las nanopartículas fueron soportadas en corindón. Las nanopartículas soportadas fueron analizadas con TEM de alta resolución y pruebas de TPD. En el TPD se observó en todas las muestras la desorción de hidrógeno absorbido en el paladio alrededor de los 400 ^{o}C en proporciones que evidenciaban la formación de beta paladio. Se encontró que todas las muestras frescas presentaban nanopartículas de paladio entre 5 y 15 nm. Las nanopartículas de paladio por impregnación además presentaron paladio atómico y nanoclusters de menos de 2 nm. En las muestras de nanopartículas de paladio realizadas por diferentes métodos, pasadas por ciclos continuos de adsorción y desorción de hidrógeno a temperatura programada, se evidenció la formación de Beta paladio (hidruro de paladio) y estructuras amorfas.

Únicamente los átomos de paladio y los nanoclusters se mantuvieron inalterados. De esto se propone que la actividad y la estabilidad de los catalizadores de paladio obtenidos por impregnación son debidas a los nanoclusters y átomos de paladio ya que éstos no formarían hidruro de paladio en las condiciones de reacción. Posiblemente, los nanoclusters son los responsables, en mayor medida, de la presencia del hidrógeno quimisorbido en todos los ciclos, ya que su mayor superficie de contacto y poca masa hace que el hidrogeno en estos esté predominantemente adsorbido en la superficie y no absorbido; es decir, son por una parte menos vulnerables a la formación de hidruros y por otra más catalíticamente activos.

En conclusión, los reactores catalíticos de membrana con paladio impregnado son una opción eficaz para aplicaciones medioambientales en condiciones suaves a nivel industrial. Debido a su carácter modular se abre la posibilidad de ser escalados para aplicaciones a mayor escala. Más estudios son necesarios para optimizar la eficiencia de las diferentes aplicaciones testadas.

ABSTRACT

Catalytic membrane reactors are well known because of their versatility to develop various industrial processes. This versatility lies in the ability to run two functions in a single device, filtration and catalysis. In this regard, catalytic membrane reactors can act: 1) as extractors: wherein a reaction product is removed from the reaction zone by the membrane. 2) As distributors: In this mode, the membrane controls the amount of the one reactant that enters in the reaction zone. 3) As contactor: In this mode, the membrane facilitates the contact between the reactants and catalyst. The membrane may be intrinsically catalytic or by the supported catalyst. The catalytic membrane reactor acts in interfacial mode when the reactants enter from opposite sides of the membrane. Then, the reactants and the catalyst are put in contact on the membrane surface. In the through flow contact mode both reagents come together and flow through the membrane, subsequently coming in contact with the catalyst in the membrane.

Catalytic membrane reactors for interface mode have advantages such as: 1) economically, they are inexpensive devices as a result of using inert porous membranes that act as a support for the catalyst and as reaction interface. Furthermore, the requirement of catalysts, usually a noble metal, is minor compared to the other modes. 2) Since, the input of the reagents are made from opposite sides of the membrane, this device allows reaction between immiscible compounds or reagents in different phases. For example, this mode enables contacting a solid catalyst with a reagent in gas phase and another in a liquid phase.

Due to the advantages of catalytic membrane reactors in interface mode, this thesis is focused on the development of catalytic membrane reactors to be tested in industrial applications, focusing on environmental remediation.

For the preparation of catalytic membrane reactors, commercial hollow fiber membranes made of corundum were used. Palladium as the main

active phase was synthesized by different methods such as impregnation, sputtering and micro-emulsion. Moreover, copper palladium alloy nanoparticles were obtained by the polyol route. The palladium was chosen as the active phase due to its ability to perform hydrogenation reactions as well as promoting the hydrogen peroxide generation.

The reactors obtained were tested in the following reactions: In situ generation of hydrogen peroxide, phenol oxidation, phenol hydrogenation, chromium (VI) reduction and ibuprofen hydrogenation. Reactions were performed at mild conditions: atmospheric pressure and low reaction temperatures (< 60 °C). In all cases, the hydrogen passed through the membrane. It was dosed to one end of the membrane whilst the other end was kept closed. In addition, all the compounds were in aqueous solution. For the in situ generation of hydrogen peroxide and the oxidation reactions, air or oxygen were bubbled into the water or into the aqueous solution. Thus, the oxygen was dissolved into the water solution or water. The catalytic membrane reactor was placed within the aqueous solution. Thus, the catalytic membrane reactor put in contact the hydrogen gas, the liquid containing the reactants and/or gases such as oxygen and the catalyst.

In the proposed experimental assembly the palladium activates the hydrogen. In the generation of hydrogen peroxide the activated hydrogen reacts with the dissolved oxygen in the water to form hydrogen peroxide, which further forms hydroxyl radicals. These radicals are utilized in the oxidation of organic matter. Moreover, the activated hydrogen by the palladium can reduce the inorganic compounds or produce the hydrogenation of the organic matter.

The results of the different tests were as follows:

Regarding to the reduction of chromium, it was found that it is essential to employ an acid pH. For this reason, it was established that pH 3 would be used in all the tests. The evolution of the reaction was monitored by spectrophotometry after adding 1.2 diphenylhydrazine in the sample as an

indicator. Catalytic membrane reactors with palladium as the only active phase, and the CMR of three phases (palladium, iron oxide and cerium oxide), were found to be effective in reducing chromium (VI) to chromium (III) to levels below 50 ppb. Chromium (III) was removed from the water by precipitation at pH 8, after which it was filtered.

It was found that all reactors were active for the in situ generation of hydrogen peroxide. However, catalytic membrane reactors with palladium loading by sputtering, microemulsion or the palladium copper nanoparticles by polyol route, suffer very fast deactivation. Only the membrane reactors containing palladium by impregnation were active in long-term experiments.

In the oxidation and reduction of phenol the CMRs with palladium by impregnation presented more promising results than the CMRs prepared by the other methods. The reactions were performed at ambient pressure and 60 °C. It was found that the CMR with a smaller pore size (4 nm) was more effective compared to the CMR with a larger pore size (1400 nm). All reactions were monitored by HPLC-DAD and TOC. In addition, the final solutions were extracted with ethyl acetate and analysed using GC-FID. In the reactions with air, the phenol elimination was between 34 % and 60 %. In these reactions, it was found that simultaneously with phenol oxidation its hydrogenation also occurs. In the oxidation reactions using oxygen, the conversion of phenol was approximately 40 %, obtaining a mineralization degree of approximately 60%. Under these conditions hydrogenation products were not detected. Finally, in the experiments for only hydrogenation, the phenol removal was lower than 40 %. Cyclohexanol and cyclohexanone were found as hydrogenation products. Depending on the amount of dissolved oxygen in the water, oxidation, hydrogenation or both reactions may occur. When the solution is saturated with oxygen only oxidation occurs. At low levels of dissolved oxygen both oxidation and hydrogenation reactions take place. In the absence of oxygen the activated hydrogen hydrogenates the phenol.

For the hydrogenation of ibuprofen, only the catalytic membrane reactor

containing palladium single phase and 4 nm pore size was used. The results were followed by HPLC-DAD. It was found that even at room temperature the reaction occurs. It was also found that it is essential to establish a pH below the pKa of ibuprofen. It was found that more than 90 % of ibuprofen was eliminated using only hydrogen. By the mass analysis HPLC-QTOF confirmed that hydrogenation reactions take place.

In order to understand how the palladium nanoparticles obtained by different methods are affected during the experiments, additional samples were prepared. Powder samples were prepared by different methods such as impregnation, sputtering and microemulsion; concurrently, palladium copper nanoparticles by polyol route were also prepared. These Pd nanoparticles were supported on corundum. Supported nanoparticles were analysed with high resolution TEM and with TPD-MD tests. The purpose of this study was to determine whether the Pd is affected during the different application of the CMRs. Using the high resolution TEM, palladium nanoparticles ranging between 5 and 15 nm in size, were observed. In the sample prepared by impregnation they have been observed also Pd nanoclusters and single atoms. In all samples, it was found that the 5-15 nm Pd nanoparticles are severely affected by H_2. In contrast, Pd nanoparticles with sizes < 2nm and the single atoms are not affected by H_2. The presence of these specimens of the Pd only in the impregnated samples may explain the differences in the activities for hydrogen activation between the two samples. Based on these findings a tentative explanation of the activity for the CMRs can be stated. The results suggest that long term activity of CMRs as well as Pd/corundum for the hydrogen activation could be attributed to the Pd small clusters and single atoms that are presented only in the impregnated samples.

In general, the proposed catalytic membrane reactors have shown to be promising devices that can successfully be used in different processes regarding the industrial processes at mild conditions. Due to the modular character of the reactors, the process is easily scalable and opens the possibility for large scale applications. Therefore, further study is

recommended in order to optimize and increase the efficiency of the proposed reactors.

INDEX

TABLES

FIGURES

CHAPTER I

Introduction

1.Introduction

1.1. Catalytic membrane reactors

1.1.1. Membranes for membrane reactors

A membrane is a permeable or semi-permeable barrier made from a variety of materials ranging from inorganic solids to polymers. The main role of the membrane is to control the exchange of materials between two adjacent fluid phases. The membrane acts as a barrier separating different species, either by filtering or by controlling their relative rate of transport through itself. The membrane action results in two fluid streams: retentate and permeate (see figure 1.1). Transport processes across the membrane are the result of a driving force, which is typically associated with a gradient of concentration, pressure, temperature, electric potential, etc. The ability of a membrane to separate mixtures is determined by two parameters, its permeability and selectivity. The mass transfer mechanisms through membranes vary, depending on many factors, such as the membrane structure, the specific interactions between the membrane and the fluid, and the overall operating conditions [1].

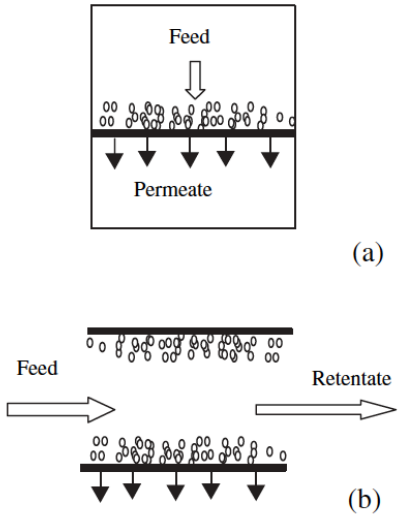

Figure 1.1: Schematic diagram of the filtration process [2]

The membranes are classified according to their nature, which may be biological and synthetic. Other classifications are based on their chemical composition, such as organic e.g. polymeric, inorganic as ceramics, metallic, and organic/inorganic. Regarding their geometry, membranes are classified into flat, tubular, multi-tubular, hollow-fiber, or spiral-wound (see figure 1.2). Membranes are also classified according to their structure, which may be symmetric (homogeneous) or asymmetric [1,3].

Figure	Membrane module	Advantages	Disadvantages
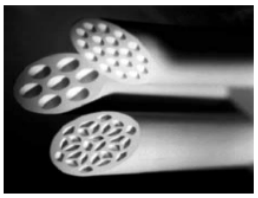	Tubular	• Easy to clean • Feed stream with particulate matter can be put through membrane • Good hydrodynamic control • Individual tubes can be replaced	• Relative high volume required for unit membrane area • High energy consumption • Relatively expensive
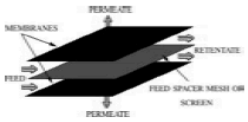	Flat sheet/plate and frame	• Moderate membrane surface/ volume ratio • Well-developed equipment • Easy membrane replacement	• Susceptible to plugging at flow stagnation points • Difficult to clean • Expensive
	Spiral wound	• Compact • Good membrane surface/ volume ratio • Minimum energy consumption • Low capital/operating cost	• Not suitable for very viscous fluid • Difficult to clean • Faulty membrane – change whole module
	Hollow fibre	• Compact • Excellent membrane surface/ volume ratio • Low energy consumption	• Susceptible to end-face fouling • Susceptible to plugging by particulates • Single fibre damage – replace entire module

Figure 1.2: Advantages and disadvantages of the different membranes[3]

The inorganic membranes can be even subdivided into porous and dense membranes [3]. For porous membranes, the molecular size of the species to be separated plays also an important role in determining the pore size of the membrane to be utilized, and the related membrane process. According to the IUPAC classification, porous membranes with average pore diameters larger than 50 nm are classified as macroporous, and

those with average pore diameters in the intermediate range between 2 and 50 nm as mesoporous; microporous membranes have average pore diameters which are smaller than 2 nm. Current membrane processes include microfiltration (MF), ultrafiltration (UF), nanofiltration (NF), gas and vapor separation (GS), and pervaporation (PV) [1].

Figure 1.3 indicates the type and molecular size of species typically separated by these different processes. Porous membranes are made of polymers (they include those used for dense membranes and, in addition, many others including polysulphones, polyacrylonitrile, polypropylene, etc.), ceramics (alumina, silica, titania, zirconia, zeolites, etc. or their combination), and microporous carbons [1].

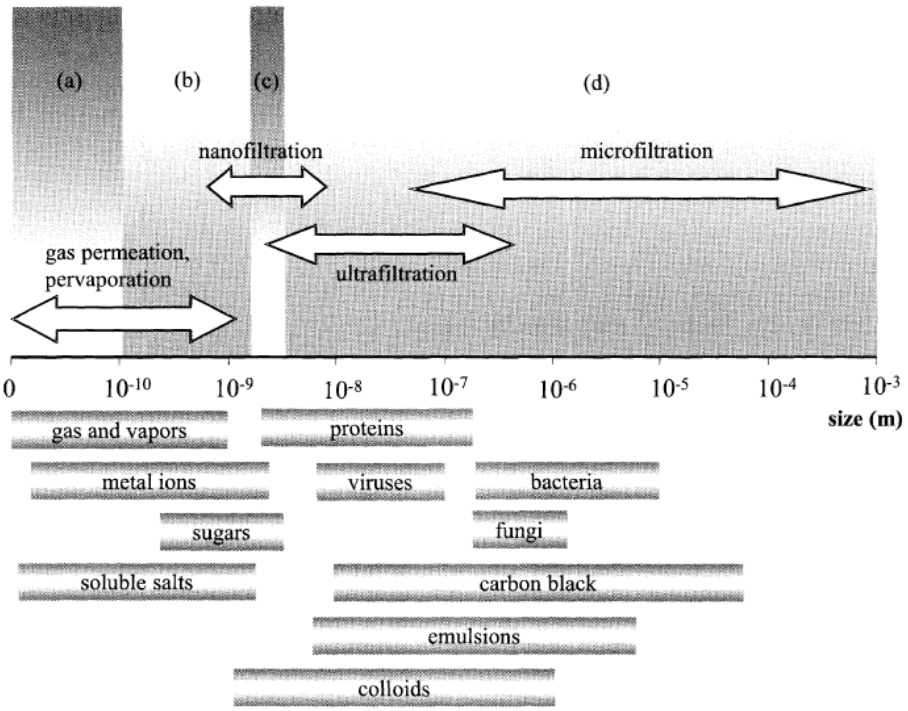

Figure 1.3: Various membrane processes and the different types of membranes and molecular species involved (a) dense and ultramicroporous, (b) microporous, (c) mesoporous, (d) macroporous [1].

Ceramic membranes can be used for a wide range of applications because of their stability and durability under harsh operating conditions; for

instance, high temperatures and different ranges of pH [1]. The inorganic membranes are more expensive than the polymeric membranes, however, they possess advantages such as resistance toward solvents, a well-defined stable pore structure (in the case of porous inorganic membranes), high mechanical stability and elevated resistance at high operating temperatures. Ceramic membranes generally have a macroporous support, one or two mesoporous intermediate layers and a microporous or a dense top layer. The bottom layer provides mechanical support while the middle layers bridge the pore size differences between the support layer and the top layer where the actual separation takes place [2].

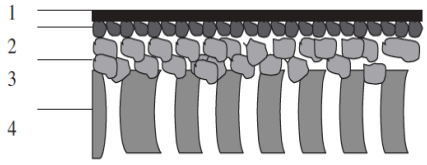

1. Modified separation layer (Dense or <2 nm)
2. Separation layer (2–50 nm)
3. Intermediate layer(s) (50–1000 nm)
4. Porous support (1–15 µm)

1 + 2 + 3+ 4	nanofiltration or gas separation membranes
2 + 3 + 4	ultrafiltration membranes
3 + 4	microfiltration membranes

Figure 1.4: Schematic representation of an asymmetric composite membrane [2].

1.1.2. Membrane Reactor (MR)

A membrane reactor is a device that combines a membrane separation or distribution process with a chemical reaction in one unit. Membrane reactors are capable of promoting a reaction process by: (1) selectively removing at least one of the products from the reaction zone through the membrane, making the equilibrium reaction shift to the product side; (2) supplying only a particular reactant to the reaction zone giving an optimum concentration ratio of the two reactant streams. As a result, the yield

can be increased (even beyond the equilibrium value for equilibrium reactions) and/or the selectivity can be improved by suppressing other undesired side reactions or the secondary reaction of products [2].

The simultaneous separation show advantages related to the process and the reaction: (1) it reduces the flow rate of the reactant stream, whilst increasing the residence time; (2) it increases the reactant concentration and hence the forward reaction rate; (3) it reduces product concentration, reducing the reverse reaction rate [4]. An important advantage is that in the reactor the membrane is able to retain homogeneous catalysts. Thus, it allows continuous operation without needing to separate and recycle catalysts [5].

Membrane reactors usually follow three generic approaches these include extractors, distributors and contactors: membrane reactors as an extractor selectively remove certain products from the reaction zone [3,5]. The MR as a distributor enhances the selectivity through optimizing the reactant dosing [5]. That is, distributing one of the reactants selectively [1]. Both a perm-selective and a nonperm-selective membrane can be used to distributive one of the reactants [3]. The membrane reactor as a contactor intensifies the contact between reactants and the catalyst [5–7]. See figure 1.5

(a)

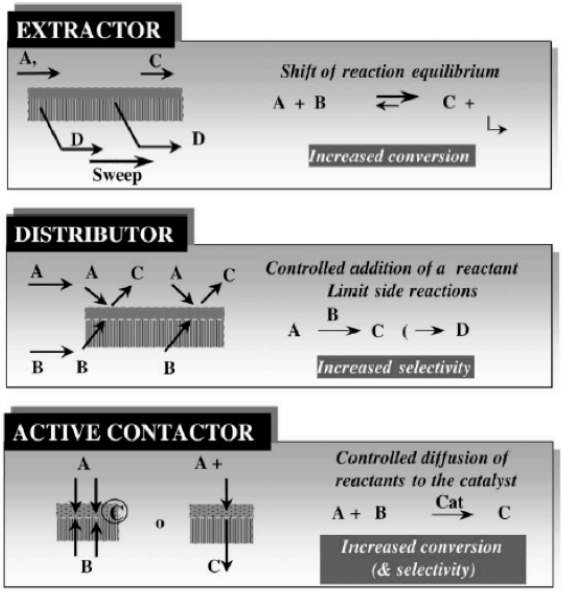

(b)

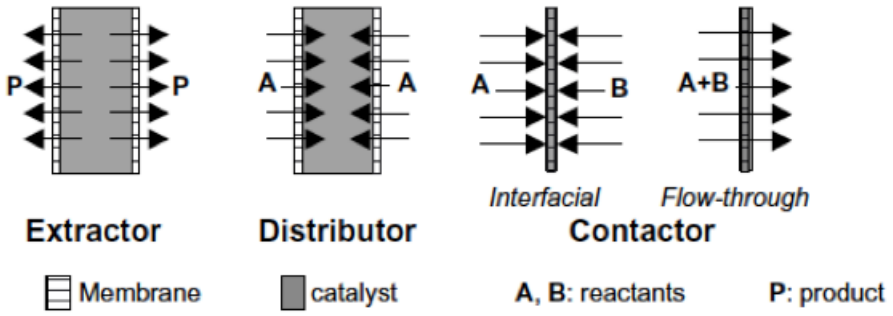

Figure 1.5: Extractor, distributor and contactor approach for (a) MR and (b) CMR [5,8,9].

The principal types of membrane reactors are [3]:

- Catalytic membrane reactor (CMR),
- Catalytic non-permselective membrane reactor (CNMR),
- Packed-bed membrane reactor (PBMR),
- Packed-bed catalytic membrane reactor (PBCMR),
- Fluidized-bed membrane reactor (FBMR),
- Fluidized-bed catalytic membrane reactor (FBCMR),
- Nonperm-selective membrane reactors (NMR),
- Reactant-selective packed bed reactors (RSPBR).

The different types of MRs are summarized in the figure 1.6

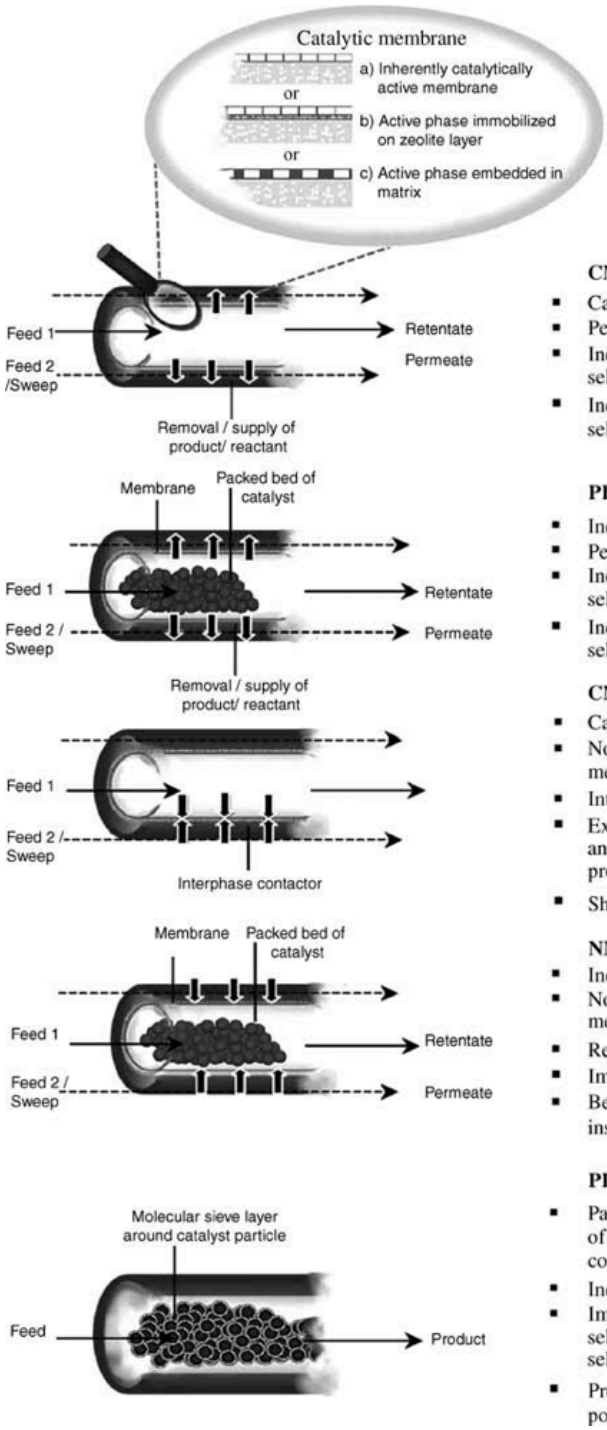

CMR

- Catalytic active membrane
- Permselective membrane
- Increase conversion through selective product removal
- Increase selectivity through selective reactant supply

PBMR

- Inert membrane
- Permselective membrane
- Increase conversion through selective product removal
- Increase selectivity through selective reactant supply

CNMR

- Catalyticly active membrane
- Non-Permselective membrane
- Interphase contactor
- Exclusion of solvents renders an environmentally attractive process
- Short contact time

NMR

- Inert membrane
- Non-Permselective membrane
- Reactant distributor
- Improved selectivity
- Better controllability – for instance explosion limits

PLMR

- Packed bed reactor consisting of permselective membrane-coated catalyst particles
- Inert membrane
- Improved selectivity, through selective reactant supply or selective product removal
- Protection against catalyst poisoning.

Figure 1.6: Classification of MRs based on the function and position of membrane [3].

1.1.3. Catalytic membrane reactors (CMR)

A catalytic membrane reactor is a device whose permselective membrane is of the catalytic type or has a catalyst deposited in or on it [10,11]. In the catalytic membrane reactor, the membrane provides simultaneously the separation and reaction functions. To accomplish this, one could use either an intrinsically catalytic membrane where the same material acts as a catalyst and membrane (e.g., zeolite or metallic membrane) or a membrane that has been made catalytic through activation, by introducing catalytic phases by either impregnation or ion exchange, in this case, a membrane only facilitate transfers [8,12]. For instance, palladium membrane were first to be used in catalytic membrane reactor applications because of their unique hydrogen permselectivity [11].

Targeted benefits of catalytic membrane reactors are focused on different levels: a) process level, eliminating process units and phase changes between them. The integration of a separation function into the reactor allows the number of process units to be decreased, b) reactor level, optimizing the contact between the phases and the dosing strategy, and c) catalyst level, influencing catalysis through the chemical nature of the membrane [13].

The catalytic membrane reactor can be used as an extractor, a distributor, contactor or a combination of these [8]. The CMR as a contactor can be used following two modes, that is interfacial and flow-through (see figure 1.5) [8].

In the interfacial contactor mode, the reactants are separately introduced from each side of the membrane, and meet in the catalyst zone [8]. The interfacial catalytic contactor approach provides an opportunity for a one stage process. Using hydrophobic porous membranes, three principal functions are performed: (i) the gas–liquid interface is well defined and easily controlled, (ii) it provides catalyst accessibility for gaseous reagents, (iii) high gas mass transfer [14].

For an unselective interfacial contactor, two different reactants of the

same phase are separated by a porous membrane forming an interface inside the membrane. The reactants remain separated until they reach the catalytically active centers on the pore surface where the reactions take place. In this arrangement a permselectivity is not required, the membrane only provides the reaction zone. The partial pressure difference forces the reactants to diffuse towards each other until they meet in the catalytic zone. If the reaction is faster than the mass transport in the membrane, a reaction front is formed which prevents the permeation of unreacted components [6].

The other contactor mode is the flow-through contactor. In this mode, the mixture of reactants is forced through the membrane, i.e. through the catalytic pores. Contact time and are permeation regime in the active pore itself, can directly be adjusted from the operative conditions and adapted to required values, which is hardly feasible in conventional reactors [8]. In this concept an unselective porous catalytic membrane is applied in the dead-end mode, forcing the reactants to flow through the membrane. The function of the reaction is to provide a reaction space with short controlled residence time and high catalytic activity. Even for low solubility high pressures are not required, e.g. the gas is supplied directly where it is consumed. Catalytic membrane reactors in flow-through mode is mostly applied to gas-phase reactions, with a few exemptions of liquid phase or multi-phase reactions [6].

The unselective interfacial contactor is the concept most closely related to the flow-through catalytic membrane reactor. Both use unselective catalytic membranes and in both concepts the membrane provides the reaction space. Consequently, the applications are somewhat similar. The difference is, that in the interfacial contactor mode the reactants are fed from different sides of the membrane, whereas in forced flow-through mode the premixed reactants are supplied from the same side in dead-end mode [6].

Among the different potentially promising applications for catalytic membrane reactors are the hydrogenation and oxidation processes:

Hydrogenation reactions can be performed using catalytic porous membrane reactors. The CMRs act as a contactor between the liquid and gaseous reactants as well as host for the catalyst, which is placed in the porous framework of the membrane. The porous membranes create a triple-point interface between the three different phases (gas, liquid, and the solid catalyst on the membrane); this decreases the mass transfer limitations typically encountered with classical slurry or trickle-bed reactors [12].

The selective catalytic hydrocarbon oxidation reactions are difficult to implement because, in general, the intermediate products are more reactive towards oxygen than the original hydrocarbons. The result is often the total oxidation of the original substrate. One of the ways to increase the selectivity towards the intermediate products is to control the oxygen concentration along the reactor length. This can conveniently be implemented by the use of the catalytic membrane reactor approach. The use of a membrane allows for the oxygen and the hydrocarbon reactants to be fed into different compartments. The most preferable configuration is the CMR containing the catalytic phase providing a reactive interface where the reaction takes place [12].

1.2. Objectives

The main objective of this thesis was to prepare catalytic membrane reactors following different methods and applying them in diverse applications regarding water treatment. The prepared catalytic membrane reactors must be able to generate hydrogen peroxide directly from hydrogen and oxygen. The palladium will be used as a main catalytic phase in order to promote the reaction in near ambient conditions.

The specific objectives are summarized as follow:

- To establish different methods for palladium nanoparticle preparation.

- To develop methods for preparation of CMRs by depositing the Pd phase obtained by the different routes into the reaction zone.

- To test the catalytic membrane reactors in abatement of organic and inorganic pollutants in water.

- To test the catalytic membrane reactors in hydrogenation processes.

- To study whether the hydrogen affects the palladium nanoparticles during the experiments by means of different techniques e.g. TPD-MD, XRD, TEM and HRTEM.

1.3. Contents

The thesis is divided into five chapters described briefly below.

After the introductory chapter, chapter II presents the procedures developed for the preparation and characterization of the catalytic membrane reactors. It includes detailed descriptions of the methods used for the synthesis and loading of cerium and iron oxide by impregnation into the CMRs. It also includes the methods used to prepare and load the Pd nanoparticles obtained by impregnation, sputtering, microemulsion as well as the method for synthesis of palladium copper alloys using the polyol route. Moreover, the methods used to characterize the catalytic membrane reactors, such as transmission electron microscopy (TEM), X-ray diffraction (XRD) and temperature programmed desorption (TPD) are described.

In Chapter III a discussion is presented about the different applications in which the catalytic membrane reactors were tested. In section 3.1, the catalytic membrane reactors used to reduce chromium (VI) to chromium (III) with hydrogen as a reducer are analyzed and compared. In section 3.2, the results for phenol abatement in a water solution using the proposed CMRs are presented. Special emphasis is made about the chemical

reactions involved during the phenol elimination. Finally, the elimination of ibuprofen from an aqueous solution using the CMR is studied.

In chapter IV a description is provided for the different methods used for Pd deposition, but here applied for deposition on corundum powder. Thereafter, the attention is focused on the different interaction between the Pd and the hydrogen in conditions similar to those used in the experiments with the CMRs. The results obtained by different techniques e.g. TPR/O, HRTEM are presented. Finally a tentative explanation for the Pd deactivation caused by the hydrogen is also presented.
Finally, in chapter V the conclusions and recommendations for future work are summarized.

CHAPTER II

Catalytic Membrane Reactors: Preparation and Characterization

2.1 Preparation of catalytic membrane reactors (CMRs)

2.1.1 Corundum hollow fibers

2.1.2 Methods of preparation of the catalytic membrane reactors

a. Cerium and iron oxide by impregnation

b. Palladium by impregnation

c. Palladium by sputtering

d. Palladium by microemulsion

e. Palladium and copper alloy by polyol route

2.2 Characterization of catalytic membrane reactors (CMRs)

2.2.1 Transmission electron microscopy (TEM)

2.2.2 X-ray diffraction (XRD)

2.Catalytic membrane reactors: Preparation and characterization

2.1. Preparation of catalytic membrane reactors (CMRs)

2.1.1. Corundum hollow fibers

Corundum hollow fiber membranes of 4 nm, 200 nm and 1400 nm of porous size for ultra and nano filtration manufactured by Ceparation $_{TM}$ were used as the starting material for the preparation of the catalytic membrane reactors. Each hollow fiber is made of alpha alumina (α-Al_2O_3). The hollow fiber membranes present chemical resistances to different chemicals in a wide range of pH (1-14). Additionally, these fibers have high thermal stability and as a result, they may be used at temperatures up to 1000 °C. The porosity of the membranes varied from 10 % to 15 %. The used membranes have an inner diameter of 2 mm and an outer diameter of 3 mm with a total length of 300 mm. Each catalytic membrane reactor was prepared by using a 150 mm fragment of the membrane.

Figure 2.1: A corundum hollow fiber membrane that is 150 mm in length.

2.1.2 Methods used to prepare the catalytic membrane reactors

The catalytic membrane reactors used in this study are obtained after the active phases are supported within the corundum hollow fiber membrane. Different routes and methodologies have been developed and followed in order to incorporate the palladium catalytic phase into the ceramic supports. Two kinds of catalytic membrane reactors were prepared. In the

first case, only Pd was deposited by impregnation. In the second case, additional active phases were incorporated prior to the Pd loading.

a. Cerium and iron oxide on CMR obtained by impregnation method.

The CMRs that contain cerium oxide and iron oxide were prepared using the impregnation technique starting with water soluble precursor salts: $Ce(NO_3)_3.6H_2O$ (purity grade > 99.9 %, Aldrich) and $FeCl_3.6H_2O$ (purity grade > 99 %, Sigma–Aldrich). Each solution was prepared in an adequate concentration in order to obtain around 2 % (w/w_m) in weight of each oxide per weight of the membrane.

In the cases that the CMRs contain transition metal oxides, the iron and cerium salt precursors were impregnated from an equimolar water solution into the hollow fiber membrane. Once the impregnation was finished, the membrane was dried in a special vessel under vacuum for 30 min. During this step the fiber was rotated along its axis in order to avoid preferential deposition of the salts onto the ceramic support. Thereafter, the CMR was dried at 120 ^{o}C for 2 h, and finally was calcined at 450 ^{o}C for 6 h.

The amounts of oxides deposited were calculated by the weight difference between the originals and the modified membranes. Once, the CMRs containing cerium oxide and iron oxide were obtained, subsequent incorporation of the Pd was performed. The palladium or palladium alloys were introduced following different methods:

- By impregnation of the soluble Pd precursor.

- By sputtering using a specially prepared device.

- Synthesis of Pd or Pd-Cu nanoparticles in microemulsions following different methods. Once the active phases were prepared the deposition onto the CMRs was done by filtration.

b. Palladium on CMR obtained by impregnation method.

Palladium was added by impregnation from its soluble salt to the original membrane or to the membrane incorporated with transition metal oxides (cerium and iron oxides).

The procedure of Pd deposition onto the membrane has been thoroughly described by Osegueda. et al. [15,16]. The precursor salt solution of palladium was $PdCl_2$ (Johnson Matthey) with 59.83 % of the noble metal. Firstly, a known amount of the precursor salt was added into Milli-Q water, whilst stirred. Then, concentrated hydrochloric acid (purity grade of 37 %, sigma Aldrich) was added in a drop wise manner into the solution until the salt was completely dissolved. Finally, the concentration was adjusted with Milli-Q water in order to achieve approximately 1 % of weight of Pd per weight of the membrane.

The palladium precursor solution was impregnated into the membrane. Once the impregnation was complete, the catalytic membrane reactors were dried in a special vessel under vacuum for 30 min. In this step, the CMR was rotated along the horizontal axis in order to avoid preferential deposition of the salts onto the ceramic support. Furthermore, the CMR was dried at 120 ^{o}C for 5 h and finally calcined at 450 ^{O}C overnight. The palladium loaded onto the CMR was further activated by reduction under 20 sccm/min flowing hydrogen at 350 ^{O}C for 3 h.

The amount of palladium deposited was calculated by the weight difference between the original and the modified membrane.

c. Palladium on CMR obtained by sputtering method

The incorporation of the catalytic phases onto the membranes by impregnation is a well known technique that achieves homogeneously distributed active phases within the supports. However in the case of the

proposed CMRs, the chemical reactions occur at the external surface of the membranes. In order to assure more efficient use of the precious metal it

has been developed a new method was developed for Pd deposition onto the membranes by the use of a conventional sputtering chamber.

After the incorporation of cerium oxide and iron oxide in the hollow fiber membrane, according to the method reported by Osegueda et. al. [16], the catalytic phase of palladium was directly incorporated by sputtering. The palladium was pulverized from a palladium target, Hauner metallische werkstoffe with 99,95 % purity, in a standard sputtering chamber and deposited on the external surface of the CMRs, using the K575X sputter coater (Qourom Technologies). The equipment has a turbomolecular pump working at a background vacuum in the low, 10^{-5} Pa. Deposition was carried out using pure argon as a working gas. Palladium deposition was carried out at 30 mA for 60 seconds of exposition.

In order to obtain a homogenous distribution of the noble metal, a special assembly was used to rotate the catalytic membrane reactor continuing the transition metals while the palladium was pulverized. Hence, palladium was placed on the external surface of the catalytic membrane reactor. The CMR was placed in a special support of gears within the assembly, which was coupled to a small dc motor. The current was supplied from 2 x 1,5 V batteries. The rate of rotation for the CMR was adjusted to 90 rpm. A schematic diagram and pictures of the proposed device are presented in figure 2.2.

At the same height, a glass plate was placed as a reference material adjacent to the membrane, which was used to determine the thickness (amount) of the Pd layer by means of X-ray reflectometry using a Bruker-AXS D8-Discover diffractometer. The thickness of the Pd layer was calculated from the X-ray diffractogram using the fast Fourier transform (FFT) method.

Thereafter, the amount of palladium deposited onto the membrane

was estimated taking into account the effective membrane area exposed to the palladium beam as well as the rotation velocity.

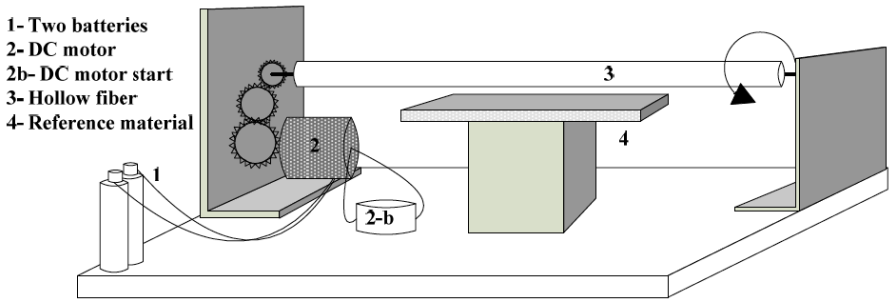

Figure 2.2: Schematic diagram of the assembly [17] used for sputtering of Pd onto the ceramic membrane fibers.

Finally, the catalytic membrane reactor was dried at 120 °C for 2 h, calcined at 600 °C overnight, and reduced at 350 °C under 20 sccm/min H_2 for 2 hours.

d. Palladium on CMR obtained by microemulsion method

Another method was developed for the selective Pd deposition into the reaction zones of the membranes. It consists of two steps; firstly, Pd nanoparticles are synthesized in microemulsions. Secondly, after the proper washing procedure the suspension containing the Pd nanoparticles was filtered with the membrane (from the outer to the inner part of the membrane) assuring the deposition of the active phase on the desired membrane surface.

The microemulsion containing the Pd precursor was synthesized following the procedure described by Wang et al. According to the authors, the obtained palladium nanoparticles are 8 nm in size [18]. The nanoparticles were obtained by mixing two microemulsions of water in oil. Both microemulsions contained 17.78 % w/w of hexadecyltrimethylammonium bromide (CTAB) as a surfactant (purity ≧ 96 %, Fluka Analytical), 22.22 %

w/w of n-butanol as a co-surfactant (purity 99.8 %, Sigma Aldrich), 40 % w/w of iso-octane (from Pareac) and 20 % w/w of an aqueous solution of the metal precursor or reducing agent. The palladium precursor aqueous

solution was 0.01 M $Pd(NH_3)_4Cl_2$. The second emulsion containing the reducing agent was prepared using 0.5 M of hydrazine solution.

The solution of 0.01 M of the $Pd(NH_3)_4Cl_2$ was prepared by dissolving $PdCl_2$ (Johnson Matthey, 59.83 % metal content) in 0.5 N hydrochloric acid. The solution was adjusted to pH 9 using ammonium hydroxide (Sigma Aldrich). The solution of 0.5 M H_4N_2 was obtained by dissolving H_4N_2.OH (hydrazine monohydrate with approximately 64 % of hydrazine, Sigma Aldrich) in Milli-Q water. The two microemulsions were obtained under vigorous stirring at ambient temperature after mixing the corresponding parts described above.

In order to obtain the palladium nanoparticles, both microemulsions were mixed and rapidly stirred at 450 rpm. In approximately 20 minutes the palladium ions were reduced by the hydrazine and the Pd particles were formed. The formation of the Pd particles was change was easily detected due to the color change.

$$2Pd(NH_3)_4^{2+} + H_4N_2 + 4OH^- \Rightarrow 2Pd + 8NH_3 + N_2 + 4H_2O$$

To eliminate the excess surfactant, the solution was washes with ethanol until no surfactant was observed. A simple test was used in order to verify the presence of surfactant in the spent washing solution. A drop of the spent solvent was placed on dark paper and after the ethanol was evaporated a white stain remains indicating the presence of residual surfactant. In order to separate the palladium nanoparticles from the liquid after the alcohol addition, the mixture was centrifuged with a BR4i centrifuge. The first separation was performed at 9000 rpm for 40 min; the next was set at 8000 rpm for 20 min. In all cases, ¾ parts of the liquid

was withdrawn and tested for the presence of the surfactant. If the test confirmed that are surfactant was still remaining in the solution, more ethanol was added and the steps described above were repeated.

Finally, the washed palladium nanoparticles were obtained in the form of a suspension in ethanol. Their deposition onto the external surface of the chosen membrane was performed by a simple filtration procedure from the outside to the inside of the membrane.

A schematic diagram of the process used is presented in figure 2.3

The Pd nanoparticles suspended in ethanol were placed in a 100 ml test tube. The suspension was agitated using a magnetic stirrer. The chosen CMR was placed in the test tube. One end of the CMR was tightly closed and the other end was connected to vacuum. A cold trap was coupled to the vacuum line in order to recover the permeated ethanol. The level of liquid in the tube was maintained by continuously adding fresh ethanol.

During the filtration the Pd nanoparticles were retained on the external membrane surface in a homogeneous manner assured by the stirring process.

In order to measure the amount of palladium loaded onto the CMR, samples from the different solutions were collected. Those solutions were the initial and final feed solution from the test tube containing the suspended Pd nanoparticles and the permeate solution retained in the cold trap.

The Pd content in those samples was analyzed using inductively coupled plasma spectroscopy, (Spectro ICP) after the appropriate digestion with HCl and HNO_3 acids. Once the palladium was placed in the CMR, it was dried in a special vessel under the vacuum for 30 min. Furthermore, the CMRs were dried at 120 ^{o}C for 2 h and finally calcined at 550 ^{o}C overnight.

The CMRs containing palladium were reduced under hydrogen flow adjusted to 20 sccm/min using the Allicat Scientific mass flow controller at 350 ^{o}C for 3 h.

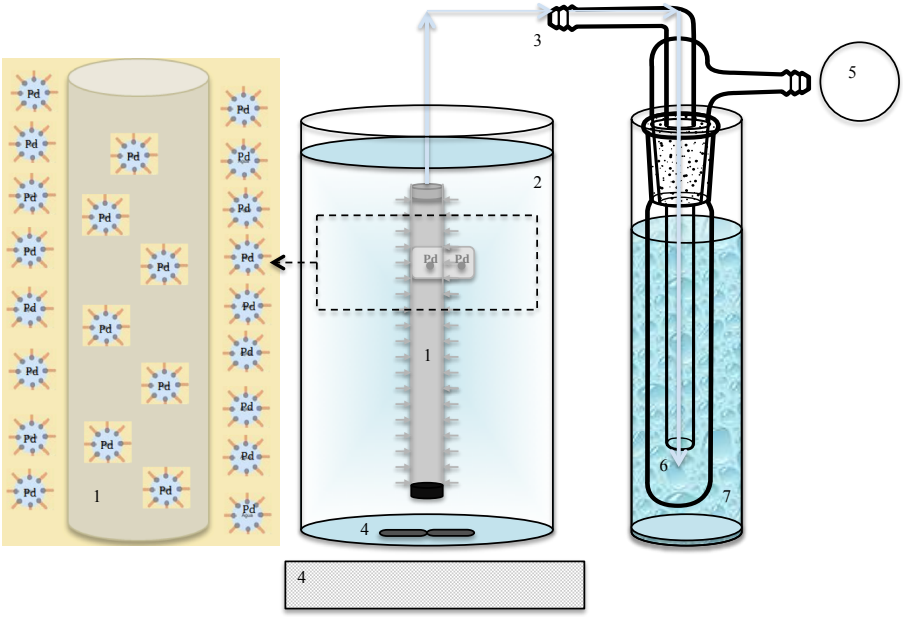

Figure 2.3: Schematic diagram for deposition of the palladium nanoparticles prepared by the microemulsion method on the hollow fiber membrane 1) CMR, 2) suspension of Pd nanoparticles 3) permeate 4) stirred plate 5) vacuum 6) cold trap 7) glass with ice.

e. Palladium copper alloy nanoparticles on CMR obtained by polyol synthesis route

The incorporation of copper into the crystal lattice of Pd does not decrease the capacity of the resulting alloy for hydrogen activation in respect to the pure Pd, but at the same time it stabilizes the crystal structure, such that the formation of β-palladium (PdHx, x > 0.58) is prevented. In order to check this assumption, Pd-Cu nanoparticles were synthetized in different ratios. In order to synthesize the Pd-Cu alloy nanoparticles, the procedure reported by Meshesha et al. [19] with some modification was followed. The $Pd(C_5H_7O_2)_2$ (Heraeus with 34.97 % of palladium) and $Cu(NO_3)_2.3H_2O$ (Sigma Aldrich of 98 % – 103 %) were used as precursors salts for palladium

and copper, respectively. The palladium salt was dissolved in ethylene glycol (99 % purity, Sigma Aldrich). The amount of palladium salt used was adjusted in order to obtain a 0.05 M concentration. In another flask, a 0.05 M solution of copper salt in ethylene glycol was prepared. To each of those solutions 1-hexadecylamine (HDA) (Aldrich, purity 90 %) was added in molar ratio of 3:1 with respect to the metal content. In order to adjust the Pd:Cu molar ratio to 4:1 the corresponding volumes from both solutions were taken and mixed.

The mixture was stirred for one hour in an ice bath in order to avoid an early metal reduction. The homogeneous mixture was then heated at 140 ºC in a reflux for 12 h. During the temperature increase a color variation of the liquid was observed; the initial green gradually transformed to blue, then red to black in the end. The changes indicate the formation of Pd-Cu alloy particles obtained by the reducing effect of ethylene glycol. The surfactant molecules of HAD act mainly as stabilizers in the particles formation. Finally, the nanoparticles were extracted with toluene.

The nanoparticles were deposited into the CMR containing the cerium and iron oxide using the same procedure as described before for palladium nanoparticles obtained by the microemulsion method (see figure 2.3).

2.2 Characterization of catalytic membrane reactors (CMRs)

2.2.1 Transmission electron microscopy (TEM)

In order to determine the size of the Pd nanoparticles in the catalytic membrane reactor, transmission electron microscopy was employed. The equipment used was the transmission electron microscopy, TEM, JEOL model 1011 from Servei de Recursos Científics i Tècnics of URV.

A piece of the CMR was crushed and the powder was dispersed in ethanol. Then, a drop of the sample in suspension was placed into a copper grid. The grid was dried and placed in the TEM to be observed.

The sizes of the observed Pd particles were determined using the ITEM software (Olympus).

2.2.2 X-ray diffraction (XRD)

In order to identify the palladium and corundum crystals, pieces of the catalytic membrane reactor were analyzed using X-ray diffraction. XRD measurements were performed using the Bruker-AXS D8-Discover diffractometer equipped with a parallel incident beam (Göbel mirror), a vertical θ-θ goniometer, an XYZ motorized stage and a General Area Diffraction System (GADDS). Samples were placed directly on the sample holder and the area of interest was selected with the aid of a video-laser focusing system. An X-ray collimator system allowed the analysis of 500 μm areas. The X-ray diffractometer was operated at 40 kV and 40 mA to generate Cukα radiation. The GADDS detector was a HI-STAR (multiwire proportional counter of 30 x 30 cm with a 1024 x 1024 pixel) placed 15 cm away from the sample. A frame (2D XRD patterns) covering 24 – 56^{o} 2θ was collected. The exposure time was 900 s per frame and it was chi-integrated to generate the conventional 2θ vs. intensity diffractogram. Image scale: small lines separation corresponds to ≈ 100 μm. The average area analyzed was represented by an ellipsoid centered in the cross with a constant short axis of 0.5 mm (N-S direction) and a variable long axis (from 1.5 to 0.6 mm in the W-E direction). The analysis of the XRD diffractogram was performed by the ICDD database (release 2007) using Diffracplus Evaluation software (Bruker 2007).

2.3 Results

Table 2.1 summarized the catalytic membrane reactors obtained by the different methods. The notation used to name the CMR has three parts:

- Beginning, active phase(s) included in the CMR: Pd (palladium), Fe (iron oxide) and Ce (cerium oxide). * M means corundum hollow fiber membrane without active phase(s).

- Middle, pore size of the hollow fiber membrane: 4 (4 nm), 200 (200 nm) and 1400 (1400 nm).

- End, first letter of the method used to obtain palladium or copper palladium nanoparticles: i (impregnation), s (sputtering), m (microemulsion), and p (polyol route).

Table 2.1: Catalytic membrane reactors

CMR	Method	Pores size (nm)	% Fe_2O_3	% CeO_2	% Pd
FeCe_1400_i	Impregnation	1400	2.15	2.15	-
FeCePd_1400_i	Impregnation	1400	1.5	1.5	0.3
FeCePd_200_s	Sputtering	200	1.8	1.8	0.02
FeCePd_200_m	Microemulsion	200	2.15	2.15	0.1
FeCePdCu_200_p	Polyol route	200	2.15	2.15	0.5 (20 % Cu 80 % Pd)
Pd_1400_i	Impregnation	1400	-	-	0.9
Pd_4_i	Impregnation	4	-	-	0.75
M_1400	-	1400	-	-	-
M_4	-	4	-	-	-

In figure 2.4 a picture of the catalytic membrane reactors with commercial hollow fiber membrane are shown, CMR with iron oxide and cerium oxide and in the bottom CMR with iron oxide, cerium oxide and palladium.

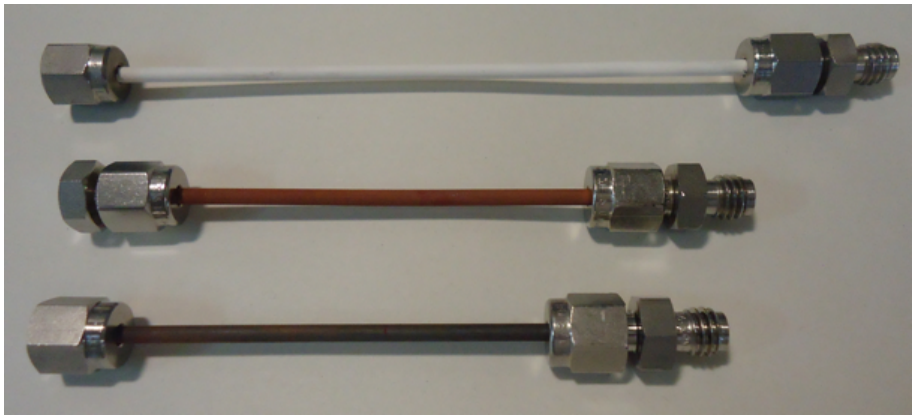

Figure 2.4: Picture of different CMRs. Hollow fiber used for the blank tests, CMR with iron and cerium oxide, and CMR with three phases, iron and cerium oxide and palladium.

2.3.1 TEM

a. Pd particles on the three active phases CMRs obtained by impregnation

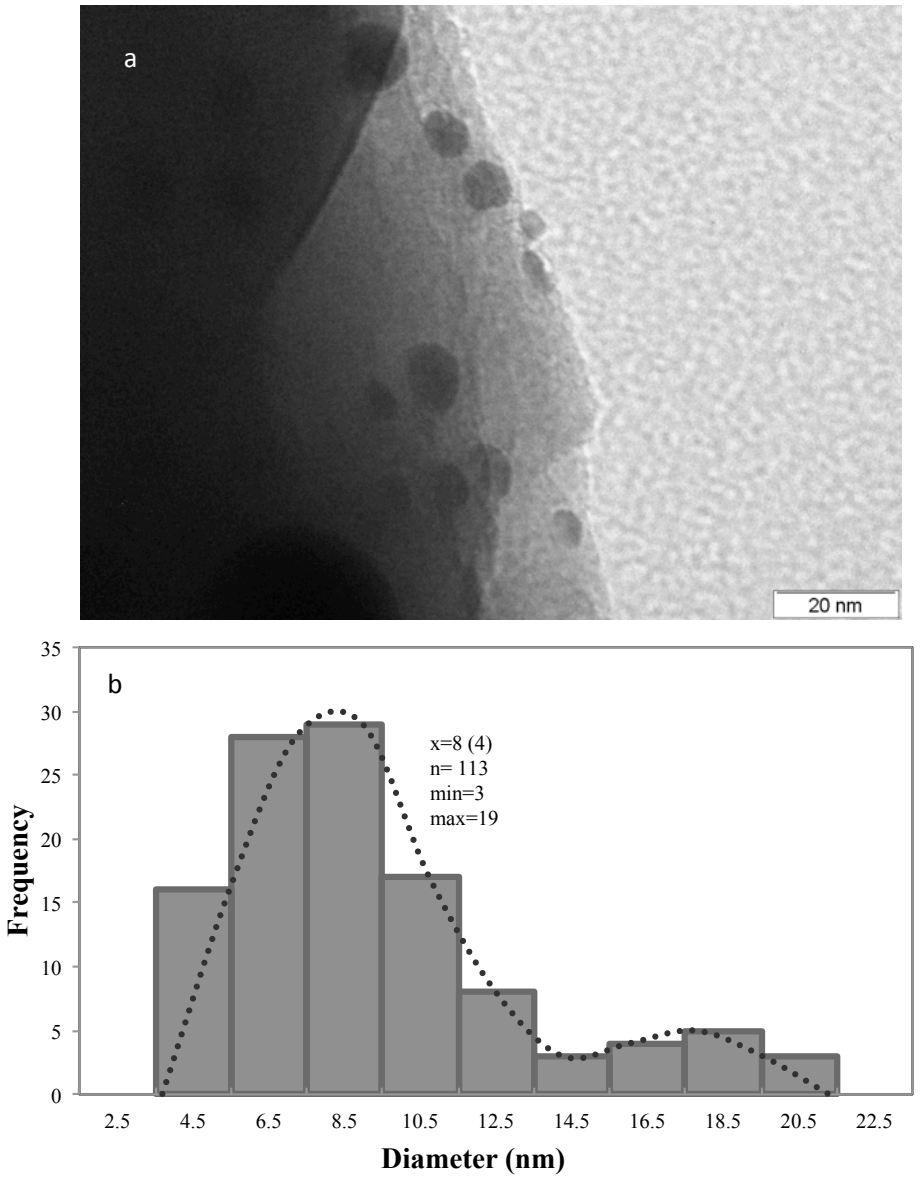

Figure 2.5: TEM image of powder obtained from catalytic membrane reactor of CMR FeCePd_1400_i after grinding.

In order to examine the Pd particles on the CMRs, pieces of the reactors were grinded into a fine powder. After the proper pretreatment of these powder samples they were observed using TEM.

A representative picture corresponding to CMR PdFeCe_1400_i is shown in fig. 2.5.

The Pd particle size distribution was determined after counting more than 113 particles. The obtained particle mean size was 8 nm with a standard deviation of 4 nm. The minimum size was 3 nm and the maximum 19 nm.

Figure 2.5b also shows a histogram for the Pd particle size distribution obtained in this analysis.

2.3.2 XRD

a. μ-XRD analyses of palladium on a hollow fiber membrane used as base of the CMR

An image of the 4 nm hollow fiber membrane with nominal pores and diffractograms at five different points, are presented in figure 2.6. The pieces of the hollow fiber of corundum are shown in figure 2.6a.

The diffractorams can be seen in Fig. 2.6b. The first two points represent the inner part and the others three points below to the outer part of the membrane. In the diffractogram, two high peaks characteristic of the corundum at 2θ of 37.7 and 43.3 and three peaks more at 2θ of 25.5, 38 and 52.6.

This confirms the crystallinity of the corundum used in the hollow fiber membrane. The XRD analysis of the CMR pieces confirmed the homogeneity of the corundum membrane.

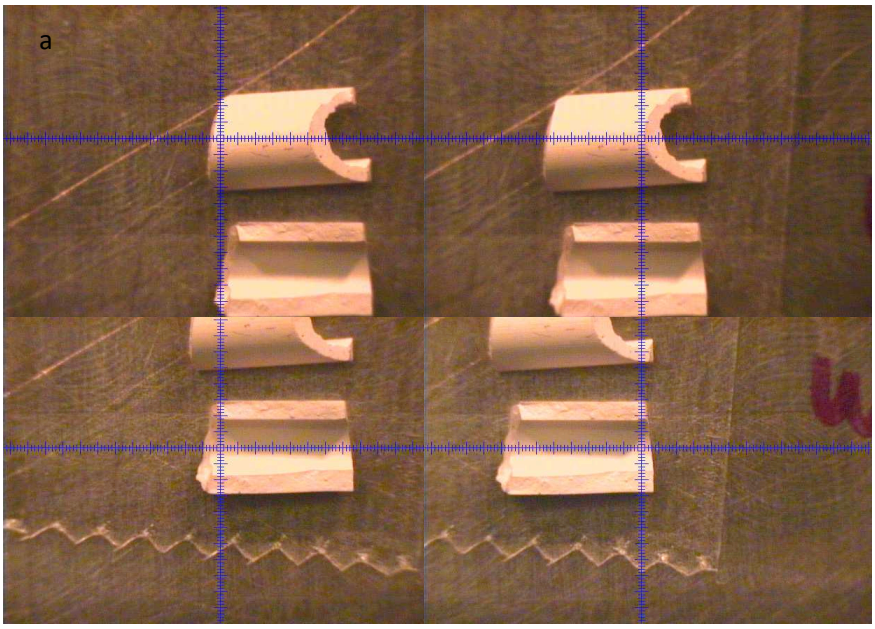

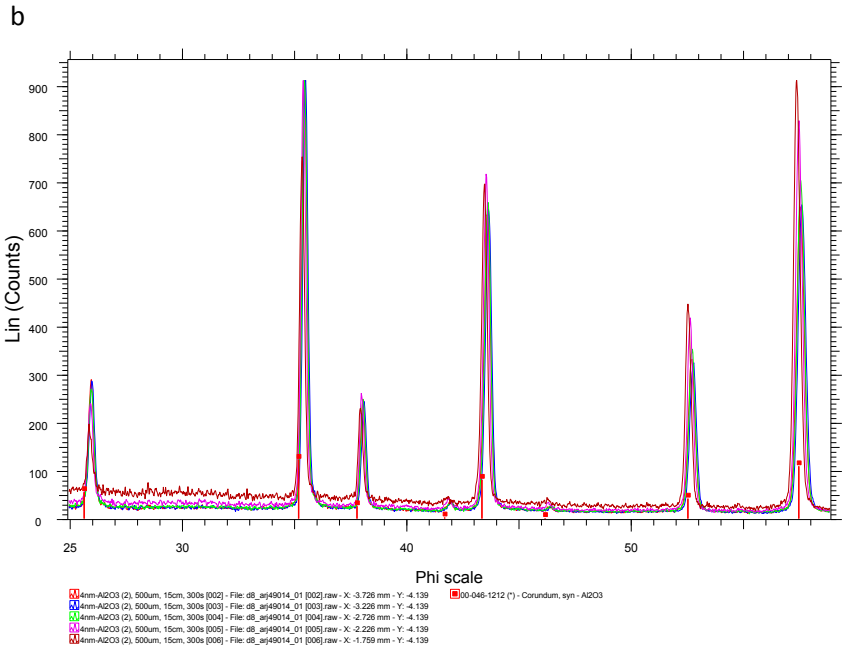

Figure 2.6: a) Pieces of M_4 measured at five points, two on the inner and three on the outer surface. b) X-ray diffractograms obtained for the four points.

b. μ-XRD analyses of palladium on a catalytic membrane reactor obtained by impregnation.

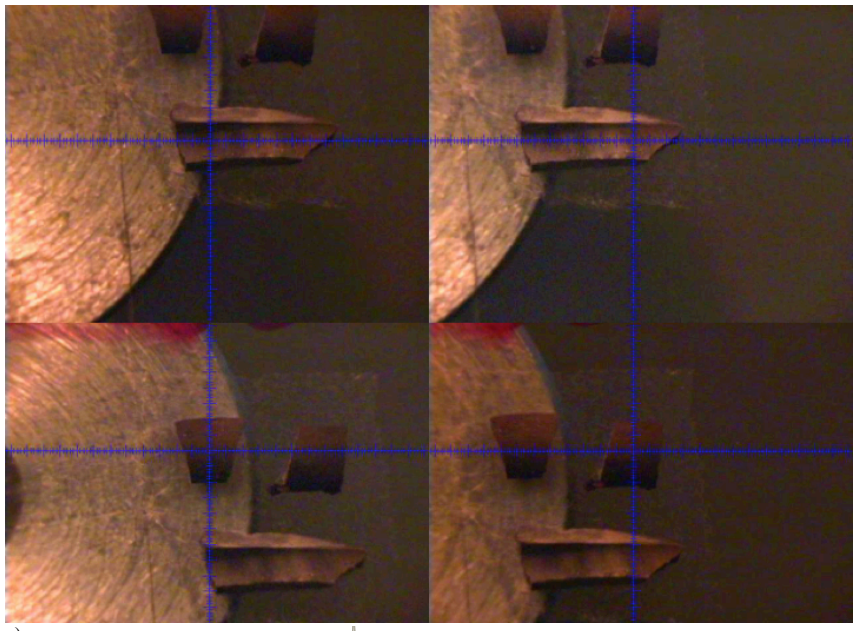

a)

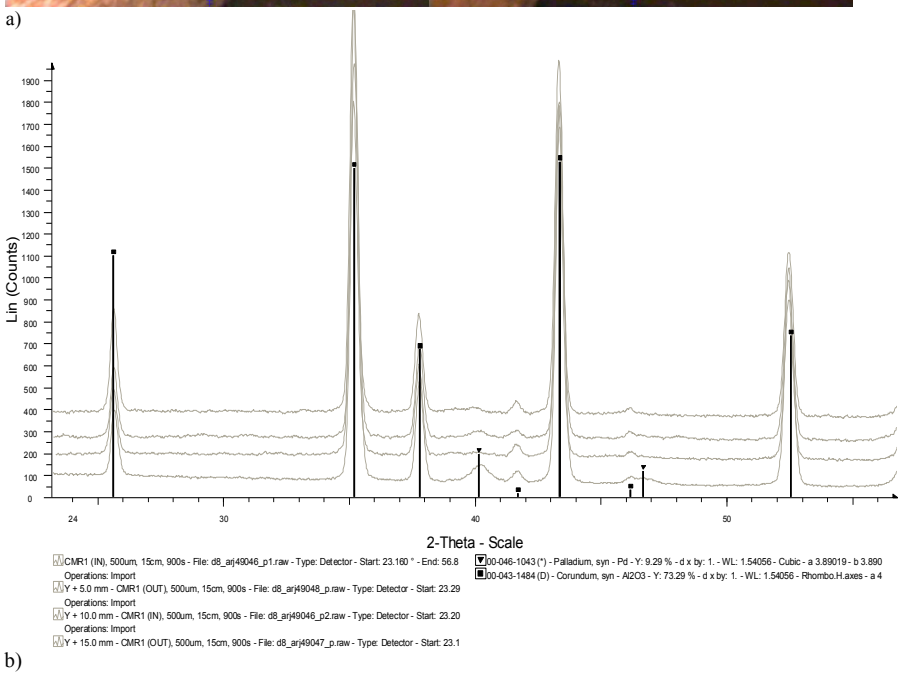

b)

Figure 2.7: a) Pieces of CMR Pd_1400_i measured at four points, two on the inner and two on the outer surface. b) X-ray diffractograms obtained for the four points.

An image of the CMR piece and diffractograms at different points are presented in figure 2.7 for the case of CMR Pd_1400_i. The registered diffraction patterns on the outer and the inner membrane surfaces are shown in figure 2.7a. The obtained diffractorams for this case can be seen in Fig. 2.7b.

A piece of the membrane reactor is placed under the beam and the reflected rays are collected at specific angles. The registered patterns correspond to the area of 500 um^2 and 20 um depth. The diffraction patterns are obtained from two zones of each side of the membrane reactors. The two characteristic high peaks of the corundum can be seen at 2θ of 37.7 and 43.3. It is confirmed that the crystallinity of the material is not disturbed. Moreover, a little peak of palladium is presented at 2θ of 40.2. The XRD analysis of the CMR pieces confirmed a homogeneous active phase distribution across the entire membrane.

c. μ-XRD analyses of palladium, iron and cerium oxide on a catalytic membrane reactor obtained by impregnation.

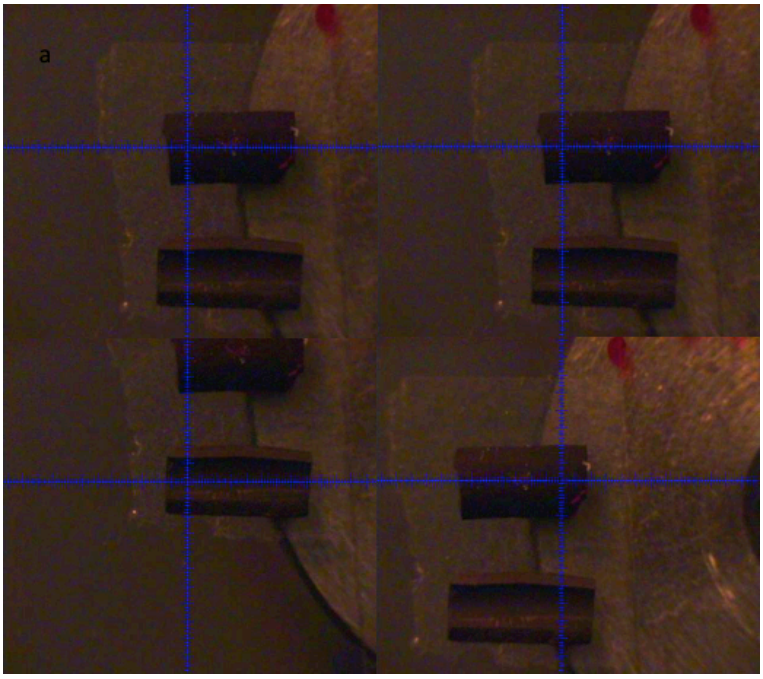

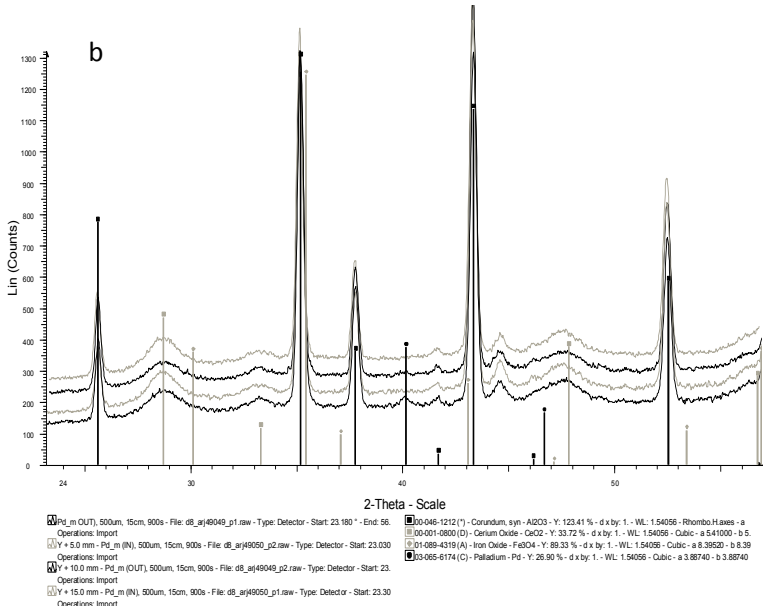

Figure 2.8: a) Pieces of PdFeCe_1400_i measured at four points, two on the inner and two on the outer surface. b) X-ray diffractograms obtained for the four points.

An image of the CMR pieces and diffractograms at four different points is presented in figure 2.8 for the case of CMR PdFeCe_1400_i. The diffraction patterns on the outer (in black) and the inner (in gray) membrane surfaces are shown in figure 2.8a. The diffractorams can be seen in Fig. 2.8b. In the diffractogram, two characteristic high peaks of the corundum at 2θ of 37.7 and 43.3 can be seen as well as three peaks more at 2θ of 25.5, 38 and 52.6 without disturbances. A peak at 2θ of 40.2 corresponds to palladium. The three peaks at 2θ of 28.8, 33.3 and 47.9 correspond to cerium oxide. The peak at 2θ of 47 corresponds to iron oxide. The XRD analysis of the CMRs pieces confirmed a homogeneous active phase distribution across the entire membrane.

CHAPTER III

Applications of Catalytic Membrane Reactors

3.1 Chromium (VI) reduction

3.1.1 Introduction

3.1.2 Methods and Materials

3.1.3 Results and Discussion

3.1.4 Conclusions

3.2. Application of the prepared CMRs in the treatment of waste waters polluted with organic contaminants

3.2.1 Introduction

3.2.2 Methods and Materials

3.2.3 Results and Discussion

3.2.4 Conclusions

3.Applications

3.1. Chromium (VI) reduction

3.1.1. Introduction

Chromium, the 21st most abundant element in the earth's crust, is a metallic element naturally found in rocks and soil. Although it exists in several oxidation states, the zero, trivalent, and hexavalent states are the most common [20]. In water, chromium is commonly found in the (III) or (VI) oxidation state [21]. Chromium (IV) and (V) are transient intermediates during the reduction of the hexavalent chromium and both are instable in water forming chromium (III) or (VI) [22]. Trivalent chromium has very low solubility and reactivity at neutral pH resulting in low mobility in the environment and low toxicity in living organisms. Cr (III) is considered essential for living organisms [20]. Hexavalent chromium, however, is very soluble in water and it is considered to be the most toxic form of the metal. In drinking water, according to a number of studies, soluble Cr (VI) compounds may cause cancer [23]. EPA has an enforceable drinking water standard, that is 100 ppb for total chromium, which includes chromium (VI) and chromium (III) [24]. WHO recommended a maximum allowable concentration of 50 ppb of hexavalent chromium [23]. The wastewater contaminated with chromium (VI) must be treated before discharge or reuse. The conventional treatment process generally involves two steps: (1) reduction of Cr (VI) to Cr (III) and (2) precipitation of Cr (III), for total removal of the chromium after filtration [25].

In an aqueous medium, taking into account the pH and concentration, hexavalent chromium occurs in oxy anions, such as $HCrO_4^-$; $Cr_2O_7^{2-}$ or CrO_4^{2-} with the chromate ion being predominant in basic medium [26]. At pH values below 6, chromate ion accept protons and converts it into $HCrO_4^-$ and $Cr_2O_7^{2-}$. The equilibrium between both ions is dependent on their concentration. In concentrated solutions, dichromate is predominant; while, in dilute solutions, hydrogen chromate ion predominates [27].

The dichromate is well known as a very strong oxidant in acid medium, while a less oxidant chromate predominates in basic solutions [22]. When reducing agents are present in the aqueous solution, these oxyanions are reduced to trivalent chromium. The trivalent chromium at pH values between 8 to 10 forms $Cr(OH)_3$ that has very low solubility in water, resulting in precipitation [28]. Thus, the trivalent chromium hydroxide can be removed by filtration.

The most common way to reduce hexavalent chromium in aqueous medium is to employ iron and ferrous ions as electron donors while the chromium is the electron acceptor [25]. The reduction of Cr (VI) to Cr (III) occurs through the formation of pentavalent and tetravalent chromium as intermediate states [29,30]. It is suggested that the presence of cerium (III) accelerates the conversion of Cr (IV) to Cr (III) acting as one-electron reducing agent [31].

Several studies have been developed to reduce Cr (VI) to Cr (III) in aqueous medium and acidic conditions [25,26,29–45]. Most of them used iron or ferrous ions as a reducing agent [25,26,29,30,36,37,42,43,45]. The majority of the studies were performed with synthetic wastewater containing hexavalent chromium, while a few deal with wastewater from the electroplating industry with Cr(VI) concentration exceeding 400 ppm [36,37]. Alternatives to address the problem includes the use of biological agents to reduce hexavalent chromium in synthetic wastewater [32,33,38,39]. The photo catalytic reduction of chromium presented in synthetic water and in wastewater polluted with chromium and EDTA from printed circuit boards [41] has also been studied. The redox reaction between chromium (VI) and arsenic (III) from acid mine drainage (AMD) wastewater in the presence of H_2O_2 as a promoter has also been studied [40].

Only few of the studies focused on chromium (VI) reduction at low concentrations, e.g. in the range 5 to 10 ppm. In those cases, different proposals have been made e.g. reduction with iron wires, packed-bed bioreactors and by the use of photoelectrocatalysis with nanotube array electrodes. In the former case, the process involved simultaneous

reduction of chromium combined with phenol oxidation in synthetic wastewater [25,35,38].

This work proposes a novel method for Cr (VI) to Cr (III) reduction using hydrogen gas as a reducer. In order to accomplish the final goal, catalytic membrane reactors using commercial corundum hollow fiber membranes were developed and prepared. Different active phases were introduced to the membranes by impregnation of the water-soluble precursors, by means of sputtering, microemulsion or the polyol route. The catalytic tests were performed in a semi-batch mode at ambient conditions, room temperature, and atmospheric pressure. One end of the membrane was closed and the hydrogen gas, adjusted by a mass flow controller, was supplied to the other end.

The reactors were submerged into a vessel containing the chromium solution. It was found that the presence of palladium by impregnation is essential for reduction of chromate anions. The CMRs containing palladium loaded by sputtering or deposited from microemulsions or from Pd nanoparticle suspension presented very poor activities and suffered very fast deactivation under the experimental conditions.

The experiments were performed with two types of water, Milli-Q and mineral water, both contaminated with chromate in concentrations between 0.5 and 18 ppm. It was found that the initial adjustment of the solutions pH to values below 4 is necessary to completely reduce Cr (VI) to Cr (III). Additionally, by using the proposed method, once Cr (VI) is reduced to Cr (III), followed by adjusting the pH the final solution to 8, the chromium can be completely removed from the water by simple filtration of the low soluble Cr(III) hydroxide.

It is important to note that no sub products are generated and no excess of chemical reagents remained in the final solution. The tested catalytic membrane reactors showed a steady performance during the Chromium (VI) reduction without losing activity in repetitive runs.

3.1.2. Methods and materials

a. Preparation of the chromate containing water

A stock water solution of 179 ppm CrO_4^{2-} was prepared from K_2CrO_4 salt, Panreac. An aliquot of this solution was added to Milli-Q or mineral water in order to obtain 0.5, 3.4, 12 or 18 ppm of CrO_4^{2-} solutions corresponding to 0.2, 1.5, 5.4 or 8 ppm of Cr (VI), respectively.

The composition of the mineral water, as stated by the supplier, was: 28 ppm dry residue, 21 ppm bicarbonates, 0.6 ppm chlorides, 5.26 ppm calcium, 0.91 ppm magnesium and 1.36 ppm sodium.

b. Chromate analysis.

The chromate concentration in the withdrawn samples was measured using the Jasco V-630 spectrophotometer. Samples were prepared in accordance with the standard methods 3500-Cr (colorimetric method for the examination of water and wastewater) [46]. 1,5 biphenyl carbazide was added to the samples as an indicator and its absorbance was measured at 540 nm.

A calibration curve for the chromium (VI) determination was prepared using standard solutions according to the standard method. Following the above standard method, the low detection limit for the chromium (VI) was 28 ppb. This value is lower than the maximum limit 50 ppb allowed according to the WHO.

Once the reaction was complete, the pH of the solution was adjusted to 8 using sodium hydroxide. The solution was then filtered using a 0.45 μm cellulose acetate filter. The filter was washed with 5 % HCl acid in order to recover the Cr (III). The amount of chromium was measured in both solutions, the acidic solution containing the Cr (III) and the filtrate containing the unreacted Cr (VI). The measurements were performed using inductively coupled plasma spectroscopy (ICP), Spectro.

c. Preparation of the catalytic membrane reactors.

Commercial corundum hollow fibers for micro-ultra filtration were used for the preparation of the catalytic membrane reactors. The preparation procedures of the catalytic membrane reactors used for this application are described in details in chapter II.

Seven different CMRs were used for Cr (VI) reduction in aqueous media. The active phase compositions and the nominal pore size of the ceramic membranes were as follow:

- Pd_1400_i: 0.9 w/w % of Pd.
- Pd_4_i: 0.75 w/w % of Pd.
- FeCe_1400_i: 2.1 w/w % of Fe_2O_3 and 2.1 w/w % of CeO_2
- FeCePd_1400_i: 0.3 w/w % of Pd, 1.5 w/w % of Fe_2O_3, and 1.5 w/w % of CeO_2.
- FeCePd_200_s: 0.02 % Pd by sputtering and 1.8 % of Fe_2O_3 and 1.8 w/w % of CeO_2.
- FeCePd_200_m: 0.1 % Pd by microemulsion, 2.2 % of Fe_2O_3 and 2.2 w/w % of CeO_2.
- FeCePdCu: 0.5 % Pd Cu by polyol route, 2.2 % of Fe_2O_3 and 2.2 w/w % of CeO_2.

* For more details see Table 1 in chapter II

d. Experimental setup.

The catalytic membrane reactors were tested in a semi-batch mode of operation. The hydrogen flow was adjusted using a mass flow controller and supplied to one end of the reactor whilst the other end was kept

closed. The CMR was submerged into a glass reactor containing 100 ml of water polluted with Cr (VI) ions. The hydrogen crossed the membrane wall reaching the water on the external surface. All the tests were performed at room temperature.

The hydrogen supply was maintained at 10 sccm/min in all experiments. Different experiments were performed from a variety of chromate concentrations in the range of 0.5 to 18 ppm. The pH of the water solution was varied between 3 and 7. Thereafter, it was maintained at 3 in all experiments.

Two types of water were used in the tests. Initially, Milli-Q water was used and later the experiments were performed using mineral water with the composition as described above. In order to quantify the chromate reduction, samples were withdrawn from the reaction vessel during the experiments.

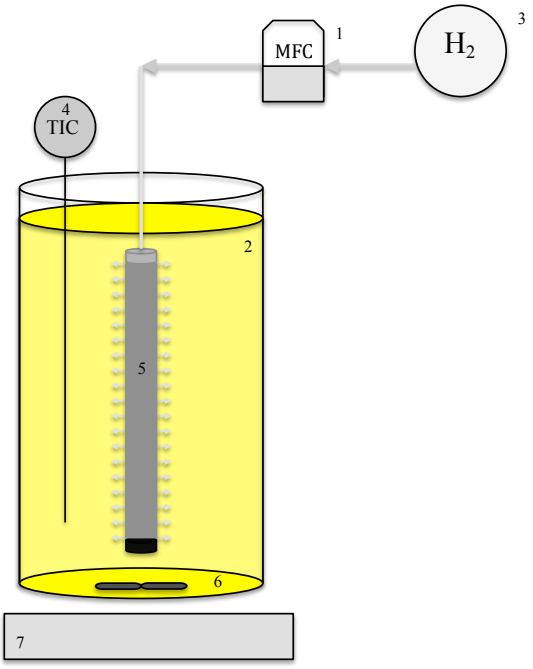

Figure 3.1: Experimental setup for the chromium (VI) reduction tests using CMR. 1) Mass flows controller 2) Chromium (VI) solution 3) Hydrogen supply 4) Temperature indicator and controller 5) CMR 6) and 7) stirrer plate.

3.1.3 Results and Discussion

a. Initial tests of chromium (VI) reduction.

These tests were performed using the CMR FeCePd_1400_i. The model solution was a water solution of 5.4 ppm of Cr (VI) prepared with Milli-Q water without any pH adjustment. The hydrogen supply was fixed to 10 sccm/min. No chromate reduction was observed in this case as can be seen in figure 3.2 for the case of neutral pH.

It is well known that the redox potential of the Cr (VI)/Cr (III) depends on the pH of the aqueous medium and it increases at higher acidity. At neutral pH the Cr (VI) mainly exists as CrO_4^{2-}. As a next step, the pH of the solution was decreased to 3 by adding hydrochloric acid. For the chosen Cr (VI) concentration, at pH 3, the predominant form of Cr (VI) is $HCrO_4$- and traces of H_2CrO_4 are probably also present. After acidifying the water, the chromate concentration decreased steadily during the experiment. The results are presented in figure 3.2.

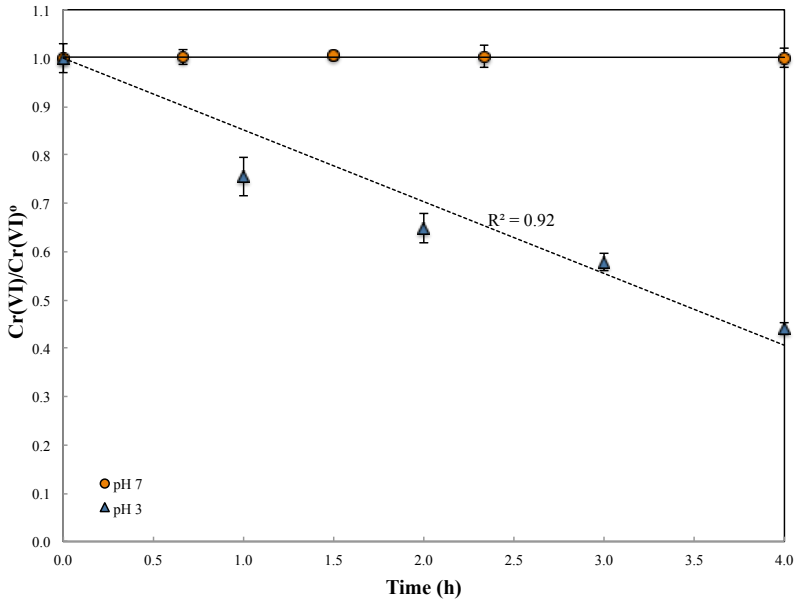

Figure 3.2: Cr (VI) reduction in Milli-Q water with FeCePd_1400_i at pH 3 or 7, and 10 sccm/min of H_2 supply, 5.4 ppm Cr (VI) at room temperature.

It is important to note that the amount of hydrogen supplied is much higher than the one consumed in the reaction (e.g. 1 sccm H_2/h). There are two main reasons for the use of such high excess hydrogen. Firstly, the hydrophilic nature of the catalytic membrane reactors imply that the hydrogen must be supplied at higher pressure in order to overcome the capillary pressure of the water occupying the porous structure of the membrane.

Secondly, the non-uniform pore size distribution requires the application of pressures higher than the bubble point of the main part of the pores. This ensures that the hydrogen could, practically, reach the entire outer surface of the reactor where the reaction takes place. All experiments were performed at room temperature, and due to the same initial nominal pore size of the ceramic fibers, 1.4 um, the hydrogen reached pressures between 1.2 and 1.5 barg in the inner part of the CMRs.

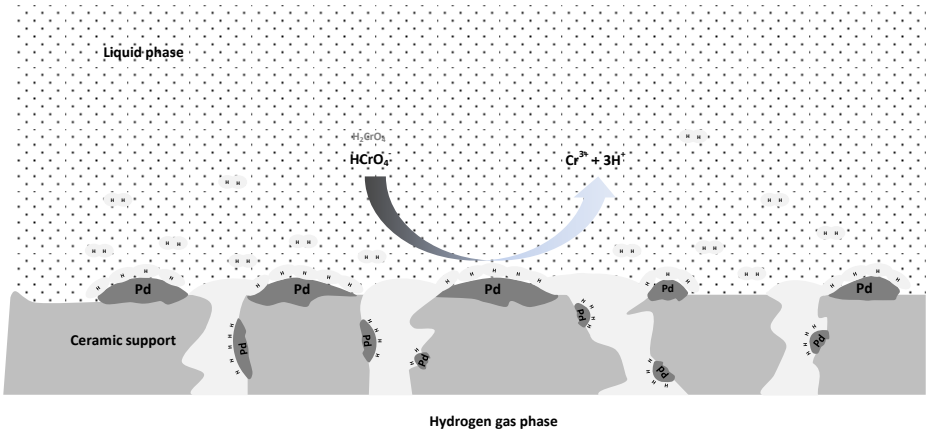

Figure 3.3: Reaction mechanism of reduction of chromium (VI) to chromium (III).

The proposed reaction mechanism is depicted in figure 3.3. The hydrogen flows from the inner CMRs side through the pore structure, reaching the outer surface. Part of it is activated on the Pd domains loaded uniformly into the reactor. The activated hydrogen reduces the two forms of chromate forming Cr (III). The reaction takes place predominantly at the solid-liquid-gas contact point.

b. Chromium (VI) reduction by means of the CMRs containing Pd deposited by sputtering, microemulsion or polyol route.

After the initial screening of the CMR activity for chromate reduction, the rest of the experiments were carried out with a hydrogen supply fixed at 10 sccm/min and pH of the water medium adjusted to 3. The Cr (VI) concentration was varied between 0.2 and 8 ppm.

In figure 3.4 the results for Cr (VI) reduction, when the CMRs (FeCePd_200_s and FeCePd_m) were used can be seen. The figure also includes the results for the Cr (VI) reduction using the CMR containing the PdCu nanoparticles used in consecutive run (FeCePd_200_p). The results show, that in all cases, the activity for Cr (VI) reduction is very low especially when compared to the activity of the CMR containing Pd loaded by impregnation e.g. see figure 3.7. In contrast, the second test using the CMR FeCePdCu_200_p the activity was insignificant.

The tests were performed at different Cr (VI) concentrations but the activities were very low in all cases. These results indicate that the Pd loaded on the CMRs as a metal phase, by sputtering or as nanoparticles (microemulsion, polyol route), have some specific features that favor this fast deactivation and low activity despite its high concentration in the reaction zone.

At this stage it can be speculated that, in the cases of CMRs with Pd loaded by impregnation the interaction between the support and the metal is much stronger than in the cases of sputtered or deposition from microemulsion Pd. This strong metal support interaction stabilizes the Pd such that its stability is enhanced.

In the last chapter of the present thesis some additional results are presented and a more detailed discussion is provided about the Pd deactivation.

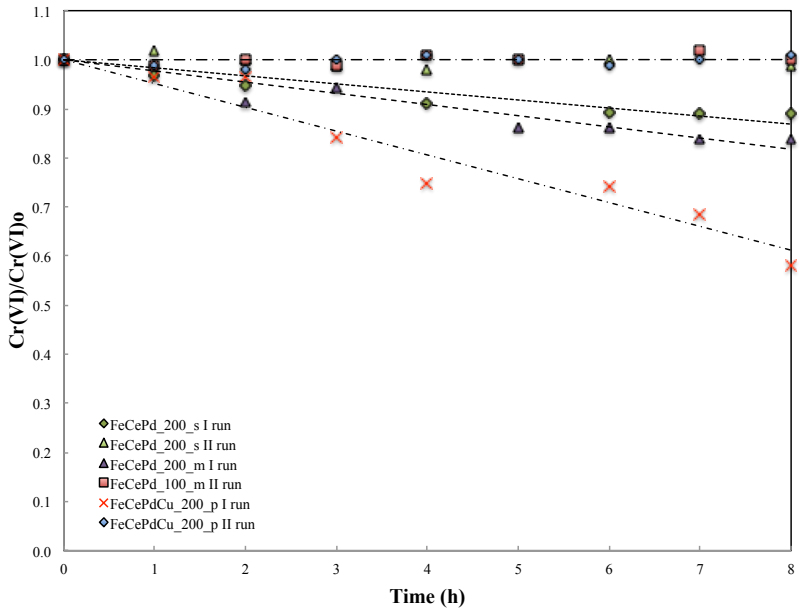

Figure 3.4: Cr (VI) reduction in Milli-Q with FeCePd_s, FeCePd_m and FeCePdCu at pH 3 and 10 sccm/min of H2 supply, 8 ppm Cr (VI) at room temperature.

c. Cr (VI) reduction in Milli-Q and mineral water with CMRs containing Pd loaded by impregnation.

In order to check whether any specific adsorption of the different forms of Cr (VI) occurred on the ceramic reactors at different pH, additional experiments were performed with catalytic membrane reactors that did not contain palladium.

The tests were done with the hollow fiber membrane, M_1400 that was free from an active phase as well as with CMR FeCe_1400_i that only contained a mixture of iron and cerium oxides. For both reactors, no change in the Cr (VI) concentration was observed for 8 h under the experimental conditions.

Figure 3.5 shows the results for two types of water at pH 3.

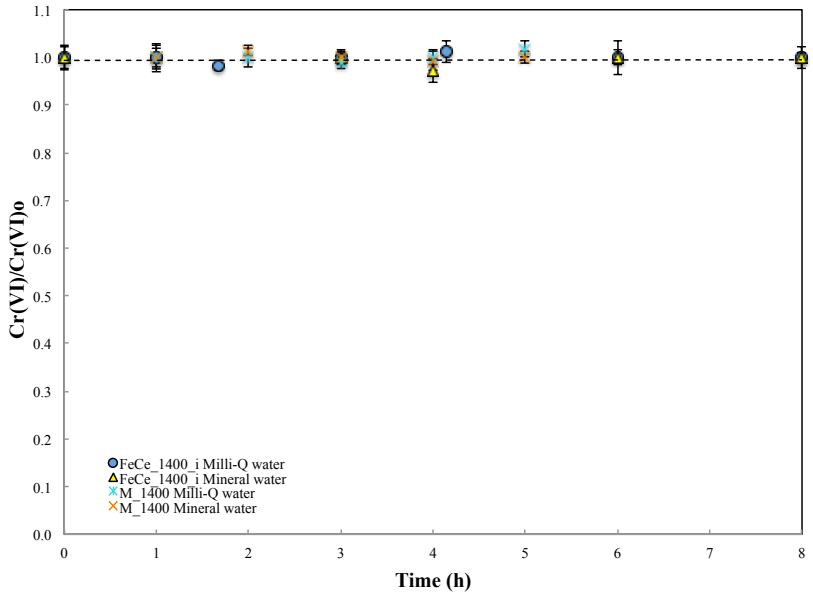

Figure 3.5: Cr (VI) reduction in Milli-Q or mineral water with M_1400 and FeCe_1400_i at pH 3 and 10 sccm/min of H_2 supply, 8 ppm Cr (VI) at room temperature.

On the other hand, experiments with CMR Pd_1400_i and CMR FeCePd_1400_i were performed at pH 3 simulating a heterogeneous catalytic system. In those experiments, the reactor was submerged into the reaction vessel supplying the hydrogen to the solution by bubbling. No activity for Cr (VI) reduction was observed.

CMR Pd_1400_i contained only palladium as an active phase. Chromium reduction with this reactor was performed using two types of water, Milli-Q and mineral. The initial Cr (VI) concentration was 8 ppm.

For the two types of water the chromate concentration steadily decreased below 28 ppb (the low detection limit of the analytical method used).

The results are presented in figure 3.6. The graphs include error bars that were calculated from the repetitive runs.

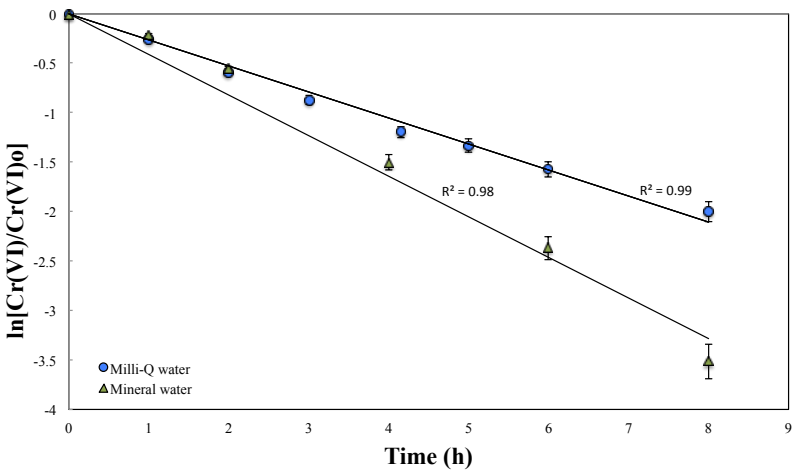

Figure 3.6: Cr (VI) reduction in Milli-Q or mineral water with CMR Pd_1400_i at pH 3 and 10 sccm/min of H_2 supply, 8 ppm Cr (VI) at room temperature and their exponential line.

The reaction proceeds most likely as a first order reaction with respect to the chromium concentration as can be seen from the exponential fits and the corresponding regression coefficients. As mentioned before, we assumed that the hydrogen concentration does not vary during the reaction. In order to compare the performance of CMRs for chromate reduction, the first 4 h of the experiments were used assuming linear trends. The rate of chromium reduction in the catalytic membrane reactor of Pd_1400_i water was 1.4 ppm Cr (VI)/h during the first 4 h of the test.

It is important to note that the chromium reduction by the proposed system is not affected by the presence of other ions as demonstrated by the tests with mineral water. It is worth noticing that CMR of Pd_1400_i was tested in consecutive experiments and no decrease of its activity was observed. No special activation procedures were performed between the different tests with either Milli-Q or mineral water.

As described in the experimental section, cerium and iron oxides were loaded in CMR before palladium deposition by impregnation. It is well known that in the cerium oxide part of the Ce is in the 3^+ oxidation state [47].

The proportion between Ce (III) and Ce (IV) depends on different factors.

In the present case, due to the close contact between the oxide, the palladium, and the activated hydrogen on its surface, it can be expected that the presence of Ce (III) will be rather high. Therefore, the aim of the preparation of this CMR was to verify whether the activity of the catalytic membrane reactors would be increased with the incorporation of the mixed oxides and whether this would also increase the efficiency of hydrogen use. At the same time the amount of the noble metal in the CMRs of three phases were reduced compared to the CMR containing only palladium.

Figure 3.7 presents the obtained results for the chromate reduction in two different aqueous media, Milli-Q and mineral water. Similarly to the tests with CMR of Pd_i, this reactor was used in nine consecutive experiments and no decrease of activity was observed.

The FeCePd_1400_i catalytic membrane reactor reduced the chromate efficiently in the two types of water at pH 3 and room temperature, as observed in figure 3.7. Similarly to Pd_i CMR, the results also show that the activity of the CMR is slightly higher when the Cr (VI) reduction occurs in mineral water. Further investigation is required in order to give a plausible explanation for the observed behavior.

Contrary to the results obtained with Pd_i CMR, the decrease in Cr (VI) concentration is linear with time over the entire range of the test (see also the reported regression coefficients). The linear trend of chromate reduction is also an indication that the reaction is most likely to be of a zero order in respect to the chromate.

For the full duration of the experiment, the rate of Cr (VI) reduction can be roughly estimated to 1 ppm Cr (VI)/h. Compared to the CMR of Pd_1400_i, it is somewhat lower, but it should be kept in consideration that the Pd content in the FeCePd_1400_i CMR is three times lower compared to Pd_1400_i CMR.

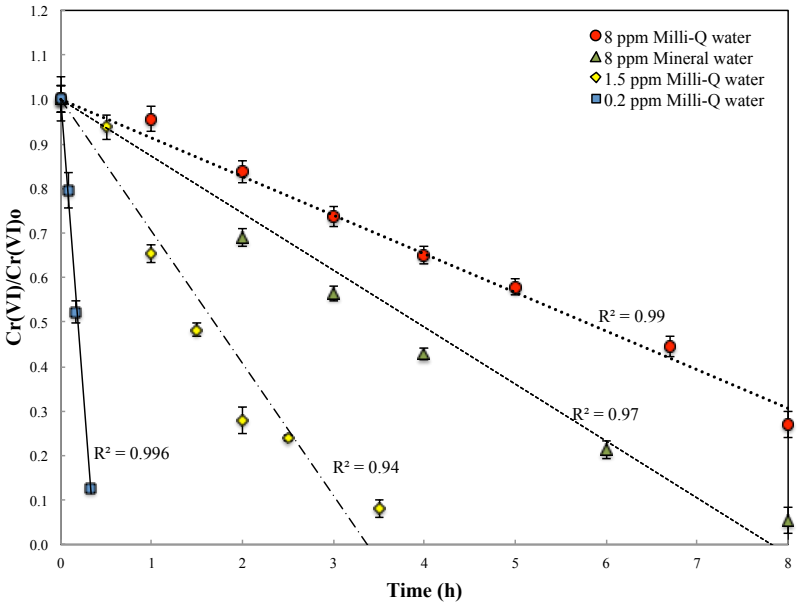

Figure 3.7: Cr (VI) reduction in Milli-Q or mineral water with CMR FeCePd_1400_i at pH 3 and 10 sccm/min of H_2 supply at room temperature.

For the case of the CMR of FeCePd_1400_i an additional test was performed using 0.2 and 1.5 ppm as initial concentrations of Cr (VI). As observed in figure 3.7 it was confirmed that at lower concentrations the reaction rate decreases, e.g. 0.7 ppm/h vs 0.5 and 0.4 ppm/h of Cr (VI) reduction for high and low concentrations, respectively.

Taking into account the prolonged linear trend of Cr (VI) reduction as well as the higher activity of FeCePd_1400_i compared to Pd_1400_i CMR, it can be speculated that the Ce (III)/Ce (IV) pair participates in the chromate reduction; however, it is too premature at this stage to draw definitive conclusions.

Table 3.1 summarizes the experimental conditions and the results obtained in the different tests of the catalytic membrane reactor with one or two catalytic phases.

Table 3.1: Experimental conditions and results obtained with the different CMRs in the Cr (VI) reduction tests.

CMR	M_1400		Pd_1400_i		FeCe_1400_i		FeCePd_1400_i					
Cr(VI), mg L^{-1}	8.0	8.0	8.0	8.0	8.0	8.0	5.4	5.4	0.2	1.5	8.0	8.0
pH	3	3	3	3	3	3	3	7	3	3	3	3
H_2 flow, cm^3/min	10	10	10	10	10	10	10	10	10	10	10	10
Type of water*	MQ	M	MQ	M	MQ	M	MQ	MQ	MQ	MQ	MQ	M
Cr(VI) reduction, mg/Lh first 4h	0.0	0.0	1.4	1.6	0.0	0.0	0.7	0.0	0.4	0.5	0.7	1.1
Cr(VI) reduction, mg/h·g of Pd	-	-	9.2	10.4	-	-	15.2	0.0	8.6	10.9	15.2	23.9
Cr(VI) reduction, mg/h.m^2 of membrane	0.0	0.0	109	115	0.0	0.0	53	0.0	30	38	53	84

*MQ Milli-Q water, MW mineral water

The catalytic membrane reactors without palladium did not possess any activity for Cr (VI) reduction as shown in table 3.1. It is also important to mention that at neutral pH no chromate reduction occurred. The results indicate that the process is faster in mineral water than in model solutions. At this stage, it is rather difficult to give a plausible explanation for this finding. Therefore, more tests are planned in order to investigate the effects of other anions presented in the water, paying special attention to sulfates, phosphates, and nitrates. In order to compare the performance of different CMRs for chromium reduction the rates are calculated for the first 4h of the reaction assuming linear trends for all cases. As mentioned before, for CMR_ FeCePd_i containing cerium and iron oxides, the trend of Cr (VI) was linear for the entire period of the experiments in all tests.

In respect to the activity as a function of the amount of palladium contained by catalytic membrane reactors (see the penultimate raw in

table 3.1), it appears that CMR_FeCePd_i is two times more active than CMR_pd_i. It can be suggested that this is due to the Ce^{3+}/Ce^{4+} contribution to the reaction by increasing the number of active sites involved in the reaction. Full characterization of the processes related to the catalytic reduction of Cr (VI) described here call for additional research to evaluate the effects of parameters, such as the hydrogen flow rate and composition of the catalyst as a means of optimizing the performance of the reactors. As mentioned above, a new set of experiments is under consideration in order to address this issue.

The modular nature of the catalytic membrane reactors, easily, allow the proposed process to be scaled up. The data representing the capacity for Cr (VI) reduction expressed per one square meter of the catalytic membrane reactor is shown in the last row of the table. No loss of catalytic activity was registered in repetitive runs nor during the entire period the experiments were performed, i.e. for more than 4 months.

Additional experiments were performed in order to check whether full elimination of the chromium ions from the solution was possible at these relatively low concentrations.

The final solution after the Cr (VI) reduction was separated and its pH was adjusted to 8 by sodium hydroxide solution. At this pH the Cr^{3+} precipitates forming $Cr(OH)_3$. Thereafter, the solution was filtered using a standard laboratory 0.45 μm filter. After filtration the filter was washed with 5 % HCl solution and the liquid was kept. The content of chromium was measured in both solutions (the filtrate and the washing solution) using the ICP apparatus.

The measured concentration of chromium (unreduced Cr (VI)) in the filtrate confirmed the results obtained by the photometric method. The measured amount of chromium in the acidic solution is the same as the amount of Cr (VI) reduced during the reaction.

d. Cr (VI) reduction in Milli-Q water with CMR with nominal pore size of 4 nm containing Pd loaded by impregnation.

The CMR Pd_i and CMR FeCe Pd_i were prepared starting from commercial membranes with a nominal pore size of 1400 nm. The incorporation of the

active phases to the membrane support does not significantly alter the final pore size of the prepared reactors. This issue was discussed with more details in the previous chapter. In the process of chromate reduction the dosing of hydrogen through the porous wall of the reactor is essential in order to accomplish the reaction. From the results obtained with the CMR Pd_1400_i and CMR FeCePd_1400_i it can be deduced that part of the hydrogen gas flowing through the porous membrane matrix is activated on the Pd surface. Thereafter, the activated hydrogen reacts with the chromate anions that were dissolved in the water.

The proposed mechanism is also supported by the results obtained in the experiments when the hydrogen is dosed by bubbling to the reaction vessel. In this case, no activity for Cr (VI) reduction was observed. It can be expected that the efficiency of the CMRs for the Cr (VI) reduction will be increased if membranes with a smaller pore size are used.

In the studied reaction, a CMR_4nm_Pd, that was prepared with a 4nm nominal pore size membrane, was used. The amount of Pd loaded onto the membrane by impregnation in the CMR Pd_4_i was similar to the one loaded into the CMR Pd_1400_i, 0.75 and 0.9 w/w %, respectively. Figure 3.8 presents the results obtained for the CMR_4nm_Pd_i used for the reduction of Cr (VI) in Milli-Q water. The initial Cr (VI) concentration was 8 ppm and the reaction conditions were similar to the ones used in the experiments with the other CMRs.

Similar to the case of CMR_1400_Pd_i the Cr (VI) reduction follows first order kinetics in respect to the chromate concentration. On the other hand, the expected improvement in the activity of this CMR in respect to the CMR with a 1400 nm nominal pore size was not observed.

The calculated rate of Cr(VI) reduction for the first 4h was 1.4 ppm/h, that is, the value obtained with CMR_1400nm_Pd_i in similar experimental conditions. For the case of CMR_4nm_Pd_i, the amount of Pd, 0.75%, is lower than for the CMR_1400nm_Pd_i, 0.9%. Taking this difference into account, it seems that the CMR with a lower nominal pore size is more active. However, considering the differences between the pore sizes of both reactors the obtained activity is lower than the expected one. This result can be attributed to the lack in uniformity of the pore size distribution of the starting membrane. Another possibility is that the chromate reduction at this concentration and experimental conditions is kinetically limited. More experiments are planned in order to achieve a better understanding of the processes involved.

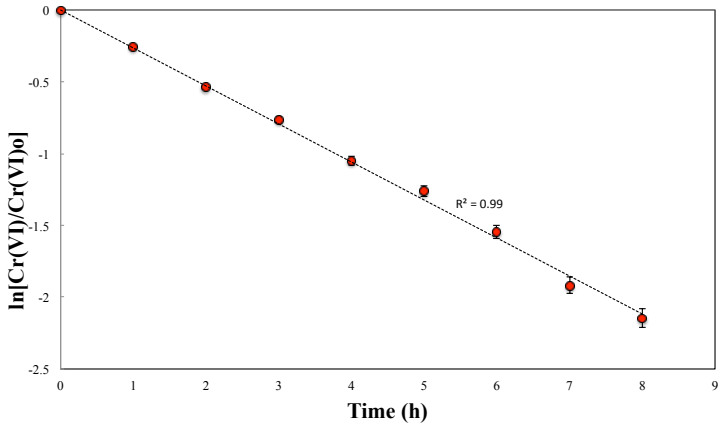

Figure 3.8: Cr (VI) reduction in Milli_Q water with CMR Pd_4_i at pH 3 and 10 sccm/min of H2 supply, 8 ppm Cr (VI) at room temperature.

3.1.4. Conclusions

The present work demonstrates an efficient method for Cr (VI) reduction in the concentration range between 0.2 to 8 ppm using specially prepared catalytic membrane reactors in aqueous medium. The presence of palladium by impregnation as an active phase in the CMRs is required for the reaction to take place. Also, the water solution must be acidified to a pH of 3.

Surprisingly the CMRs containing Pd loaded as a metal by sputtering or from solutions containing reduced metal nanoparticles presented very poor activities as well as very fast deactivation in the studied reaction.

The addition of cerium oxide to the membrane reactors enhanced the activity in the Cr (VI) reduction indicating that the Ce^{3+}/Ce^{4+} pair may be involved in chromate reduction. The membrane reactor prepared from membranes with lower nominal pore sizes did not demonstrate to be more active than the CMR with larger pore sizes in the Cr (VI) reduction.

The proposed reaction system using CMRs can also be used, very efficiently, to reduce chromate present at low concentrations in the model and real water sources using only hydrogen as a reagent. Remarkably, the proposed CMRs did not present any loss of catalytic activity in repetitive runs. By a final pH adjustment to 8, the chromium can be eliminated completely from the contaminated aqueous source after filtration. Due to the modular character of the starting commercial ceramic membranes used in the present study, the process is easily scalable. From a practical point of view the obtained results are promising and encourage further work in this direction.

3.2. Application of the prepared CMRs in the treatment of wastewaters polluted with organic contaminants.

3.2.1. Introduction

Phenol is a colorless or white crystalline solid with a potent antiseptic odor. It exists in ecosystems with a natural or anthropogenic origin [48]. Phenol is highly irritating after short-term inhalation or dermal intake, and it is quite toxic when taken orally [49].

Phenol is a compound widely studied as an environmental pollutant as well as a reagent for industries. As far as are environment is concerned, phenol is found in some raw sources and wastewater; the last one is its major source; it comes principally from industrial effluents and landfills [46]. Due to its toxicity, it is mandatory, to eliminate phenol from the water.

In this aspect, the advanced oxidation processes (AOP) are one of the most effective methods for removing organic pollutants such as phenol from wastewater [50]. Advanced oxidation processes (AOPs) are considered a highly competitive water treatment technology for organic pollutants not treatable by conventional techniques [51]. Advanced oxidation processes include O_3, O_3/H_2O_2, UV, UV/O_3, UV/H_2O_2, $O_3/UV/H_2O_2$, Fe^{2+}/H_2O_2, and photo catalysis. AOP are characterized by the ability to exploit the high reactivity of $OH^{\cdot}$ radicals in driving oxidation processes which are suitable for achieving the complete abatement and through mineralization of even less hazardous pollutants [52].

Different AOPs to eliminate pollutants from water have been developed using phenol as a model contaminant compound, such as electro-catalytic oxidation of phenol [53–57], photocatalytic degradation of phenol [58–66] and photo sonochemical degradation of phenol [63].

Among the different types of advanced chemical oxidation processes, the H_20_2/Fe^{2+} systems named Fenton systems, are effective in decomposing organic pollutants [67]. The radical species involved in the oxidative

degradation of contaminants in Fenton are the hydroxyl radicals ($OH^{\cdot}$), peroxyl radicals ($ROO^{\cdot}$), the hydroperoxyl radicals ($HO_2^{\cdot}$) and its conjugated base, the superoxide anion (O_2^{-}) [68]. Principally, the hydroxyl radicals are generated in an acidic solution by the catalytic decomposition of hydrogen peroxide [69].

The mechanism of phenol oxidation comprises different consecutive steps. It is generally accepted that catechol is the primary oxidation product, indicating that hydroxylation takes place predominantly in the ortho position. The concentration of the other oxidation products, such as hydroquinone (para-hydroxylation), resorcinol (meta-hydroxylation), and p-benzoquinone are less predominant than catechol. The ring opening of the aromatic intermediates lead to the formation of organic acids such as muconic acid, maleic acid, formic acid and malonic acid. As a result, a decrease in the pH takes place. In fact, all of the intermediates are finally oxidized to formic acid and oxalic acid. Formic acid is also oxidized to CO_2 and H_2O, whereas oxalic acid shows quite refractory behavior and may remain in solution [58].

One way to generate hydrogen peroxide in situ and consequently use it in AOPs is the direct synthesis of H_2O_2 from hydrogen and oxygen in the presence of a catalyst [70]. Two main problems have to be taken into account:

1) H_2/O_2 mixtures are explosive over a very wide range of hydrogen concentrations (4-75 mol % in air, 4-94 mol % in oxygen at 1 atm pressure; and 2) the low selectivity toward hydrogen peroxide by the fact that materials catalyzing its formation generally are also active for its decomposition as well as the parallel formation of water [71].

In order to avoid these problems, the catalytic membrane reactors are an alternative since CMRs prevent the direct contact between O_2 and H_2 reagents [70]. Moreover, the contactor CMRs can improve the selectivity toward H_2O_2. Thus, in order to accomplish the entire Fenton process the catalytic membrane reactors must be able to promote both steps, that is,

the generation of H_2O_2 and formation of $OH^{\cdot}$ radicals.

The ability of palladium to promote the generation of hydrogen peroxide is well known[72]. In fact, in many studies the Pd has successfully been used to obtain H_2O_2 directly from hydrogen and oxygen [15,71,73–81]. Different reaction mechanisms for the hydrogen peroxide generation can be found in open scientific literature. In this work, we considered that the most probable reaction pathway is as described below. The hydrogen gas passes through the porous membrane structure and it is activated on the palladium surface. Thus, the activated hydrogen reacts with the dissolved oxygen in the aqueous phase. The reaction occurs on the three phase contact point comprised between the solid catalyst, the gas phase hydrogen and the liquid phase containing the dissolved oxygen. In this sense, the reaction can be considered as a hydrogenation of the oxygen. Moreover, following this reaction mechanism it can be speculated that the activated hydrogen may also hydrogenate any other species that are present in its vicinity, such as phenol. In fact, palladium is well known as a catalyst for hydrogenation of phenol to obtain cyclohexanone. Until now, limited amount of work has been reported on the hydrogenation of phenol in mild conditions [82–85], typically involving processes at high temperature and pressure [86–90]. Moreover, the catalysts specially designed for this reaction have several disadvantages, such as long and complicated synthesis procedures [91–104].

Another potentially interesting catalytic phase is the cerium oxide. It can store and release oxygen, enhance the oxygen mobility, form surface and bulk vacancies, and also improve the catalyst redox properties of the composite oxides [105]. Therefore, it can be expected that the near contact between the Pd clusters where the hydrogen is activated and the ceria phase will enhance the hydrogen peroxide production.

Iron (II) is well known for promoting the generation of $OH^{\cdot}$ from the hydrogen peroxide. One disadvantage when a homogeneous catalysis is used, is that the iron salt cannot be retained in the process, thus requiring further separation to prevent additional water pollution [106].

A way to overcome this problem is to immobilize the iron e.g. iron oxide, on a solid support as a strategy to avoid sludge formation as well as to expand the effective pH range of the Fenton reaction [68].

The objective of this work is to evaluate the capability of the catalytic membrane reactor with a main catalytic phase of palladium in the treatment of wastewater polluted with organic matter. In order to demonstrate this a model solution of phenol or ibuprofen was used.

In the first part of this work, the results obtained with the different catalytic membrane reactors in the production of hydrogen peroxide are presented. The experiments were performed at ambient temperature and atmospheric pressure. The hydrogen peroxide was produced in Milli-Q water starting from hydrogen gas and air born oxygen. It has been demonstrated that the Pd is essential for the production of H_2O_2. It has also been shown that the activity for hydrogen peroxide production depends on the method used for Pd loading onto the initial membrane. The membrane reactors containing Pd deposited by sputtering or deposited from Pd nanoparticles suspended in a solvent lost their activities very fast.

In order to reactivate those CMR complexes regeneration consisting of calcination and reduction have to be performed. On the other hand, the CMRs containing Pd loaded by impregnation demonstrated very stable behavior and no loss of activities in repetitive tests.

In the second part of the present chapter possibilities are explored for the proposed CMRs to promote different reactions depending on simple experimental parameters that can easily be controlled. The experiments were performed using a 100 ppm synthetic solution of phenol. It has been demonstrated that depending on the availability of dissolved oxygen the phenol can be oxidized following the Fenton like process and in contrast, in absence of oxygen, it can be hydrogenated to cyclohexanone and cyclohexanol. This new feature of the CMRs was used for treatment of 30 ppm of ibuprofen water solution prepared with Milli-Q water.

3.2.2 Methods and Materials

a. Synthetic solutions of phenol or ibuprofen in water

A 100 ppm synthetic water solution of phenol was prepared using Milli-Q water and phenol, Riser s.a (98.5 %).

A 1000 ppm synthetic water solution of ibuprofen (IBP) was prepared as a mother solution with milli-Q water and ibuprofen sodium salt (98 %, Sigma Aldrich). Then, 100 mL of 30 ppm of IBP water solution was prepared with Milli-Q water. For some tests, the pH of the solution was adjusted to 4 with hydrochloric acid (Sigma Aldrich).

b. Catalytic membrane reactors (CMRs)

Seven different CMRs were used to test the phenol abatement in aqueous media. The active phase compositions and the nominal pore size of the CMRs were:

- Pd_1400_i: 0.9 w/w % of Pd.
- Pd_4_i: 0.75 w/w % of Pd.
- FeCePd_200_i: 1.2 w/w % of Pd, 1.5 w/w % of Fe_2O_3 and 1.3 w/w % of CeO_2.
- FeCePd_200_s: 0.02 % Pd and 1.8 % of Fe_2O_3 and 1.8 w/w % of CeO_2.
- FeCePd_200_m: 0.1 % Pd, 2.2 % of Fe_2O_3 and 2.2 w/w % of CeO_2.
- FeCePdCu: 0.5 % PdCu (3/1), 2.2 % of Fe_2O_3 and 2.2 w/w % of CeO_2.

More information about the CMRs preparation and characteristics can be found in chapter II.

c. Experimental setup

c.1. Test of generation of hydrogen peroxide

First, the activities of the CMRs were tested in the generation of H_2O_2. All CMRs were tested for in situ production of H_2O_2 in water in semi-batch mode. Each CMR was introduced in a vessel containing 100 mL Milli-Q water. Hydrogen flow of 6 sccm/min was supplied to one end of the CMR whilst the other end was kept closed. In this way, the hydrogen is passed across the membrane wall reaching the external surface. Air was bubbled into the water as an oxygen source in the reactor vessel.

c.2. Test of treatment of 100 ppm of phenol in aqueous solution

The catalytic membrane reactors were tested in 100 ppm of phenol water solution in semi-batch mode. The hydrogen flow was adjusted using a mass flow controller and supplied to one end of the reactor whilst the other end was kept closed. The hydrogen supply was 6 sccm/min. The hydrogen crosses the membrane wall reaching the external surface. The CMR was submerged into a glass reactor containing 100 mL of the phenol water solution. All the tests were performed at 60 ^{o}C for 7 h at atmospheric pressure. Thereafter, the experiments were divided into four groups: a) air supply; b) pure oxygen supply, c) argon supply and d) no external gas supply to the reaction vessel containing the model solution. When an external gas was supplied, in order to saturate the solution, this gas was bubbled into the vessel 10 minutes before introducing the membrane with hydrogen.

In order to determine the elimination of the organic substances by stripping, individual tests for phenol, cyclohexanol and cyclohexanone were done. The stripping test for phenol was done in the same condition as the oxidation tests with air using a hollow fiber membrane without a catalytic phase. The stripping tests for cyclohexanol and cyclohexanone were done with a hollow fiber membrane with the same conditions as that of the hydrogenation tests but using argon as a sweep gas.

c.3. Test of hydrogenation of 30 ppm of ibuprofen in aqueous solution

Ibuprofen hydrogenation was performed in semi-batch mode of operation. The hydrogen flow was adjusted using a mass flow controller and supplied to one end of the reactor whilst the other end was kept closed. The hydrogen supply was 30 sccm/min in all tests. The hydrogen crossed the membrane wall reaching the water on the external surface. The CMR was submerged into a glass reactor containing 100 mL of the 30 ppm of ibuprofen water solution. The tests were performed at 60 °C or at room temperature for 7 h. Initial tests were done at neutral pH. In a second series of experiments the pH of the solutions were adjusted to 4, a value lower than the pKa of IBP. Test bubbling oxygen into the vessel was also performed. A blank test using a hollow fiber of 4 nm membrane reactors without catalytic phases was performed at room temperature and pH 4.

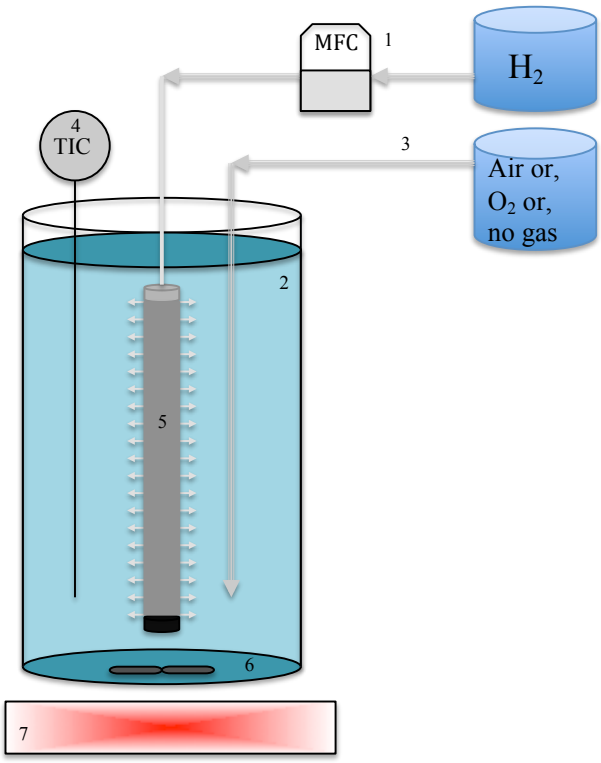

Figure 3.9: Experimental setup used in the phenol, IBP abatement tests. 1) Mass flow controller; 2) 100 ppm of phenol aqueous solution or 30 ppm of IBP water solution (pH 4); 3) air, or O_2 source; 4) Temperature controller; 5) CMR 6, and 7) heating and stirrer plate.

d. Analytical techniques and methods.

d.1.High performance liquid Chromatography (HPLC)

High performance liquid chromatography, HPLC Shimadzu, equipped with LC 20AB system and with a diode array detector SPD-M10Avp, was used to measure the concentrations of hydrogen peroxide, phenol and ibuprofen.

Hydrogen peroxide was analyzed at a wavelength of 193 nm after direct injection of the sample without a column. The mobile phase was Milli-Q water.

A column C-18 (Omnisphere, Varian) was used to separate the reaction intermediate products from the phenol or the ibuprofen, ID. 4.6 mm, length 250 mm.

The concentrations of phenol or ibuprofen during the tests were measured every hour. The analysis of the phenol was made at a wavelength 254 nm. The mobile phase of 1 mL/min was a mixture of 60 % water at pH 3 adjusted with acetic acid and 40 % of acetonitrile (Aldrich).

The ibuprofen was detected at 230 nm. The mobile phase of 1 mL/min was a mixture of 60 % acetonitrile (sigma Aldrich) and 40 % of Milli-Q water. 10 mMol of acetic acid was added in each liter of the mobile phase.

Additionally, in some cases, the final samples from the ibuprofen tests after previous derivatization with trimethylsilyl ether were analyzed by HPLC-QTOF.

d.2.Total organic carbon (TOC)

The total organic carbon was measured with TOC-L Shimadzu CSN equipment. Only the initial and the final samples were assessed.

d.3.Gas chromatography (GC)

Hydrogenation products of phenol were assessed in the end of each experiment using the gas chromatograph Shimatzu GC-2010 with ZEBRON ZB-WAX column and FID detector.

The hydrogenated products were extracted from the aqueous solutions, previously saturated with NaCl, with ethyl acetate (Sigma). The analyses GC conditions were: 115 kPa head column pressure, helium flow 144 mL/min, split ratio 15, injector and detector temperature 250 ^{o}C. The temperature ramp was from 60 ^{o}C to 180 ^{o}C and hold for 5 min.

The obtained values were corrected by a relative response factor [107]. A calibration curve was prepared for cyclohexanone (Fluka), for cyclohexanol (Sigma Aldrich) and for 2-cyclohexen-1-one (Aldrich).

d.4.Dissolved oxygen measurements.

In the reaction vessel the dissolved oxygen was measured in each experiment using a dissolved oxygen meter SG6 (MettlerToledo).

3.2.3 Results and Discussion

a. Hydrogen peroxide generation

Initially the activities of the CMRs were tested in the generation of H_2O_2. The measured initial velocities of hydrogen peroxide generation with the different catalytic membrane reactors can be seen in Table 3.2.

Except for the blank membrane reactors in all cases hydrogen peroxide was generated. The results confirmed that the Pd is essential for the production of hydrogen peroxide. In this process, the hydrogen is activated on the palladium surface and then reacts with the dissolved oxygen forming hydrogen peroxide or water. Indeed, the reaction may be considered as oxygen hydrogenation.

Table 3.2: Hydrogen peroxide generation at room conditions with the different CMRs.

CMR	Trans-membrane pressure (barg)	Max H_2O_2 ppm	% Efficiency mol H_2O_2 / mol H_2	mol H_2O_2 / h.mol Pd*	mol H_2O_2 / h.m^2 membrane
FeCePd_200_i	2.3	57	34	85	9.7
FeCePd_200_s	1.8	7	0.5	3.24	0.08
FeCePd_200_m	1.7	11	0.2	4.79	0.05
FeCePdCu_200_p	2.4	15	0.56	6.26	0.13
Pd_1400_i	2.3	11	0.45	0.57	0.06
Pd_4_i	3.7	7	0.22	0.34	0.03
M_1400	0.6	0	0	0	0
M_4	3.4	0	0	0	0

* Initial hydrogen peroxide generation rates measured in the first ten minutes of the tests.

The CMRs FeCePd_200_s, FeCePd_200_m and FeCePdCu_200_p reached the maximum concentration of H_2O_2 after twenty minutes. For the case of CMR FeCePd_200_i, the maximum concentration of peroxide was reached approximately in one hour. Then, in all cases, no more hydrogen peroxide was produced. A possible reason to explain this apparent inactivity can be attributed to palladium deactivation caused by the H_2O_2 produced [15]. For the CMRs containing cerium and iron oxide more hydrogen peroxide is produced. Cerium oxide is well-known as an oxygen storage material. So, it is possible that ceria participates in the process as an oxygen donor.

It is important to remark other important differences that were found comparing the long term activities of CMRs with Pd loaded by impregnation and the ones with Pd loaded as metal. In the cases of CMRs with impregnated Pd, once a maximum H_2O_2 was reached, an apparent inactivity was observed. The reactors were activated only by passing hydrogen through them (taking out the reactor from the vessel without stopping the hydrogen flow). In contrary, this simple procedure was not effective for reactivation of the CMRs with Pd deposited as metal and these reactors were not active in subsequent tests. A possible drawback in the process is the peroxide decomposition caused by the palladium. In order to check this, once a maximum in the peroxide concentration was

reached the hydrogen supply was stopped and the H_2O_2 concentration was monitored. No variation in the peroxide concentration was measured for at least 20 min.

It is reasonable to expect that if the hydrogen peroxide is produced in waters contaminated with organic matter it will be directly involved in subsequent oxidative reactions especially if peroxide radicals are formed.

In the following a description is provided for the results obtained with the CMRs in the treatment of phenol contaminated model solutions. The results are classified as follow:

Section b.1 describes the results obtained with the CMRs with palladium deposited on the membrane as metal e.g. by sputtering and Pd nanoparticles. Section b.2 describes the results with the CMRs containing palladium loaded by impregnation.

b.1. Oxidation of phenol in water solution with CMRs containing palladium as the active phase loaded as metal e.g. by sputtering or from Pd or PdCu nanoparticle suspensions.

The incorporation of cerium and iron oxides to the CMRs prior to the palladium loading will potentially optimize the AOP. Cerium oxide is capable of improving the oxygen mobility enhancing the oxygen availability close to the active sites; thus, the formation of the hydrogen peroxide.

On the other hand, the iron oxide promotes the hydroxyl radical formation from the hydrogen peroxide. The oxidation potential of these radicals is very high and they are the principal species that oxidize the organic compounds.

The CMRs FeCePd_s, FeCePd_m and FeCePdCu_p presented very low activities in the elimination of phenol. For all of them, in the first hour of the test, a small decrease of the phenol concentration in the reaction vessel e.g. about 3 ppm was observed. For the next 6-7 h, no changes of

the phenol concentration was observed (the tests were carried out for 7-8 h). As commented in the previous section, once deactivated, the reactivation of those CMRs were not possible following simple procedures as used in the case of CMRs with impregnated in which the passing of hydrogen through the membrane results in complete recovers of the reactors activity. Some possible reasons for the fast deactivations of those catalytic membrane reactors are presented in the last chapter of this work.

b.2. Treatment of phenol solution with catalytic membrane reactors containing palladium loaded by impregnation.

The CMRs prepared with a ceramic hollow fiber membrane and Pd as the active phase are able to catalyze different reactions in one set-up, depending on the operational conditions. The CMRs proved to be effective in the production of hydrogen peroxide under very mild conditions starting from hydrogen and airborne oxygen. In the studied conditions, H_2 can hydrogenate the dissolved oxygen leading to the production of H_2O_2. The newly formed peroxide becomes a source of hydroxyl radicals which are capable of oxidizing species with lower redox potentials, e.g. organic pollutants [16]. However, in the absence of dissolved oxygen, the activated hydrogen may reduce the species present in the medium.

In our proposed assembly (figure 3.9), as mentioned above (section c.2), the hollow fiber CMR is closed at one end, while the gas, in this case hydrogen is introduced through the other end. Thereafter, the CMR is submerged into the reaction vessel containing the aqueous solution. The hydrogen gas is passed through the pores of the membrane and is activated on the surface of the impregnated Pd, making it susceptible to reactions with the species dissolved in the reaction medium. The CMRs can hydrogenate the organic matter in mild conditions. There is currently little understanding about how to produce cheap and stable systems possessing different catalytic properties depending on the conditions used.

Herein, we report for the first time a CMR able of catalyzing different reaction pathways. The dominant reaction route depends on parameters

that can easily be modified and controlled. To demonstrate our findings, we have studied the well-known reaction of phenol elimination from an aqueous solution.

Depending on the reaction conditions, phenol can either be oxidized or hydrogenated to the corresponding cyclohexanone and cyclohexanol under atmospheric pressure and 60 °C (figure 3.10).

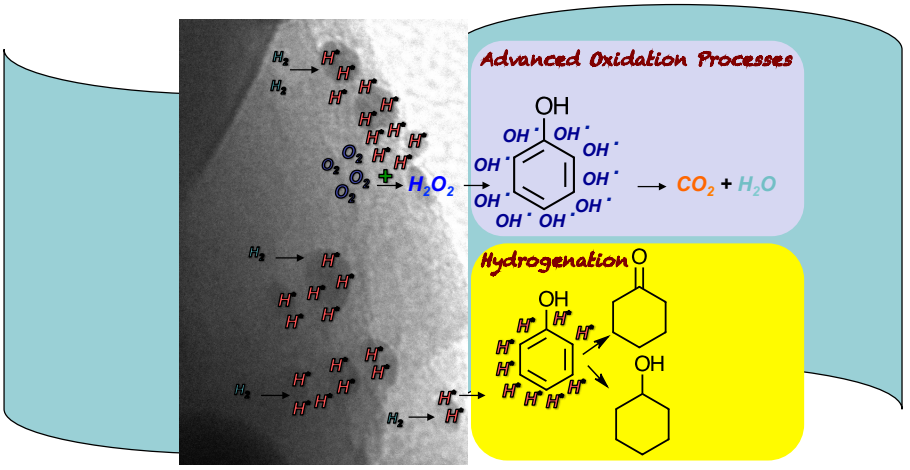

Figure 3.10: Reaction pathways in the phenol abatement in water solution at 60 °C and atmospheric pressure, CMRs with palladium obtained by impregnation, hydrogen flow of 6 sccm/min.

In order to prove our hypothesis, the experiments were divided into three groups. The experiments were done with CMR Pd_1400_i and CMR Pd_4_i. The first set of experiments was focused on a Fenton-like oxidation process, by bubbling pure oxygen into the reaction vessel. Under these conditions the amount of oxygen dissolved in solution was found to be 23.6 ppm (Table 3.3), leading to a phenol conversion of 39 % and a mineralization of 68 %.

In figure 3.11 the results for the phenol oxidation are shown. The kinetics of the reaction follows a zero order with respect to the phenol concentration when CMR Pd_1400_i or CMR_4_i was used.

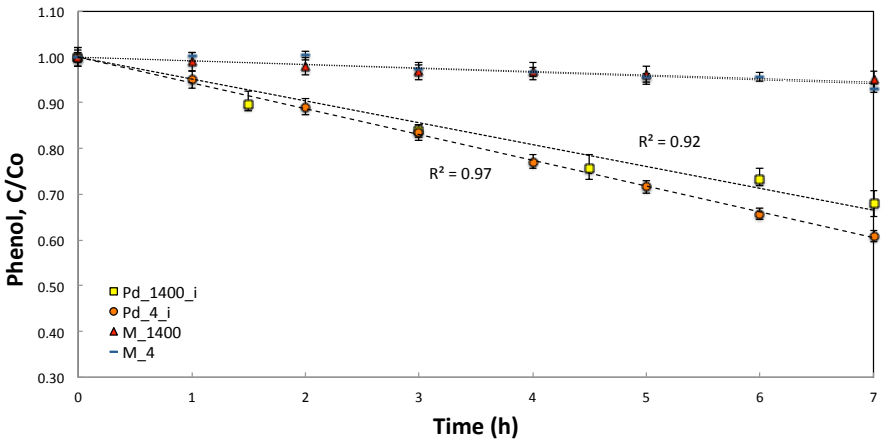

Figure 3.11: Results of the oxidation test with 100 ppm of phenol water solution at 60 °C, hydrogen flow of 6 sccm/min and pure oxygen bubbled to the solution.

In Figure 3.12 a typical chromatogram obtained with HPLC-DAD apparatus is shown. The chromatograms show the typical oxidation products, such as hydroquinone, resorcinol, catechol, and p-benzoquinone. No hydrogenation products were found, see table 3.3.

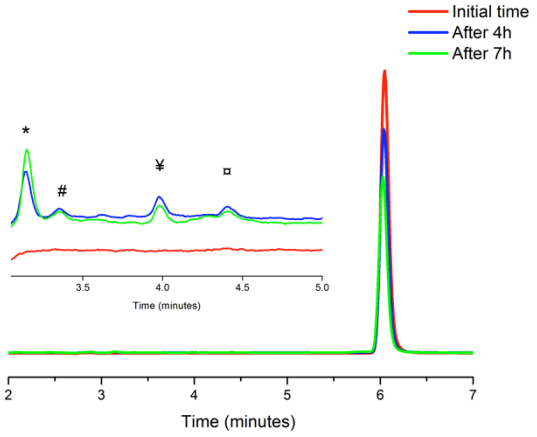

Figure 3.12: HPLC-DAD chromatograms of oxidation of phenol using oxygen. Inset graph is zoom in on the region where oxidation product appear: * - hydroquinone; # - Resorcinol; ¥ - Catechol; ¤ - p-benzoquinone.

When oxygen was exchanged by air, the HPLC results were not consistent with the TOC results, suggesting that some of the products obtained do not absorb in UV (Table 3.3). Remarkably, besides the mineralization of phenol,

cyclohexanone and cyclohexanol were detected in the reaction mixtures (table 3.3, figures 3.13 and 3.14). This contradicts previous results which state that phenol hydrogenation in these conditions is improbable to happen [16].

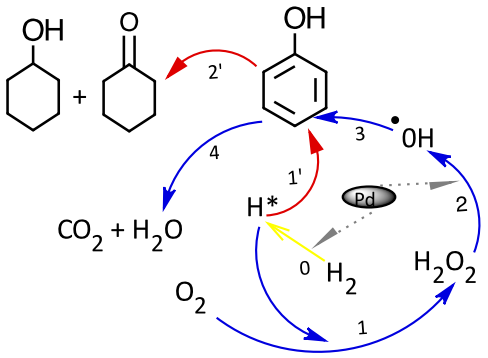

Figure 3.13: Reaction pathways in the phenol abatement in water solution at 60 °C and atmospheric pressure, CMRs with palladium obtained impregnation, hydrogen flow of 6 sccm/min and air as oxygen source.

In Figure 3.14 the typical chromatograms obtained with HPLC-DAD apparatus are shown. Oxidation products, such as hydroquinone, resorcinol, catechol, and p-benzoquinone are in very low amounts.

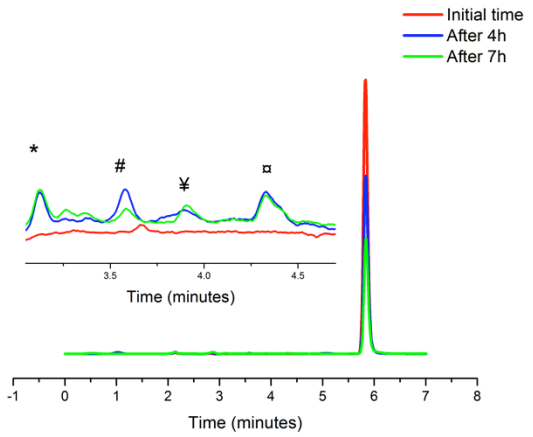

Figure 3.14: HPLC-DAD chromatograms of oxidation of phenol using air. Inset graph is zoom in on the region where oxidation product appear: * - hydroquinone; # - Resorcinol; ¥ - Catechol; ¤ - p-benzoquinone.

To prove the above results, a new experiment was done without bubbling any gas into the reaction mixture. In this case no mineralization (see fig. 3.15) was observed, only the hydrogenation products were detected (Table 3.3), demonstrating that in the absence of dissolved oxygen only the hydrogenation reaction takes place. It must be emphasized that the reaction is carried out at ambient pressure without any previous activation of the catalytic membrane reactor.

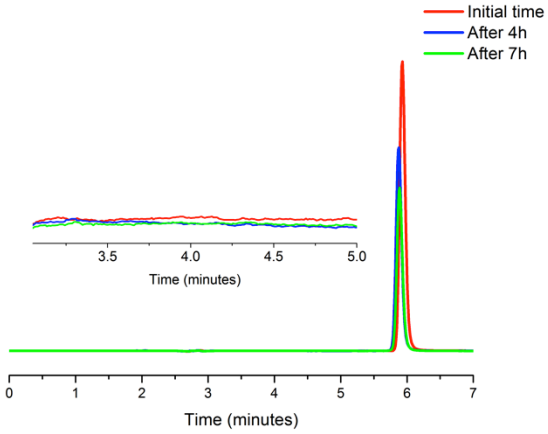

Figure 3.15: HPLC-DAD chromatograms of oxidation of phenol using no external gas. Inset graph is zoom in on the region where oxidation product appear – nothing is detected, even though the concentration of phenol decreases.

Figure 3.16 shows the results for the hydrogenation of phenol. The reaction follows zero order kinetics in respect to the phenol concentration.

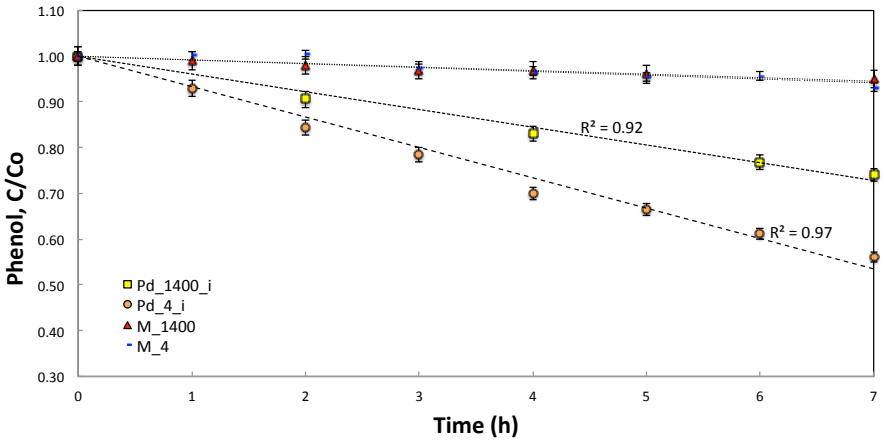

Figure 3.16: Results of the hydrogenation of 100 ppm of phenol water solution with CMR of Pd_4_i or Pd_1400_i at 60 ºC.

In table 3.3, a summary of the results obtained with CMR Pd_1400_i and CMR_4_i are shown. In the case of Pd_1400_i, the starting membrane has a much larger nominal pore size, 1400 nm vs 4 nm. The results are very similar in terms of selectivity, but the conversion obtained with the membrane reactor with a higher pore size is significantly lower. These results are not surprising taking into account that in the case of the reactor with a lower pore size, the number of pores are much higher than for the reactor with larger pores. In this context, the number of actives sites are higher for the Pd_4_i membrane reactor.

Table 3.3. Phenol conversion and different reaction pathways depending on the reaction conditions. 60 ^{o}C and 6 sccm/min of hydrogen supply in all tests, data after 7h.

CMR[a]	Gas[b]	Trans-membrane Pressure[c] (barg)	OD[d] (ppm)	% Conversion[e]	% Selectivity		
					Mineralization[f]	Cyclohexanone[g]	Cyclohexanol[g]
Pd_1400_i	O_2	0.2	23.6	32	59	00	00
Pd_4_i		4.2		39	68	00	00
Pd_1400_i	Air	0.3	5.56	34	43	12	06
Pd_4_i		7.8		53	67	09	05
Pd_1400_i	-	0.2	0.34	26	00	-	-
Pd_4_i		5.2		44	00	52	22

Typical reaction conditions: 100 ppm aqueous phenol solution, 6 sccm/min H_2, 60 ^{o}C, 7h; a CMR b gas bubbled in the reaction vessel; c transmembrane pressure in barg d directly measured with O_2 electrode; e conversion computed from HPLC-DAD; f determined from TOC analysis; g determined from GC after ethyl acetate extraction. The same set of experiments was done at room temperature, but no activity was observed in either of the cases.

The same sets of experiments were done at room temperature, but no activity was observed in either of the cases.

Furthermore, the same experiments were performed with the CMR FeCePd_1400_i (0.3 % of Pd, 1.5 % of Fe_2O_3 and 1.5 % CeO_2). In this case, the rate of phenol oxidation was 10 ppm/h regardless of the source of oxygen used (pure oxygen or air). These results confirm our previous findings that the addition of CeO_2 and Fe_2O_3 as active phases enhance the capacity of the CMR to perform the Fenton like oxidation process.

As expected from our previous studies in absence of oxygen, no hydrogenation of the phenol was observed. Most probably due to the capacity of the Ce in the CeO_2 to undergo $Ce^{4+} \rightarrow Ce^{3+}$ reduction, the activated hydrogen is trapped such that the phenol hydrogenation is prevented. Further study is needed in order to gain a better understanding of the processes involved.

This newly discovered feature of the catalytic membrane reactor was employed in the treatment of water polluted with ibuprofen at different pHs taking into account the pKa of ibuprofen (5.2). The reaction was carried out first at a neutral pH and no change in its concentration was observed when air or oxygen was bubbled in the mixture or when no gas was used.

When a pH lower than the pKa was used, more than 90 % of the ibuprofen was converted and no other products were detected by HPLC-DAD. The products from the final solution were extracted with ethyl acetate and derivatization with trimethylsilyl ether was performed, the sample was analysed with HPLC-QTOF. The hydrogenated product was identified in HPLC-QTOF analysis in all of the cases (figure 3.17). Moreover, no oxidation product was observed during these reactions (figure 3.17 and table 3.4).

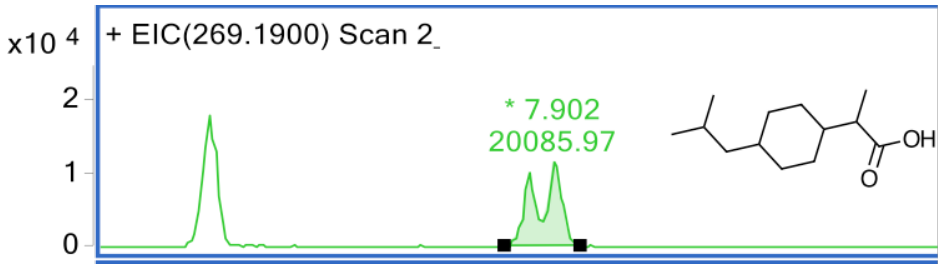

Figure 3.17: HPLC-QTOF chromatogram of the hydrogenation product of ibuprofen.

The test was performed using the CMR Pd_4_i and 30 ppm of ibuprofen water solution at room temperature or 60 ^{o}C and atmospheric pressure with 30 sccm/min of hydrogen flow. The results of the tests are shown in the figure 3.18 and table 3.4.

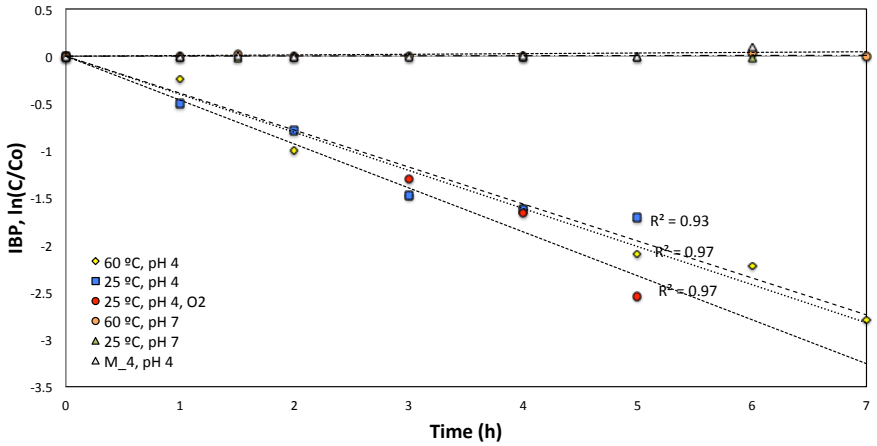

Figure 3.18: Ibuprofen hydrogenation at 60 °C or room temperature and 30 sccm/min of hydrogen supply in all tests, data after 7 h; 30 ppm IBP water solution.

The results presented in figure 3.18 shows that in all cases the hydrogenation reactions follow first order kinetics with respect to the IBP concentration. No appreciable differences in the reaction rates were observed in the studied temperature range.

In Table 3.4 the results of the IBP abatement in the different experiments are presented. The reaction can be carried out only at a pH lower than the pKa of the IBP. It is important to notice that between the tests no any activation of the CMR was performed.

Table 3.4: 30 ppm of IBP water solution; 60 °C or room temperature; 30 sccm/min of hydrogen supply in all tests.

Test	Trans membrane Pressure (barg)	Conversion
		IBP conversion by HPLC, %
H_2, pH 7, 60 ºC	3.8	0
H_2, pH 7, room temperature	4	0
H_2, pH 4, 60 ºC	3.8	72
H_2, pH 4, room temperature	4.2	100
H_2 and O_2, pH 4, room temperature*	3.2	100
Blank, pH 4, room temperature**	5.1	0

*In this experiment to the reaction vessel was bubbled oxygen

** In order to discard the ibuprofen adsorption on the corundum hollow fiber membrane, a test in the same conditions as the hydrogenation test was done using a 4 nm pore size membrane for 20 hours. No decrease of the IBP concentration was observed.

It was demonstrated that the proposed system, based on the CMR can be used in the elimination of ibuprofen. In the process, only the hydrogenation reaction takes place even when the reaction mixture is saturated with oxygen (figure 3.19).

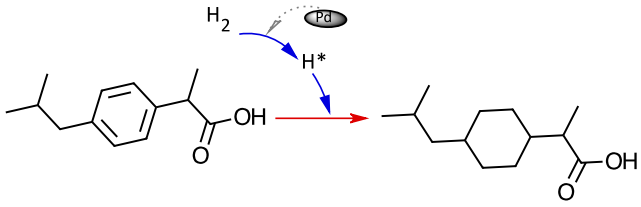

Figure 3.19: Proposal of the mechanisms of the ibuprofen hydrogenation at pH<5.2.

3.2.4 Conclusions

It has been demonstrated for the first time that a catalytic membrane reactor containing approximately 1 wt % Pd is able to catalyze different reaction pathways during the elimination of phenol present in an aqueous solution. When the reaction is carried out in the presence of air, the quantity of oxygen dissolved in solution is less than when pure oxygen is used. This decreases the oxidation reaction of phenol, but the hydrogenation reaction was observed. The same result was observed when no gas was introduced in the mixture. This new feature of the CMR was used for the treatment of water contaminated with ibuprofen. In all cases, the hydrogenation product was observed and no oxidation reaction occurred. This new property of the CMRs open a new route of developing and designing reactors that are able to catalyze multiple reactions just by employing different reaction conditions

CHAPTER IV

Palladium deactivation

4.4. Palladium deactivation

4.1 Background

The hydrogen-palladium system has been studied for nearly a century. However, in the scientific community there is no clear agreement with regards to how the hydrogen may affect the catalytic properties of the palladium.

Palladium is well-known for being able to dissociate molecular hydrogen and absorb hydrogen into the crystal matrix to form hydrides at low temperatures [108]. Among the metals, palladium is the only one that does not lose its ductility until large amounts of H_2 have been absorbed. In fact, the hydrogen has a high mobility within the lattice and diffuses rapidly through the metal. This process is highly specific to H_2 and D_2, palladium being virtually impervious to all other gases, a fact which is utilized in the separation of hydrogen from gas mixers [109].

In the hydrogen palladium system, the hydrogen is first chemisorbed at the surface of the metal but with increased pressure it enters the metal lattice and so-called α and β phase hydrides are formed [109]. The α-phase is the palladium rich phase, and the β is hydrogen rich phase [110]. Specifically, the α-phase is a solution phase that has lattice constants close to the palladium metal [111]. The ratio of hydrogen to palladium in both phases is generally non stoichiometric [112]. PdHx, x reflecting the stoichiometry, α-phase forms when 0 <= x <= 0.03. The structure is characterized by an increase of the lattice parameter of palladium metal from 3.891 to 3.894 Å, but it retains the FCC lattice of palladium atoms. When a mixture of α and β-phases is present in the range 0.03 <= x <= 0.58. For x >= 0.58, hydrogen randomly occupies the octahedral interstices in the lattice to form the β-phase. The structure is characterized by an increase of the lattice parameter of palladium metal from 3.891 to 4.025 Å [113]. Indeed, the hydrogen rich phase being closely associated with the combination Pd_2H, which is capable of taking more hydrogen into the solution [114].

The sudden rise and fall in the concentration may be associated with the appearance and disappearance of the β phase [114]. Even though, the basic lattice structure is not altered during chemisorption, the α phase causes only a slight expansion, whereas the β phase causes an expansion of up to 10 % in volume [109]. The reason for the atomic ratio for the β-phase of palladium hydride being so elusive is probably a result of the vacancies in the palladium lattice fill up, the lattice expands, creating more vacancies (Lacher, 1937) [111]. Accordingly with the theory, in both phases the hydrogen is disordered [115].

The phenomenon of the palladium–hydrogen system is of considerable interest due to the fact that in practical applications of metal hydrides, it represents a loss of efficiency [116]. Some methods to measure the hydrogen-palladium system have been developed, such as quantitative neutron radiography techniques [117]; x-ray absorption spectroscopy [108]; x-ray [110,114,118]; electrical resistance at high pressure [119]; measuring Pd resistivity [120]; electrical resistance [116,121,122]; Partial pressures [123]; X-ray diffraction (XRD) and gravimetric hydrogen [124].

The traditional theory claims that removing the hydrogen by heating at approximately 300 ^{o}C, in air, inert gas or in a vacuum, the original dimensions of a palladium specimen are almost completely restored [112]. However, it appears that the absorbed hydrogen atoms push the palladium atoms further apart, and in this state the palladium atoms take up positions that are slightly different from those occupied by the atoms in the normal face-centered lattice. A high temperature is needed to produce sufficient thermal agitation to cause the palladium atoms to return to their true positions of equilibrium [110]. Nevertheless, studies have demonstrated that it is not possible for palladium to recover its proprieties after β-hydride formation, at least, palladium may eventually be markedly altered when a large number of absorption cycles and violent expulsion of hydrogen palladium metal has transpired [112].

The hydrogen-palladium system is an extensively studied system and as a result it has long been recognized that the hysteresis of the absorption-

desorption isotherms is in apparent violation of the phase rule [125]. When hydrogen is dissolved in palladium, the α phase forms first; the β phase nucleates and grows. Furthermore, due to the large volume change that accompanies the α-to-β transition, plastic deformation of the α phase occurs as it is stretched beyond the elasticity limit. Hence, absorption is accompanied by the growth of the β phase under the compressive stress of the α phase, but desorption takes place from the β phase of the plastically deformed solid. Since this is not a thermodynamically reversible process, hysteresis results [125]. The distortion of the β phase lattice remained after the gas had been removed from the metal. It was concluded that the gas is not in its normal state when it leaves the metal [114]. A reversible pathway between the two phases may not exist [125].

In order to understand the factors involved in the hydride formation, the particle size effect was studied. Studies found that the formation of palladium hydrides is strongly dependent on the particle size [108,126].

The existence of a hysteresis provides evidence for a phase transition even in small Pd–H clusters. Structural studies of 6 nm clusters show a transition between two cubic phases. The 3.8 nm Pd–H clusters always show an icosahedral structure in the low and high concentration regime. For an intermediate size of 5 nm Pd–H clusters, the lattice structure changes during hydrogen absorption, from cubic to, most probably, icosahedral [127].

The phase transition from the solid solution (β phase) of Pd and hydrogen to the hydride (α phase) takes place with an accompanying apparent pressure hysteresis, and the miscible gap in the hydrogen pressure-composition isotherm is narrowed. Expansion at temperatures above 30 ^{o}C may show size dependence; for instance, the difference in the lattice expansion for the nanoparticles becomes smaller than that for the bulk with increasing temperature. With increasing temperature, the gap widths for the smaller nanoparticles became smaller [126].

There are striking similarities and notable differences between the properties of Pd nanoparticles with 2-3 nm diameters and that of bulk Pd.

For example, it was found that there is a significant increase in α max and a significant decrease in β min, relative to the values reported for the bulk, i.e., a shrinking of the miscibility gap [124].

There is a well-known gap between these two concentration ranges, called the miscibility gap. The existence of the miscibility gap is due to the structural transition between the two phases: an energy barrier associated with the incorporation of the hydrogen atoms onto the crystallographic sites and the resultant phase transformation. A study showed that there is a narrowing, but no closure of the miscibility gap in Pd-H nanoclusters when the cluster size is decreased. This narrowing is due to effects at both ends of the miscibility gap: i) the existence of the α phase at higher hydrogen concentrations, and ii) the existence of the β-phase at lower hydrogen concentrations as the cluster size decreases [128].

In conclusion, nanoparticles can reach different concentrations of hydrogen depending on their size [128]. Large particles provide more interstitial places for the formation of hydrides and subsequently lead to a more intense new anti-bonding state when compared to smaller particles, that is, less hydrogen per palladium atom can be absorbed in the smaller particles. Due to the higher surface to bulk ratio, the smaller particles showed more surface adsorbed hydrogen [108]. Moreover, the hydrogen-storage capacity of Pd decreases with decreasing crystalline size [126].

Furthermore, with respect to the size control, a way to avoid the β-phase formation is the addition of another metal in the palladium. For instance, alloying Pd with about 20 % Ag which provides the additional advantage of increasing the permeability of the Pd to hydrogen [109]. Alloying with platinum and iron leads to disaggregation down to the isolated primary particles that has a major effect on the catalytic activity. Alloying reduces the availability of hydrogen. So, it has a stronger impact on decreasing the β-phase hydride formation [129].

Other alloys tested were Pd-Cu and Pd-Ag. These alloys showed a lower lattice distortion [130]. Furthermore, the lattice variation with temperature

and pressure has also been observed to be dependent upon the nanoparticle size. Thus, it can be inferred that hydrogen absorption increases by increasing the pressure or by decreasing the temperature. Furthermore, the rate of hydrogen absorption is higher for smaller nanoparticles in comparison to the larger ones for Pd-Ag and Pd-Cu nanoparticles. The calculated values for the hydrogen to metal ratio in Pd-Ag and Pd-Cu alloy nanoparticles in the hydrogenated state are found to be 0.57 in Pd-Ag and 0.49 in Pd-Cu nanoparticles. These values are quite large in comparison to the corresponding bulk values of 0.2 and 0.1 in Pd-Ag and Pd-Cu, respectively [131].

In this chapter of the thesis, the attention is focused on going a better understanding of the changes in the palladium nanoparticles when they are exposed to hydrogen, in conditions similar to those used in the experiments performed with the catalytic membrane reactors. As previously discussed, in this thesis novel methods are proposed for the preparation of contactor type catalytic membrane reactors. Additionally, to the standard impregnation method for active phase loading on the ceramic membrane support, two more routes were developed. The experiments performed with the proposed CMRs are done in semi batch mode. The hydrogen is supplied to the inner part of the ceramic fiber and is passed through the porous matrix when the active phases are loaded. The CMR is submerged in the reactor vessel containing the model solution. The reaction occurs on the external surface of the CMR when the three phases: gas, solid catalyst and liquid are in close contact. In this scenario, it can be assumed that in the reaction participate only the catalytic phases loaded on the external layer of the membrane reactors. In this sense, if proper methods for active phase are loading on the external surface of the membranes are developed the efficiency of the CMRs can be increased as well as a reduction in the cost of the reactors especially when the palladium is considered. Two novel routes for Pd deposition were developed in order to achieve our objective.

In the first route, the palladium is deposited on the external surface of the membranes by sputtering from Pd target performed in a standard

sputtering chamber. In the second method, a microemulsion containing the Pd precursor is obtained and after reduction and proper washing steps, a suspension of palladium nanoparticles in the organic solvent are obtained. Another variety of this method for preparing Pd-Cu alloy nanoparticles consisted of reducing the precursor salts in solution containing a polyol and surfactant. Finally the obtained nanoparticles were deposited on the external surface of the CMR by filtration of the suspension through the starting membranes. These new methods for Pd deposition onto the membranes allowed a decrease of the active phase by more than 200 times, and at the same time the density of the metal in the reaction zone was increased.

However, as mentioned in the previous chapters of the present work, all CMRs that contained Pd deposited as metal, in contrast to the CMRs with Pd loaded by impregnation, presented very poor activities and suffered very fast deactivation. In order to recover their initial activities complex regeneration steps, including calcination and reduction, must be followed. In order to study more deeply the possible causes for the poor Pd activity in those cases additional samples were prepared. For this purpose the sputtering technique was applied to corundum powder or the suspended Pd nanoparticles were deposited on it.

These samples can be divided into three groups:

- Pd on corundum powder loaded by impregnation.
- Pd on corundum powder loaded by sputtering technique.
- Pd on corundum powder loaded after impregnation with Pd or Pd-Cu nanoparticle suspension in the organic solvent.

The Pd nanoparticle sizes were varied by changing some parameters in routes 2 and 3. These samples were further analyzed by different techniques e.g. TEM, HRTEM, TPD-MD, XRD and hydrogen chemisorption analyses as well as the changes produced on them after H_2 treatment in

conditions similar to the ones used in the experiments with the CMRs were followed.

Finally, an attempt is made for giving a plausible explanation of deactivation observed with the CMRs containing Pd loaded by sputtering or deposited from suspension.

4.2 Methods and Materials

4.2.1 Preparation methods

Concurrently to preparing the CMRs, the same procedures were also used for loading the same active phases onto corundum powder. These samples were used for additional studies e.g. TEM, TPD, HRTEM, in order to going a better understanding of the relationship between the particle sizes of the active phases, its distribution on the support and the catalytic activities. Special attention is drawn to the Pd e.g. particle size as a function of the preparation method and the interaction of the hydrogen with the Pd at conditions similar to the experimental ones. Finally, based on these results, an attempt for a plausible explanation of the Pd deactivation is made.

a. Palladium on corundum powder obtained by impregnation method.

These samples were prepared following the same procedure as that used for the preparation of CMRs, where the Pd was loaded by impregnation (see chapter II). The impregnated corundum powder was dried at 120 ^{o}C for 5 h, calcined at 450 ^{o}C overnight and reduced under flowing hydrogen of 20 sccm/min supplied by a mass flow controller (Allicat Scientific) at 350 ^{o}C for 3 h. The amount of palladium deposited was calculated by the weight difference between the original and modified powder.

b. Palladium on corundum powder obtained by sputtering method.

For the preparation of these samples the same equipment was used as that used for the preparation of the CMRs with sputtered Pd (see chapter II

for details). In this case, the corundum powder was placed onto a petri dish as a thin layer and introduced into the vacuum chamber. Thereafter, the Pd deposition was performed at similar conditions as that used for the CMRs. The sputtering current was maintained as that used for the CMRs e.g. 30 mA. However, the time of sputtering was varied: between 30, 90 and 150 seconds.

In order to know the amount of palladium deposited on the powder, a piece of glass was located in the sputtering chamber close to the corundum powder during the sputtering. The thickness of the Pd layer in the glass was calculated from the X-ray reflectometry by the fast Fourier transformation (FFT) method. Thereafter, the amount of Pd deposited onto the corundum powder was estimated taking into account the effective corundum area exposed to the Pd beam. Finally, each of the three samples obtained at different exposition times, that is 30, 90 and 150 seconds were dried at 120 °C for 2 h; then, each sample was well mixed and separated into two parts. One part was calcined at 350 ^{o}C and the other part at 600 ^{o}C for 6 h each. All samples were reduced at 350 ^{o}C in H_2 flow of 20 sccm/min for 2 hours.

The influence of the sputtering time and the calcination temperature on the Pd particle size was studied using TEM technique. The hydrogen absorption/desorption capacity of the samples and their stabilities under hydrogen treatment was investigated at conditions similar to the experimental conditions during the tests with the CMRs. For this purpose the TPD equipment was used.

c. Palladium on corundum powder obtained by microemulsion method.

Additional samples of corundum powder with deposited Pd were prepared. In this case palladium nanoparticles were obtained from microemulsion. Indeed, the palladium nanoparticles suspension in ethanol was the same as that used for the preparation of the catalytic membrane reactor denoted FeCePd_200_m (see chapter II). The palladium concentration in this solution was measured by ICP.

The Pd nanoparticles suspended in ethanol were placed in a flask containing the corundum powder. The Pd content was determined by ICP and the volume of the suspension was adjusted in order to obtain a sample with the same amount of Pd as that present in the CMR FeCePd_200_m. The ethanol was evaporated under vacuum in a rotatory distiller. Finally, the obtained powder was dried at 120 ^{o}C for 2 h and calcined thereafter at 550 ^{o}C overnight to eliminate any traces of remaining organic compounds. It was then reduced under flowing hydrogen of 20 sccm/min supplied by a mass flow controller (Allicat Scientific) at 350 ^{o}C for 2 h.

d. Palladium copper alloy nanoparticles on corundum powder obtained by polyol route.

Palladium copper alloy nanoparticles were deposited on corundum powder. The suspension containing the nanoparticles in toluene was the same as that used for the preparation of the catalytic membrane reactor denoted FeCePd_200_p. The palladium concentration in this solution was measured by ICP. An adequate volume of the Pd nanoparticles suspension in toluene was measured to load the same amount of palladium in the corundum powder as that in the CMR FeCePd_200_p.

The PdCu nanoparticles suspended in toluene were placed in a flask containing a known amount of corundum powder. The solvent was evaporated under vacuum in a rotatory distiller. The sample was further dried at 120 ^{o}C for 2 h and calcined at 550 ^{o}C for 6 h. Finally, it was reduced under flowing hydrogen of 20 sccm/min supplied by a mass flow controller (Allicat Scientific) at 350 ^{o}C for 2 h.

4.2.2 Characterization methods

The samples of Pd or PdCu alloy loaded on corundum powder were studied using different techniques e.g. TEM, HRTEM, TPD-MD and hydrogen chemisorption. The samples are classified into two main groups; the fresh group is the samples after the deposition and the corresponding activation procedures performed and the second group, aged samples.

These second samples correspond to the samples that were treated with hydrogen performing absorption/desorption cycles.

a. Microscopy (TEM)

a.1 Transmission electron microscopy (TEM, JEOL model 1011)

In order to study the size of the palladium and palladium-copper nanoparticles loaded on the corundum powder, a transmission electron microscope was used. The equipment used was the transmission electron microscope, TEM, JEOL model 1011 located in the Servei de Recursos Científics i Tècnics of URV.

A sample of corundum powder containing palladium was dispersed in ethanol using an ultrasound bath. Subsequently, a drop of the suspension was placed on a copper grid. The grid was dried and placed in the TEM chamber. The sizes of the observed Pd particles were determined using the ITEM software (Olympus).

a.2 Transmission electron microscopy (TEM, JEM ARM 200 cF)

For a deeper understanding of how the palladium nanoparticles are affected by the hydrogen, a fresh and aged sample (samples exposed to cycles of TPD-MD with hydrogen) of each type of palladium or palladium-copper nanoparticles on corundum powder were observed with a high resolution TEM, JEM ARM 200 cF located in Centro Nacional de Microscopía Electrónica (CNME) in Complutense University.

b. X-ray diffraction (XRD)

In order to identify the palladium and corundum crystal phases, the powder samples with palladium were analyzed using X-ray diffraction. XRD measurements were performed using a Bruker-AXS D8-Discover diffractometer equipped with a parallel incident beam (Göbel mirror), a vertical θ-θ goniometer, an XYZ motorized stage mounted on an Eulerian

cradle, diffracted beam Soller slits and a scintillation counter as a detector. A spectrum was collected for the sample with palladium obtained by impregnation on corundum with an angular step of 0.02^{o} at 47.9 s per step at 25 ^{o}C; the angular 2θ diffraction range was between 36.6-44.2^{o}. Spectra were collected for the samples of corundum and of corundum with palladium obtained by sputtering or microemulsion with an angular step of 0.03^{o} at 24 s per step at 25 ^{o}C; the angular 2θ diffraction range was between 36-48^{o}.

For the samples with copper palladium alloy on corundum, the spectrum was collected with an angular step of 0.02^{o} at 900 s per step and 25 ^{o}C; the angular 2θ diffraction range was between 23-56^{o}. The X-ray diffractometer was operated at 40 kV and 40 mA to generate Cukα radiation (wavelength of 1.54056 Å). The conventional 2θ vs. intensity diffractogram was generated. The analyses of the XRD diffractograms were performed by the ICDD database (release 2007) using Diffracplus Evaluation software (Bruker 2007).

c. Temperature programmed desorption (TPD)

With the purpose of studying the hydrogen absorption/desorption behavior on palladium, a temperature programmed desorption equipment was assembled. This equipment has a tubular furnace where a quartz reactor containing the sample is placed vertically. Hydrogen, argon, synthetic air and oxygen lines were connected to the upper part of the reactor that can be supplied to the sample separately or as a mixture in a controlled way by means of mass flow controller valves (Alicat).

The reactor outlet, the bottom part, is connected to a mass detector, Omni Star^{TM}, Pfeiffer Vacuum. The processing of the MD signals obtained continuously was done using Quadstar 32 bit, version 7.02 software (Inficon AG). In general, 2-4 cycles of hydrogen saturation followed by hydrogen desorption were performed on the studied samples. The different steps for a single cycle are presented in table 4.1

Table 4.1: Different steps included in a single cycle in the hydrogen adsorption, absorption and desorption experiments.

Temperature (°C)	Time (min)	Q H_2 sccm/min	Q Ar sccm/min	Purpose
60	60	5	45	Pd saturation with H_2
60	120	0	51.2	Purge the lines
60-460	80	0	51.2	TPD, chemisorbed and absorbed H_2
460	20	0	51.2	Assure H_2 free sample

The results of each sample by TPD-MD are presented in annex 7.3

4.3 Results and Discussion

Table 4.2 resumes the studied samples supported on corundum powder. In the sample denotation the "i" corresponds to Pd obtained after impregnation, "s" to Pd obtained by sputtering, "m" to Pd deposited from microemulsion, "p" to Pd loaded from the polyol route and the number corresponds to the sputtering time in seconds.

Table 4.2: Samples of palladium on corundum powder obtained with different methods.

Type	% Pd	Method of measuring palladium	Calcination Temp (°C)/time(h)	Reduction Temp(°C)/time(h)
Pd_i	1.67	Mass difference [a]	400 °C / 5 h	350 °C / 3 h
Pd_s_30"	0.004	Reflectometry [b]	350 °C / 5 h	350 °C / 3 h
Pd_s_30"	0.004	Reflectometry [b]	600 °C / 6 h	350 °C / 2 h
Pd_s_90"	0.012	Reflectometry [b]	350 °C / 6 h	350 °C / 2 h
Pd_s_90"	0.012	Reflectometry [b]	600 °C / 6 h	350 °C / 2 h
Pd_s_150"	0.020	Reflectometry [b]	350 °C / 6 h	350 °C / 2 h
Pd_s_150"	0.020	Reflectometry [b]	600 °C / 6 h	350 °C / 2 h
Pd_m	0.22	ICP [c]	550 °C / 14 h	350 °C / 2 h
PdCu_p	0.5	ICP [c]	550 °C / 6 h	350 °C / 2 h

[a] The amount of palladium deposited into corundum powder was calculated by the weight difference between the original powder and the powder after impregnation, calcination and reduction.

[b] The amount of Pd deposited onto the corundum powder was calculated from the corundum area exposed to the Pd beam and the thickness of the Pd layer formed on a glass placed in the chamber was used as a reference during the sputtering. This thickness was calculated by X-ray reflectometry using the fast Fourier transformation (FFT) method.

[c] The Pd content on the corundum powder was determined by measuring the Pd content in the suspension used to load the pd by ICP analysis.

4.3.1 Palladium nanoparticles size obtained with TEM JEOL 1011.

The results obtained with TEM JEOL model 1011 for the palladium nanoparticles are presented in table 4.3. Some of the obtained pictures can be seen in annex 7.1. In all cases they were observed as spherical palladium nanoparticles well dispersed on corundum powder.

Table 4.3: Mean size of the nanoparticles supported on corundum obtained by different methods.

Type	Calcination Temp (°C) / time(h)	Mean Size (nm)	STD (nm)
Pd_i	400 °C / 5 h	12	5
Pd_s_30"	350 °C / 5 h	5	2
Pd_s_30"	600 °C / 6 h	7	3
Pd_s_90"	350 °C / 6 h	6	3
Pd_s_90"	600 °C / 6 h	14	6
Pd_s_150"	350 °C / 6 h	8	4
Pd_s_150"	600 °C / 6 h	13	5
Pd_m	550 °C / 14 h	8	5
PdCu_p	550 °C / 6 h	4	0.8

As expected, the different times of sputtering does not have any significant influence on the average Pd particle size. On the other hand, the temperature of calcination very strongly affects the particle size. For the presented cases, the calcination at 600 °C overnight almost doubles the Pd particle size in respect to the samples calcined at 350 °C. These results clearly indicate that Pd sintering occurs at temperature of 600 °C.

The size of the nanoparticles obtained by Pd impregnation have a similar size and standard deviation as the nanoparticles obtained after Pd sputtering and calcination at 600 ^{o}C.

The following pictures presented in Figures 4.1 and 4.2 confirm that the morphologies of the samples for Pd deposited on the corundum powder after impregnation and sputtering are very similar. The pictures for all other samples can be found in annex, no 7.1.

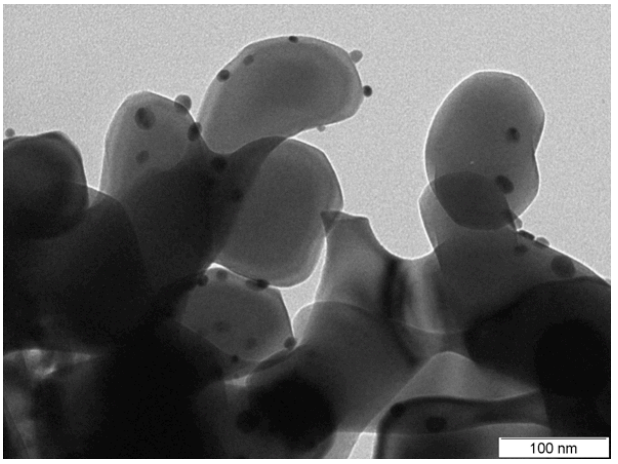

Figure 4.1: Pd deposited on corundum powder after impregnation.

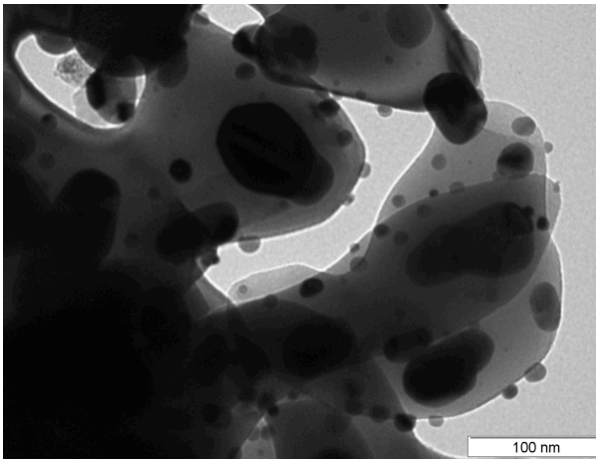

Figure 4.2: Pd deposited on corundum powder by sputtering and calcined at 600 ^{o}C.

Initially, it was believed that a plausible reason for the different activities between the CMRs with impregnated and sputtered Pd could be due to the different particle sizes of the Pd active phase. The obtained results from the TEM analyses indicate that the reasons could be different. On the other hand, it can be expected that the Pd nanoparticles obtained after impregnation of the Pd precursor salt on the corundum powder will be more strongly adhered to the support, favoring a stronger interaction between the metal and the ceramic; thus, stabilizing the active phase clusters.

The obtained results from the TEM does not demonstrate any appreciable difference between the Pd particles on the corundum as a function of the loading procedure e.g. impregnation, sputtering or microemulsion, as observed in Figures 4.1 and 4.2 and also the results summarized in annex, no 7.1.

4.3.2 XRD of the nanoparticles of palladium and copper palladium on corundum powder.

In this section, a description is provided for the results obtained with the XRD technique for the palladium nanoparticles and the nanoparticles of copper palladium supported on corundum powder.

In all the diffractograms, a low intensity peak at $2\theta = 40.2$ corresponding to palladium as well as the two characteristic peaks of corundum at 2θ of 37.7 and 43.3 without disturbance is observed. In all cases, the results are similar and indicate that the Pd is well dispersed on the support. A representative diffractogram is shown in Figure 4.3.

The XRD results for the other samples can be found in annex, no 7.2.

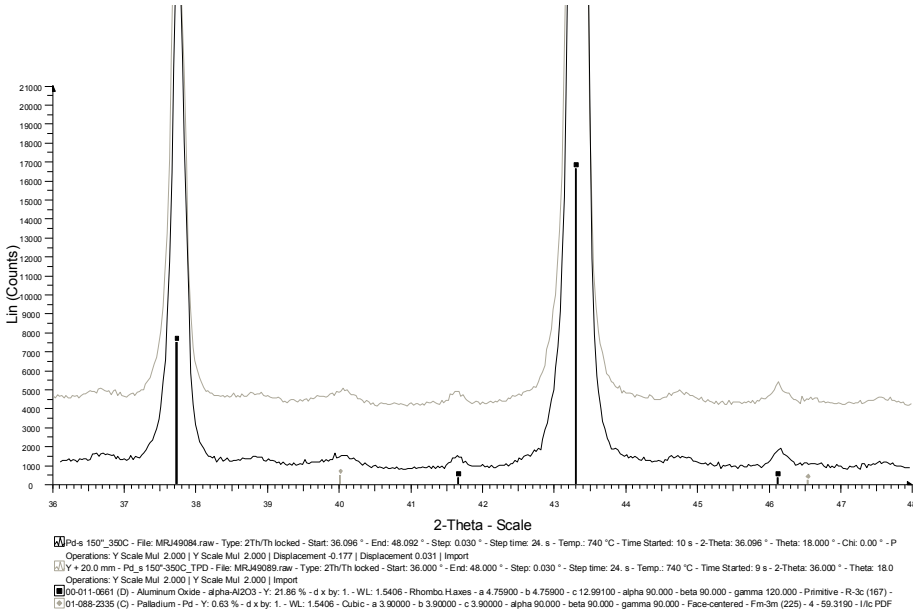

Figure 4.3. Diffractogram of palladium deposited by sputtering during 150 seconds and calcined at 350 ^{o}C fresh and aged during H_2 TP absorption/desorption cycles.

One of the initially adopted hypotheses in order to explain the catalyst deactivation in the experiments especially for cases when the Pd was loaded as metal (sputtering, nanoparticle suspension) was that the hydrogen after its absorption/desorption irreversibly affects the crystal structure of the Pd. During the process the metal crystallinity continuously decreases and finally the Pd is completely converted to an amorphous state. It is well-known Pd has a high affinity for hydrogen. When the metal is in contact with the hydrogen gas it is chemisorbed on its surface. Concerning the catalytic properties of the Pd, chemisorbed hydrogen can further be used to accomplish different hydrogenation reactions. However, the chemisorbed hydrogen can also follow a different pathway, that is, diffusion into the Pd lattice forming ß-Pd. In this form, the Pd lattice is expanded and its capacity for hydrogen activation is limited. In this case, the catalytic capability of the metal is highly decreased. The original structure of the Pd can be restored after desorbing the hydrogen at temperatures higher than 400 ^{o}C. As explained in the introduction part, the resulting structure may present some distortion e.g. expanded ß-Pd or

partially amorphous. In both cases, it can be expected that the material will partially or even completely lose its catalytic activity [109].

The obtained results from the XRD analyses do not indicate any significant difference between the fresh and the treated with hydrogen (aged) samples. It must be remembered that this analysis is appropriate for characterizing the bulk properties of the material but it is not adequate for detection of any surface changes of the sample.

4.3.3 TPD with hydrogen of the palladium nanoparticles supported on corundum.

All the palladium nanoparticles supported in corundum powder were tested by TPD-MD as previously explained. Two or three cycles were performed depending on the signals obtained by the mass detector. As a rule, when no desorption of hydrogen was detected the absorption/desorption steps was not further repeated.

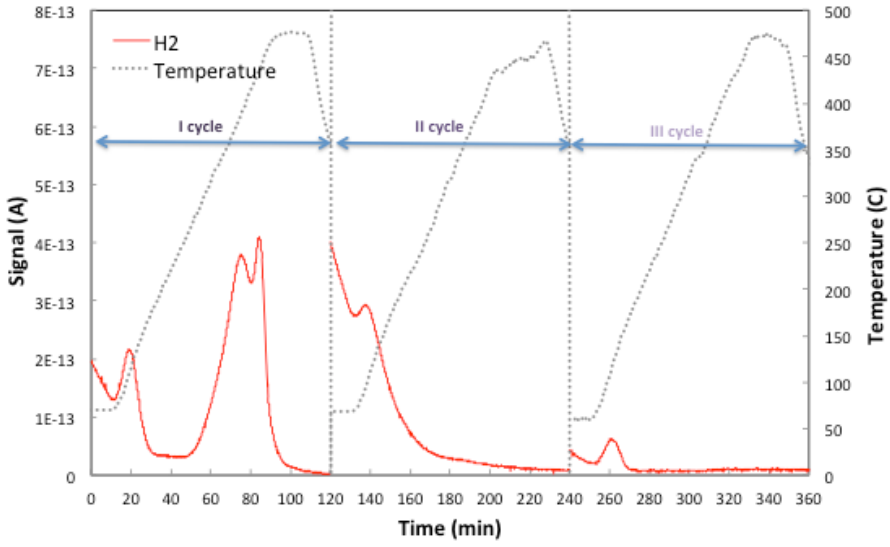

Figure 4.4: TPD-MD results for 1.67 % Pd/ corundum sample obtained by impregnation.

Figure 4.4 presents the results of the TPD experiments performed with the Pd/corundum sample obtained by impregnation. The sample is first overflown by hydrogen at 60 °C. After purging the lines with Ar, the temperature ramp is started. The mass detector coupled to the reactor outlet is used to monitor the presence of desorbed hydrogen in the argon carrier. In the first cycle, are two types of desorbed hydrogen are clearly distinguishable. The first peak with maximum intensity at 109 °C can be attributed to the chemisorbed hydrogen. The second peak is observed with, a maximum intensity at 435 °C.

The desorbed hydrogen at this temperature corresponds to the hydrogen released from the Pd lattice. A rough estimation of the amount of this hydrogen indicates that ß-Pd was formed. The obtained results are in accordance with the well described Pd-H_2 system found in the literature [108,109]. Thereafter, the absorption desorption cycle was repeated. Surprisingly only the chemisorbed hydrogen was detected during the desorption step released around 100 °C. The cycle was repeated for a third time. In the third cycle, only the chemisorbed hydrogen was detected. The chemisorbed hydrogen on the Pd surface is the responsible for the catalytic activity of the metal in the hydrogenation reaction. The TPD results indicate that the Pd/corundum sample obtained by impregnation does not lose its ability to activate the hydrogen and this feature is crucial for its catalytic activity. This result is also in complete agreement with the experiments performed using the CMRs containing Pd loaded by impregnation. In those experiments, no appreciable deactivation of the reactors were observed in repetitive runs as well as no specific reactivation of CMRs were needed. Some of these reactors were used for more than a year performing different types of reactions e.g. phenol oxidation/hydrogenation, Cr (VI) reduction.

Concerning the hydrogen desorption at higher temperatures (above 400 °C) that is released from the Pd lattice [112], the TPD-MD results clearly indicate that the Pd undergoes some changes. It seems that after the first TP Absorption/Desorption cycle the Pd is able to activate the H_2, but once it is chemisorbed it does not diffuse into the crystal lattice.

At this stage it is difficult to give a clear explanation for these changes regarding the Pd-H_2 system. The results from the HRTEM contribute to the elucidation of the ongoing processes and are discussed in the following sections.

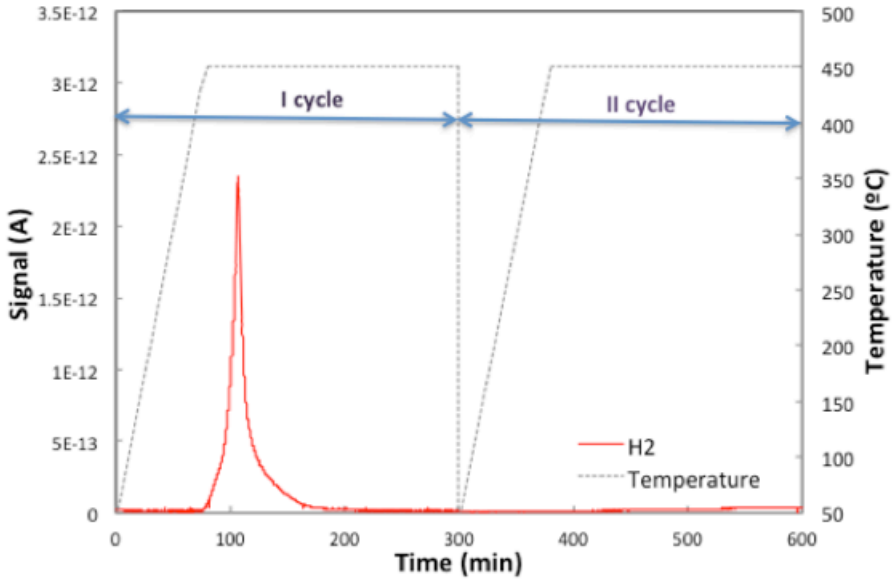

Figure 4.5: TPD-MD results for sputtered 0.004 % Pd/corundum sample; palladium sputtered for 30", sample calcined at 350 °C.

Figure 4.5 presents the results from the TPD-MD measurements performed with 0.004 % w/w Pd on corundum powder obtained by metal sputtering for 30" and calcined at 350 °C. In this case, during the desorption step, only the hydrogen released from the Pd lattice, at approximately 400 °C, was detected. No signal of chemisorbed H_2 (about 100 °C) was detected. In order to get into the crystal lattice the hydrogen must firstly be activated (chemisorbed) on the Pd surface. In this sense, we consider that the absence of detected chemisorbed hydrogen is due to its very low amount that is below the limit of detection of the MD. In the next TPD cycle after the sample was saturated with H_2, no desorbed hydrogen was detected, even at high temperatures. It can be speculated that similar to the impregnated Pd/corundum sample the capacity of the Pd lattice to dissolve

hydrogen is lost after the first cycle, but the sample is still able to activate the hydrogen and the absence of MD signal is due to the very low amount of desorbed hydrogen. However, this assumption is not supported by the experiments performed with the CMRs where very fast deactivation of the reactors with sputtered Pd was observed.

Very simple experiments were performed with the two types of Pd/corundum samples, that is, sputtered or impregnated. The same TPD-MD equipment was used for the test. The aim of the tests basically consisted of verifying the activity of the catalysts for burning hydrogen in air. For this purpose 0.2 g of Pd/corundum powder was placed in the quartz reactor, the temperature was set to 60 ^{o}C, on the reactor inlet a H_2/Ar mixture 1:50 v/v (total flow 50 sccm/min) was supplied the MD was coupled to the outlet. Once the H_2 signal was stabilized (less than a minute) the Ar was interchanged with air. Fresh and aged (samples treated in the H_2 adsorption/desorption test) samples were used.

In the following Table 4.4 are presented the obtained results.

Table 4.4. Catalytic activities of the fresh and aged samples in H_2 oxidation experiments at 60 ^{o}C.

Sample	H_2 oxidation by O_2	Observation
Impregnated Pd on corundum, fresh	Yes	MD: decreased H_2 signal, H_2O
Impregnated Pd on corundum, aged	Yes	MD: decreased H_2 signal, H_2O
Sputtered Pd on corundum, fresh	Yes	MD: decreased H_2 signal, H_2O
Sputtered Pd on corundum, aged	**No**	**MD: no change in the H_2 signal, no H_2O**
Sputtered Pd on corundum, reactivated	Yes	MD: decreased H_2 signal, H_2O

The first two rows presents the results obtained with the two samples of impregnated Pd/corundum samples. It is observed that both, samples catalyze the oxidation of hydrogen. These results are in complete agreement with the results for the CMRs obtained by Pd impregnation. The fresh sputtered Pd/corundum sample is also active in this reaction. However, the same sample after performing on it the H_2

absorption/desorption cycles is completely inactive for this reaction. As explained in the previous section, similar to the CMRs with sputtered Pd, in order to recover the initial activity, the sample must be calcined in air and finally reduced by hydrogen.

The TPD-MD results are consistent with the experimental results obtained with the CMRs, but at this stage cannot clarify the reasons for the observed differences in the activities of the two kinds of samples.

For all Pd/corundum samples prepared by loading the Pd as metal (sputtering, microemulsion, polyol route) the obtained results from the TPD-MD experiments are very similar. The TPA/D plots for all samples can be found in annex, no 7.3. In all cases, only in the first cycle the desorption of hydrogen is detected whilst in the next cycles no hydrogen was detected. As a general rule, with increasing the amount of Pd by prolonging the sputtering time, higher amount of desorbed hydrogen is detected. Also, in those cases, it seems that the samples are not completely deactivated in the first cycle as indicated by the small amount of released H_2 in the subsequent cycle. However, in the third cycle no hydrogen was detected for all samples. In table 4.5, the results of the TPD-MD obtained with all samples are presented.

Table 4.5: TPD-MD results for all studied Pd/corundum samples.

Sample \ Nº Cycle	H_2, a.u. / T ^{o}C		
	I	II	III
1.67 % Pd_i	2/109 and 22/435	1.2/94	0.4/109
0.004 % Pd_s_30"_350 ^{o}C	14/400	-	-
0.004 % Pd_s_30"_600 ^{o}C	-	-	-
0.008 % Pd_s_90"_350 ^{o}C	6/450	1.2/450	-
0.008 % Pd_s_90"_600 ^{o}C	4/450	1/450	-
0.012 % Pd_s_150"_350 ^{o}C	0.1/450	0.04/450	-
0.012 % Pd_s_150"_600 ^{o}C	3.3/450	-	-
0.22 % Pd_m	8.8/450	0.7/450	-
0.3 % Pd 0.1 % Cu_p	-	-	-

Table 4.5 shows that only for the palladium nanoparticles obtained by impregnation was detected the desorbed hydrogen corresponding to the chemisorbed hydrogen at approximately 110 ^{o}C.

The desorbed hydrogen is calculated from the area of the corresponding peak registered by the mass detector. The determination of the exact proportion between the absorbed H_2 and the amount of the Pd was not the main objective of this study. Due to the very low amount of Pd in some of the samples as well as the low H_2 signals detected by the MD, the attempt for precise calculation can induce to large errors. Moreover, the basic aim of the experiments described in this section was to gain a clearer understanding about the Pd deactivation with special emphasis on the H_2-Pd interactions. These experiments also reveal essential differences between the Pd/corundum samples prepared by different routes.

As previously commented the impregnated Pd/corundum sample chemisorbs hydrogen and it seems that its affinity to the H_2 is not lost in repetitive cycles. However during the first cycle this sample has undergone some changes and in the subsequent cycles only chemisorbed hydrogen is detected, but no absorbed H_2 is released from the Pd lattice at higher temperatures.

For the rest of the samples, it was found that they have high initial activity for hydrogen chemisorption, but their affinity to the H_2 is gradually lost. As commented before the obtained results are in complete agreement with the results obtained in the experiments using the CMRs.

In the following section, new insights are given that could help to elucidate the Pd-H_2 system.

4.3.4 Study of the palladium nanoparticles on corundum with TEM JEM ARM 200 cF, crystallographic properties.

The following figures show the results for different Pd/corundum samples obtained with the TEM, JEM ARM 200 cF. In this study four samples are analyzed, that is, fresh and aged Pd/corundum obtained by impregnation and fresh and aged Pd/corundum obtained by sputtering for 30 s (the calcination temperature for this sample was 350 ^{o}C).

a. Palladium nanoparticles by impregnation method, 1.67 % of Pd.

The fresh sample of palladium obtained by impregnation contains very well dispersed Pd nanoparticles of 6-10 nm, perfectly crystalline as monodomains with sharp edges (see figures from 4.6 to 4.8). In addition, the sample contains smaller Pd nanoparticles of 1-2 nm as well as abundant and isolated Pd atoms.

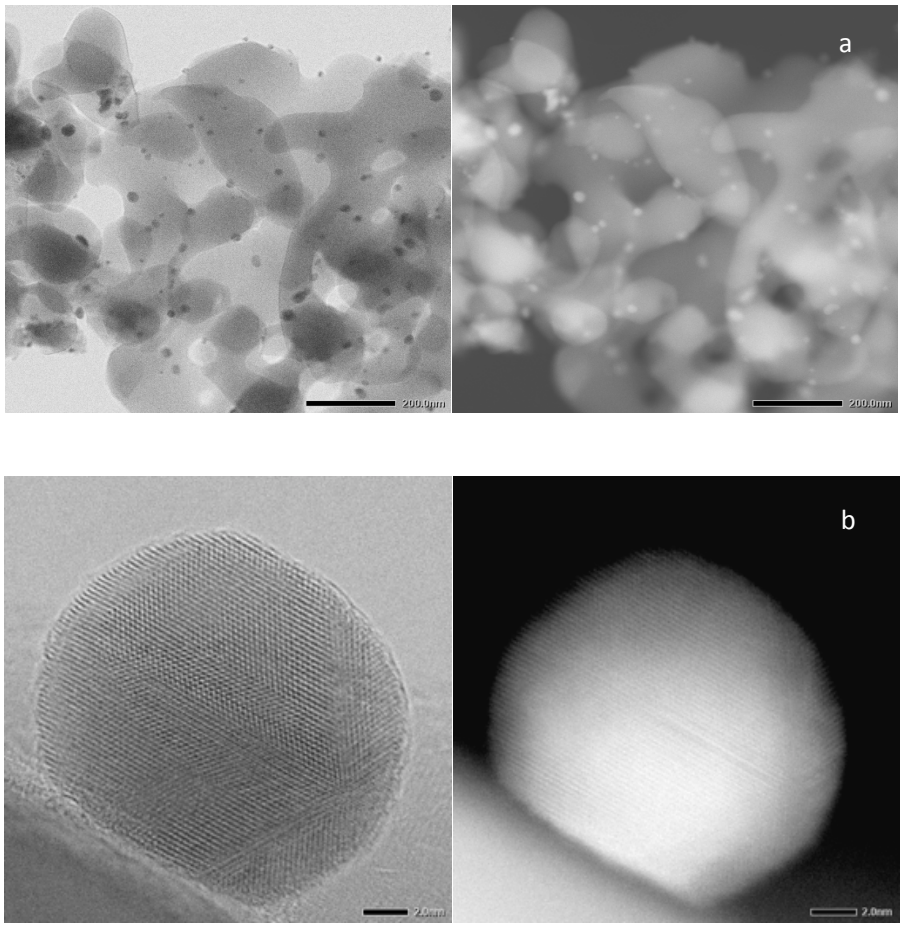

Figure 4.6: (a) and (b) JEM ARM 200 cF images of the fresh sample of palladium on corundum by impregnation method.

Figures 4.6 (a) and (b) show the palladium nanoparticles by impregnation from 6 to 10 nm of size. In figure 4.6 (a), well-dispersed spherical dark gray palladium on corundum is observed. Figure 4.6 (b) shows a palladium crystal. This corresponds to the crystal structure of Pd [110], 2.25 Å Pd (111) and 1.95 Å Pd (200). The Pd is supported on corundum with a lattice parameter of 2.54 Å, Al_2O_3 (104).

No interaction between the palladium and the corundum was found.

Surprisingly, an abundance amount of very small Pd clusters as well as single palladium atoms were observed. Representative images are shown in figure 4.7 a) and b). Nano clusters and single atoms of palladium were observed in the fresh sample of palladium on corundum obtained by impregnation.

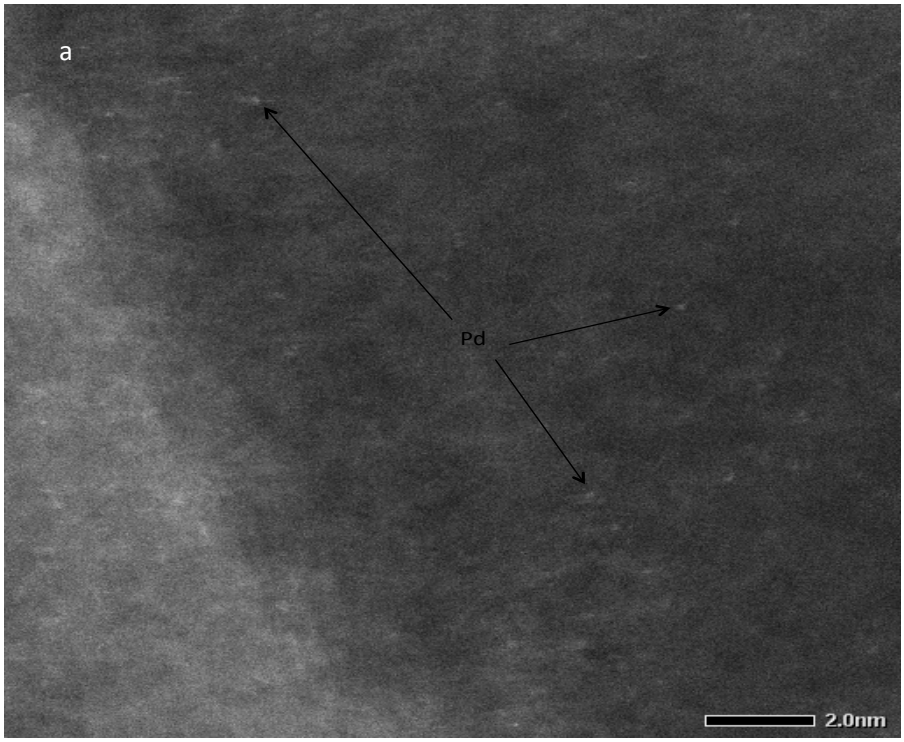

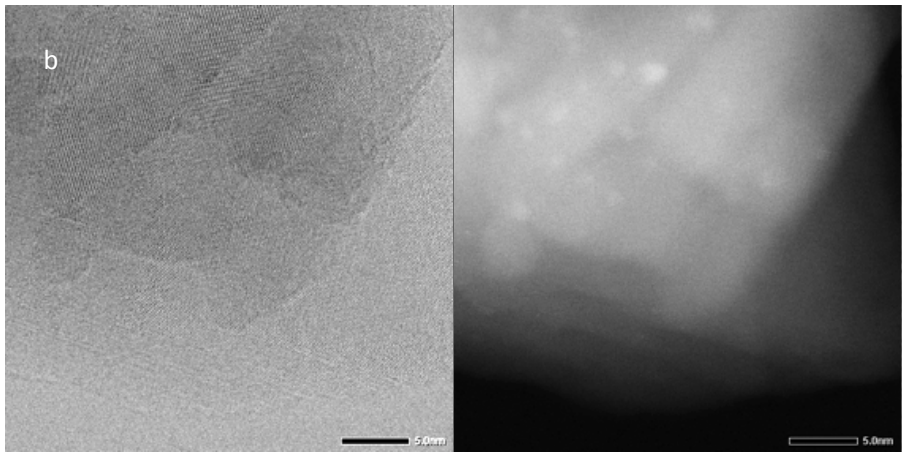

Figure 4.7: (a) and (b) JEM ARM 200 cF images of the nano clusters and single atoms in the fresh sample of palladium on corundum by impregnation method.

Figure 4.7 (a) and (b) shows free and dispersed nano cluster and single atoms of palladium around of the sample.

The sample of palladium on corundum obtained by the impregnation method and aged after performing three cycles in the TPD equipment presented the same type of nanoparticles as that observed for the fresh sample. In general, the large Pd particles exhibit a core-shell structure, with an amorphous shell and a Pd metal core. Meanwhile, the 1-2 nm Pd particles do not show any shell around them. Individual Pd atoms are found all over the sample.

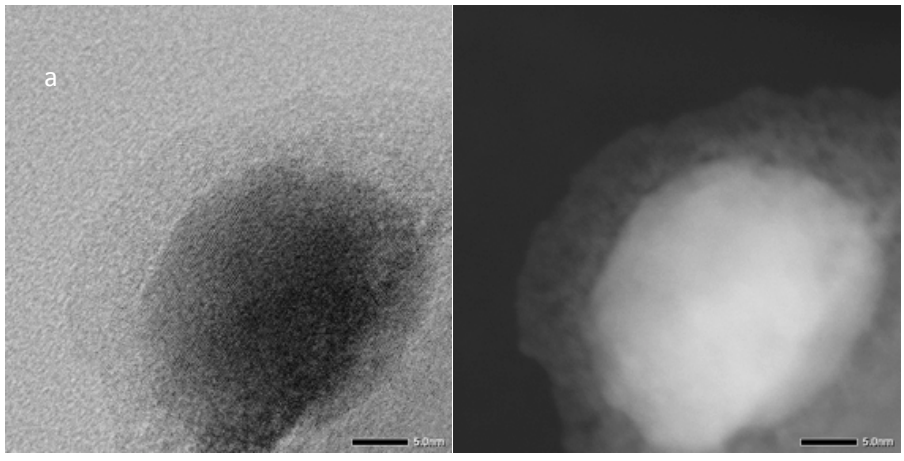

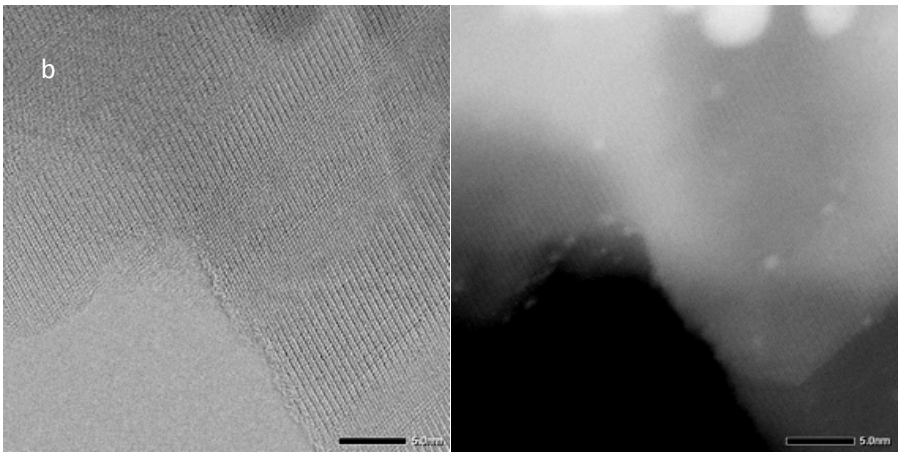

Figure 4.8: (a) nanoparticle and (b) single atom by JEM ARM 200 cF images of the aged sample of palladium on corundum by impregnation method.

In figure 4.8 (a) a crystal of palladium is showed, which corresponds to 1.95 Å Pd (200). The Pd is supported on corundum that presents a lattice parameter of 3.47 Å, Al_2O_3 (012). No interaction between palladium and corundum was found. Palladium nanoparticles have sizes between 6 to 10 nm. Differing from the fresh samples, in the aged samples amorphous zones were found in the palladium. These results clearly indicate that during the hydrogen absorption and desorption process the Pd is strongly affected and its crystal structure is partially lost and, consequently, amorphous zones are created. These zones remained after temperature treatments and the applied vacuum of the equipment. In figure 4.8 (b) single atoms and clusters are presented in all samples without an apparent change in comparison with the original sample.

b. Nanoparticles by sputtering: (a) fresh sample (b) aged sample

In this part a description is provided for the results of the Pd nanoparticles on corundum obtained by sputtering for 30 seconds and calcined and reduced at 350 ^{o}C. Representative images for the fresh sample are shown in figures, 4.9 (a) and (b). In Figure 4.10 (a) and (b) images of the aged in the TPD experiments sample are shown.

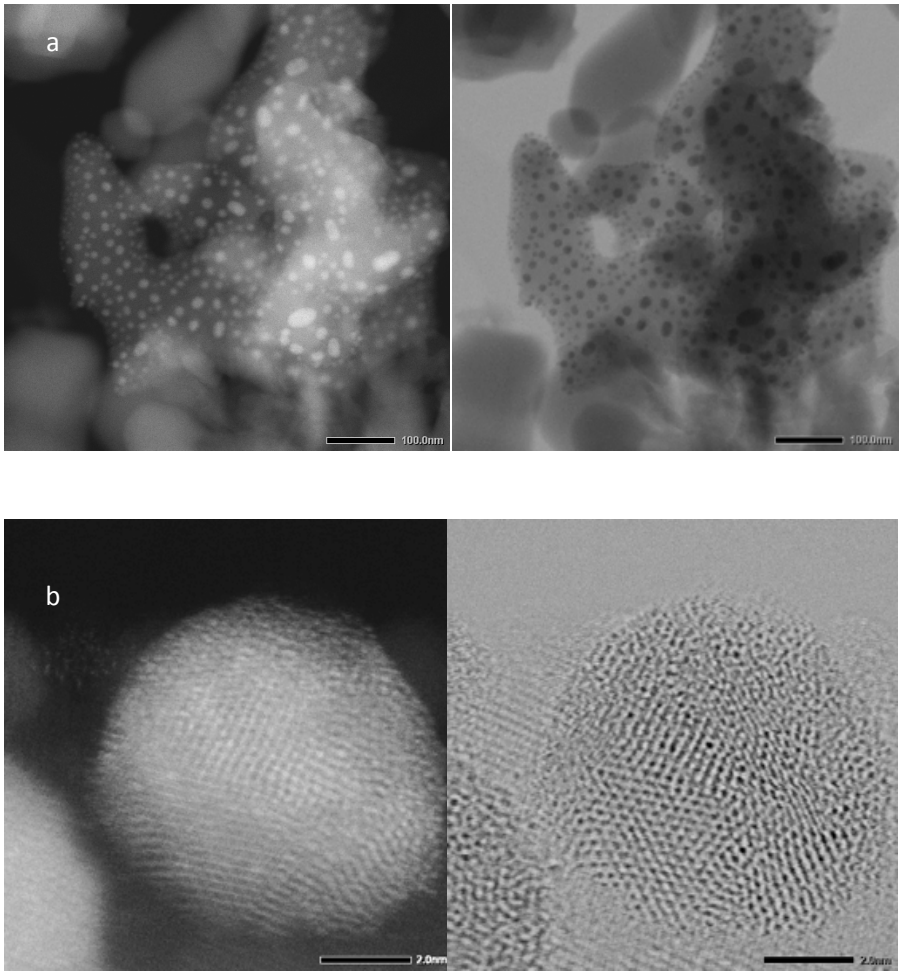

Figure 4.9: (a) nanoparticle by sputtering fresh (b) nanoparticle by sputtering fresh, crystalline core.

In figure 4.9 (a) a general view of the sample is presented. This figure shows that the fresh sputtering particles are metallic Pd. Each particle contains numerous crystalline domains and poorly ordered parts, which makes them highly stressed from a structural point of view. In figure 4.9 (b) a crystal of palladium is shown which corresponds to the crystal structure of Pd [110], 2.25 Å Pd (111) and 1.95 Å Pd (200); also the corundum support is observed at 2.54 Å, Al_2O_3 (104). Similarly to the impregnated Pd samples, no interaction between palladium and corundum was found.

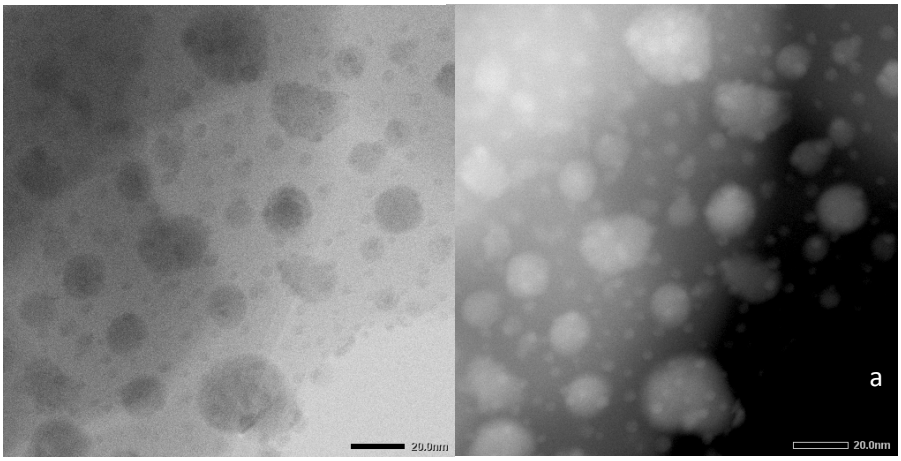
20.0nm
a
20.0nm

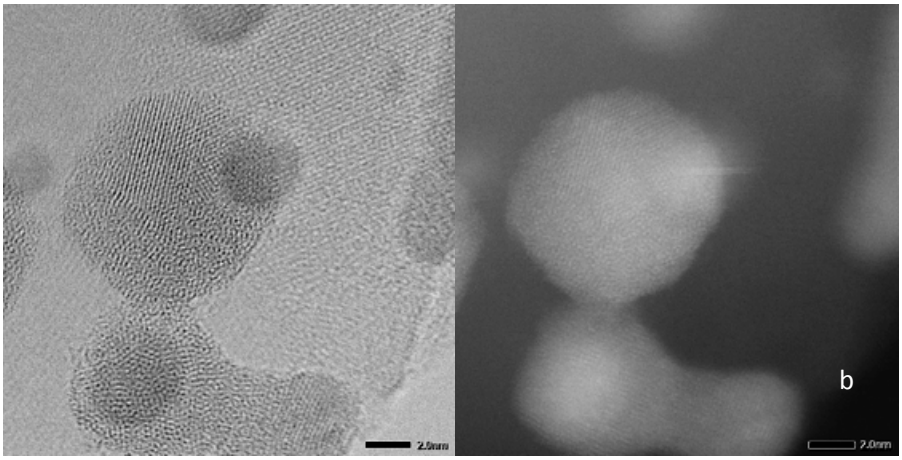
2.5nm
b
2.0nm

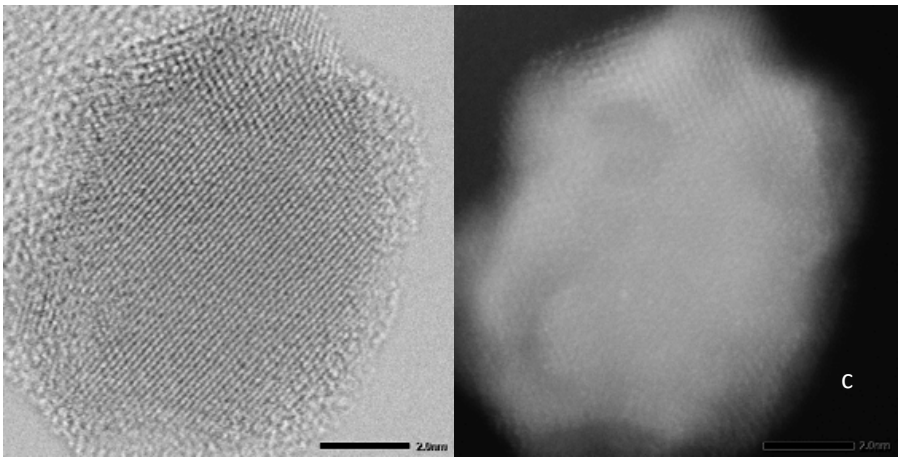
2.5nm
c
2.0nm

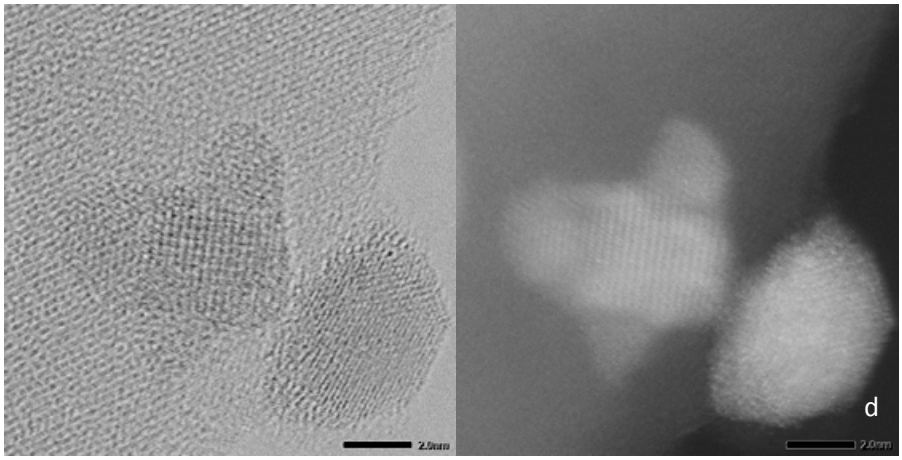

Figure 4.10: (a) nanoparticle by sputtering aged (b) nanoparticle by sputtering aged crystalline and hydride (c) amorphous shell and hydride and (d) amorphous shell, hydride and crystalline Pd.

In figure 4.10 (a) a general view of the aged sample is shown. The sputtered palladium nanoparticles show a core-shell structure with a Pd metallic core and an amorphous shell that shows no structure or, in some cases, lattice fringes that can be ascribed to palladium hydride.

Considering the large particles (4-8 nm) no important differences between the corresponding impregnated/sputtered samples were observed. Similar to the impregnated samples, no interaction between palladium and corundum was found. In figure 4.10 (b) a crystal of palladium is shown which corresponds to Pd 2.25 Å Pd (111). Structures corresponding to palladium hydride were also found at 2.31 Å PdHx (111). This result is rather unexpected. It means that after hydrogen is completely released from the sample (TPD in inert atmosphere and the vacuum of the equipment) part of the palladium lattice remains in a crystal structure that is characteristic for the PdHx.

In Figure 4.10 (b), the lattice parameter of corundum support at 2.54 Å, Al_2O_3 (104) is easily identified. In figure 4.10 (c), Pd crystal, Pd 1.95 Å Pd (200) and palladium hydride structure, 2.02 Å PdHx (200) were observed. In figure 4.10 (d), an amorphous shell, Pd crystal, Pd 1.95 Å Pd (200) in the

right and palladium hydride structure, PdHx [100], 4.03 Å PdHx (100) in the left were observed.

The results obtained by this technique clearly indicate that the hydrogen alters the crystal structure of the Pd. Moreover, the generated distortion is permanent, and the original structure cannot be restored only by heating in inert atmosphere. At first view, the two types of samples, obtained by Pd impregnation or by Pd sputtering, show very similar features. In both of them, the Pd nanoparticles do not present any kind of strong interaction with the support. Moreover, the hydrogen affects them in a similar way; for both aged samples, the surface palladium is transformed to an amorphous state and the palladium lattice partially, remains with the structure of ß-Pd. The loss of catalytic activity by the CMRs containing Pd can be attributed to the changes in the metal caused by the hydrogen. On the other hand, it still does not explain why the deactivation is observed only with the catalytic membrane reactors obtained by Pd sputtering or the methods when the loading is Pd as metal. If the small Pd clusters (2 nm and less) and the Pd single atoms are considered, a very tentative explication for the observed catalytic behavior can be stated. It should be noted that these small structures and single atoms are found only in the Pd/corundum samples obtained by impregnation. It was also confirmed that they do not undergo any alteration caused by the hydrogen. The TPD results also support this evidence.

For the samples with Pd deposited as a metal (sputtering, microemulsion), in the first cycle the hydrogen is released at temperatures above 360 ^{o}C, but in the following cycles there is no interaction with the hydrogen. In contrast, for the samples with impregnated Pd, the hydrogen in the first cycle is released at two temperatures, first in the range 90 - 120 ^{o}C corresponding to the chemisorbed H_2 and thereafter at temperatures above 360 ^{o}C corresponding to the H_2 released from ß-Pd. In the following cycles, only the hydrogen that corresponds to the chemisorbed gas is detected. It can be speculated that for all samples (obtained by impregnation or sputtering) the large Pd particles are permanently affected by the hydrogen forming on their amorphous surface layer.

Thereafter, these particles are unable to activate the hydrogen, so they will not have catalytic activities. On the other hand, the small Pd clusters as well as the single Pd atoms are not altered by the hydrogen, and in fact they are responsible for the catalytic activities of the impregnated with Pd CMRs.

In Figure 4.11 presents a schematic drawing of the proposed mechanism for Pd deactivation caused by the hydrogen. It is observed that only the particles with the capacity for hydrogen absorption are deactivated whilst the single Pd atoms and the small (< 2nm) clusters remain unaltered.

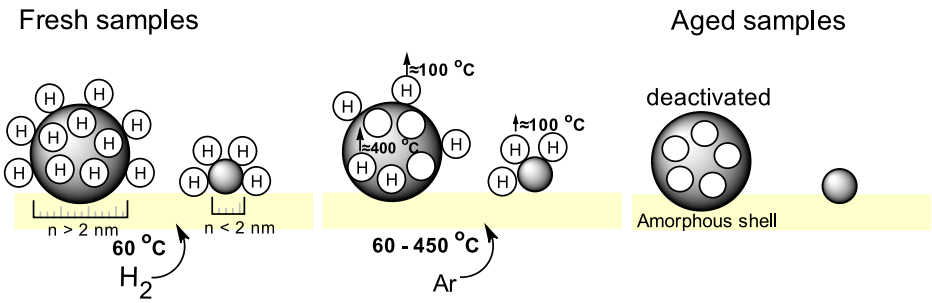

Figure 4.11: Proposed mechanism for the Pd deactivation caused by the hydrogen.

The proposed explanation is not contradictory to the results obtained by the XRD analyses where apparently no changes in the Pd have been detected. As mentioned before the XRD technique only accounts for the bulk properties of the material that is basically unchanged, but the surface characteristics of the crystals cannot be characterized by this method.

Moreover, all experimental results obtained with the CMRs presented in this work can be explained very well considering the proposed hypothesis.

4.4 Conclusions

Different pairs of Pd/corundum samples were prepared and studied by TEM, XRD, TPD-MD and HRTEM techniques. The first group was prepared

by Pd impregnation onto corundum powder, and the others were prepared by metal Pd loading on the support by means of different methods, e.g. Pd sputtering, Pd nanoparticle synthesis in microemulsion and Pd-Cu nanoparticle synthesis using polyol route. All samples were divided into two parts, the first part was only activated and the second part was studied firstly in the TPD experiments (later called the aged sample). Different Pd/corundum samples obtained by sputtering were prepared varying the sputtering time and the calcination temperature. These variations were performed in order to obtain samples with different Pd content as well as different Pd nanoparticle sizes. After calcination at 600 ^{o}C, the sputtered palladium nanoparticles were in the range of 13-14 nm almost twice the size of those nanoparticles obtained by calcination at 350 ^{o}C and very similar in size to the Pd nanoparticles obtained by impregnation (12 nm). The increased nanoparticle size is a clear indication that at 600 ^{o}C sintering of Pd occurs. The Pd nanoparticles obtained from the microemulsion were in the range of 5 to 8 nm and those obtained with the polyol method (PdCu) were at 4 nm.

On all samples at least two H_2 absorption/desorption cycles were performed in the assembled TPD-MD equipment. The obtained results have shown that all fresh samples are initially active for hydrogen sorption. However, the results indicate that the long-term behavior of the Pd/corundum samples in respect to the hydrogen is very different depending on the preparation method used. The samples can be divided into two groups. In the first group are the Pd/corundum samples obtained by impregnation. For this case, after the first absorption step the hydrogen is released at two temperatures during desorption. The first fraction is released at approximately 105 ^{o}C and the second part is desorbed at temperature above 400 ^{o}C. In the subsequent cycles only chemisorbed hydrogen is detected without any significant loss of catalytic activity. On the other hand, after the first cycle is completed, in the next, the Pd loses its capacity to dissolve hydrogen into the crystal lattice. The obtained results from the TPD-MD experiments are completely coherent with the obtained results using the CMRs containing impregnated Pd.

The second group of Pd/corundum samples comprise all samples in which the Pd nanoparticles were loaded as metal e.g. by means of Pd sputtering or synthetized in microemulsion or polyol. These samples have shown to be active for hydrogen activation only in the first adsorption/desorption cycle. Only the hydrogen released from the Pd lattice at temperatures above 400 ^{o}C was detected. Due to the very low metal content in these samples the chemisorbed hydrogen was not detected even in the first TPD cycle. In the subsequent cycles, no desorption of hydrogen was detected meaning that the samples are deactivated. The deactivation was also confirmed by performing additional tests of burning hydrogen in air atmosphere. All aged samples from this group were not active for catalyzing the hydrogen oxidation at 60 ^{o}C. The results are also consistent with the experimental results obtained using the CMRs prepared by these methods where very fast deactivation of the reactors was observed.

In addition, fresh and aged Pd/corundum samples from the two groups were analyzed using HRTEM. The obtained results prove that the hydrogen has a very strong effect on the Pd nanoparticles independent of the manner in which they were loaded on the support e.g. sputtering or impregnation. For both aged samples, it was found that the Pd nanoparticles are partially or fully covered by an amorphous Pd layer. Moreover, the results revealed that in some Pd particles the original lattice structure is not completely restored after the thermal and vacuum treatments. Unexpectedly, zones of Pd with lattice parameters corresponding to the expanded crystal structure of ß-phase were found in some aged Pd particles. These findings, satisfactorily, can explain the gradual deactivation of the Pd/corundum as well as CMRs in respect to their activities for hydrogen activation. On the other hand, an important difference was observed between the sputtered and the impregnated Pd/corundum samples. Only in the impregnated samples, apart from the well-defined Pd nanoparticles, small metal clusters (particle size < 2nm) as well as a large number of single Pd atoms were observed. These specimens and their distribution on the support are not affected by the hydrogen treatment. The presence of these specimens of the Pd only in the impregnated samples may explain the differences in the activities for

hydrogen activation between the two samples. Based on these findings a tentative explanation for the activity of the CMRs can be stated. The results suggest that long term activity of CMRs as well as Pd/corundum for the hydrogen activation could be attributed to the Pd small clusters and single atoms that are presented only in the impregnated samples. The well-defined large Pd particles (> 2nm) presented in all samples are very strongly affected by the hydrogen and irreversibly loses their ability for hydrogen activation. The rate of their deactivation depends on the experimental conditions and the support used. The experiments with the CMRs have shown that the presence of ceria an as additional active phase slows down the process probably by reacting with the activated hydrogen and preventing in some grade its diffusion into the Pd lattice.

CHAPTER V

Conclusions

5.Conclusions

5.1. General conclusions

- New routes for preparation of catalytic membrane reactors starting from commercial hollow fiber corundum membranes have been established. The palladium as the main catalytic phase was deposited into the membrane by Pd precursor impregnation or deposited as metal nanoparticles previously prepared following different routes. Such routes comprise sputtering, Pd synthesis in microemulsion and PdCu alloy nanoparticles prepared using a polyol route.

- All prepared CMRs demonstrated to be active for generation of hydrogen peroxide directly from hydrogen and oxygen when tested in contactor interfacial mode at ambient conditions.

- It has been demonstrated that the catalytic membrane reactors can successfully be used for Cr (VI) to Cr (III) reduction with only hydrogen as reducing agent. It was confirmed that the presence of palladium as an active phase in the CMRs is required for this reaction. It was found that the chromate reduction takes place at pH < 4. Applying the proposed method the Cr (VI) can be reduced to levels below 50 ppb either in synthetic or mineral water. Remarkably, the proposed CMRs did not present any losses of catalytic activity in repetitive runs. The proposed method makes possible the full chromium elimination by precipitation of chromium (III) at neutral pH and filtration. Due to the modular character of the starting commercial ceramic membranes used in the present study, the process is easily scalable.

- The catalytic membrane reactors were tested in oxidation of the phenol in a water solution at 60 ^{o}C and atmospheric pressure. The CMRs containing palladium, cerium oxide and iron oxide were found to be the most active in this reaction. The proposed reaction pathway consists of several steps: first, the hydrogen is activated on the Pd surface, secondly, it reacts with the dissolved oxygen forming hydrogen peroxide from which hydroxyl radicals are formed. These radicals, due to their high oxidation potential, oxidize the phenol.

- It has been demonstrated that the catalytic membrane reactors with a single Pd catalytic phase are active either for phenol oxidation or for its hydrogenation. The reactions can be carried out at mild conditions (atmospheric pressure and at 60 ^{o}C) and the prevailing reaction pathway can easily be chosen only by controlling the amount of dissolved oxygen in the solution. Following the oxidation pathway, the phenol can be eliminated until it is completely mineralized. On the other hand, following the hydrogenation pathway the phenol is transformed to cyclohexanol and cyclohexanone. These findings suggest that a single CMR can successfully be used in AOPs or hydrogenation reactions.

- It has been demonstrated that the catalytic membrane reactor with single palladium as the active phase can successfully be employed for hydrogenation of ibuprofen. The reaction takes place at a pH value below the pka of ibuprofen, at room temperature.

- It has been found that all CMRs obtained after palladium precursor impregnation has excellent long term stabilities and do not present any appreciable decreasing activities. In contrast, the CMRs containing Pd loaded as metal (after sputtering, Pd nanoparticle suspension), despite their good initial activities, suffer very fast deactivation. In order to recover their initial activities, a complex procedure must be followed including calcination and reduction steps.

- In order to gain a better understanding about the causes for the different activities of the CMRs prepared by different methods, additional samples were prepared using corundum powder as support. The Pd was loaded by the same methods used for the CMRs preparation. The different techniques applied for the characterization of these samples revealed:

    - In the experimental conditions used in this thesis, the hydrogen irreversibly alters the crystal structure of the Pd nanoparticles larger than 2 nm. After hydrogen absorption/desorption steps on the surface of the Pd nanoparticles an amorphous shell is formed that is not more active for hydrogen activation.

    - Moreover, only in the Pd/corundum samples obtained by Pd precursor impregnation very small Pd particles (p.s. < 2nm) as well as a large number of well dispersed Pd single atoms that remained unaltered after the hydrogen treatments were observed.

- Based on the findings from the study of the Pd/corundum powder samples as well as the experimental results obtained with the different CMRs, a tentative explanation for the Pd deactivation can be stated. In the tests performed with the CMRs, the experimental conditions favor the formation of the PdHx in β-phase that is no more active for the activation of the hydrogen; the altered Pd particles do not possess catalytic activity. The thermal and/or the high vacuum treatment applied to these particles are not sufficient for recovering their original crystal structure. The long term activities of the CMRs prepared after Pd precursor impregnation is due to the single Pd atoms as well as the small Pd domains (p.s. < 2nm) presented only in these samples and which are not affected by the hydrogen.

In general, the proposed catalytic membrane reactors have shown to be promising devices that can successfully be used in different processes regarding water treatment at mild conditions. Due to the modular character of the reactors, the process is easily scalable and opens the possibility for large-scale applications. Therefore, further study is recommended in order to optimize and to increase the efficiency of the proposed reactors.

Bibliography

6. Bibliography

1. Sanchez, M. & Tsotsis, T. in *Catalytic Membranes and Membrane Reactors.* (Wiley-VCH, 2002).

2. Lin, K. *Ceramic Membranes for Separation and Reaction*. (Wiley, 2007).

3. Gallucci, F., Basile, A. & Ibney Hai, F. in *Membranes for Membrane Reactors: Preparation, Optimization and Selection* 1–61 (Wiley, 2011).

4. Barbieri, G. & Scura, F. in *Membrane Operations: Innovative Separations and Transformations* 387–306 (Wiley-VCH, 2009).

5. in *Membrane Reactors: Distributing Reactants to Improve Selectivity and Yield* (eds. Thomas, S., Hamel, C. & Seidel - Morgenstern, A.) (Wiley-VCH, 2010).

6. Westermann, T. & Melin, T. Flow-through catalytic membrane reactors—Principles and applications. *Chem. Eng. Process. Process Intensif.* **48,** 17–28 (2009).

7. Caro, J. Basic Aspects of Membrane Reactors. (2010).

8. Miachon, S. & Dalmon, J.-A. Catalysis in membrane reactors: what about the catalyst? *Top. Catal.* **29,** 59–65 (2004).

9. Julbe, A., Farrusseng, D. & Guizard, C. Porous ceramic membranes for catalytic reactors — overview and new ideas. *J. Membr. Sci.* **181,** 3–20 (2001).

10. Cybulski, A. & Moulijn, J. A. *Structured Catalysts and Reactors*. (CRC Press, 2005).

11. Tsotsis, T. T., Champagnie, A. & Liu, P. in *Computer-Aided Design of Catalysts* (eds. Becker, R. & Pereira, C.) 471–550 (CRC Press,

1993).

12. Sanchez, M., J, & Tsotsis, T. T. *Catalytic membranes and membrane reactors*. (Wiley-VCH, 2002).

13. Dittmeyer, R., Svajda, K. & Reif, M. A review of catalytic membrane layers for gas/liquid reactions. *Top. Catal.* **29,** 3–27 (2004).

14. Volkov, V., Petrova, I., Lebedeva, V., Roldughin, V. & Tereshchenko, G. in *Membranes for Membrane Reactors: Preparation, Optimization and Selection* 531–548 (Wiley, 2011).

15. Osegueda, O., Dafinov, A., Llorca, J., Medina, F. & Suerias, J. In situ generation of hydrogen peroxide in catalytic membrane reactors. *Catal. Today* **193,** 128–136 (2012).

16. Osegueda, O., Dafinov, A., Llorca, J., Medina, F. & Sueiras, J. Heterogeneous catalytic oxidation of phenol by in situ generated hydrogen peroxide applying novel catalytic membrane reactors. *Chem. Eng. J.* **262,** 344–355 (2015).

17. Osegueda, O. Development of a novel catalytic membrane reactor: Application in wastewater treatment. (Universitat Rovira i Virgili, 2013).

18. Wang, C.-C., Chen, D.-H. & Huang, T.-C. Synthesis of palladium nanoparticles in water-in-oil microemulsions. *Colloids Surf. Physicochem. Eng. Asp.* **189,** 145–154 (2001).

19. Meshesha, B. T. *et al.* PdCu alloy nanoparticles on alumina as selective catalysts for trichloroethylene hydrodechlorination to ethylene. *Appl. Catal. Gen.* **453,** 130–141 (2013).

20. Barnhart, J. Occurrences, Uses, and Properties of Chromium. *Regul. Toxicol. Pharmacol.* **26,** S3–S7 (1997).

21. Vander Griend, D. A., Golden, J. S. & Arrington, C. A. Kinetics and Mechanism of Chromate Reduction with Hydrogen Peroxide in Base. *Inorg. Chem.* **41,** 7042–7048 (2002).

22. Cotton, F. A. & Wilkinson, S. G. *Química inorgánica avanzada*. (Editorial Limusa S.A. De C.V., 1986).

23. WHO | Guidelines for drinking-water quality - Volume 1: Recommendations. *WHO* at <http://www.who.int/water_sanitation_health/dwq/gdwq3rev/en/>

24. US EPA, O. Basic Information about Chromium in Drinking Water. at <http://water.epa.gov/drink/contaminants/basicinformation/chromium.cfm>

25. Chang, L.-Y. Chromate reduction in wastewater at different pH levels using thin iron wires—A laboratory study. *Environ. Prog.* **24,** 305–316 (2005).

26. Mekatel, H., Amokrane, S., Bellal, B., Trari, M. & Nibou, D. Photocatalytic reduction of Cr(VI) on nanosized Fe2O3 supported on natural Algerian clay: Characteristics, kinetic and thermodynamic study. *Chem. Eng. J.* **200–202,** 611–618 (2012).

27. Burriel, F., Lucena, F., Arribas, S. & Hernández, J. *Química Analítica Cualitativa*. (Paraninfo S.A., 2008).

28. Divrikli, U., Kartal, A. A., Soylak, M. & Elci, L. Preconcentration of Pb(II), Cr(III), Cu(II), Ni(II) and Cd(II) ions in environmental samples by membrane filtration prior to their flame atomic absorption spectrometric determinations. *J. Hazard. Mater.* **145,** 459–464 (2007).

29. Fendorf, S. E. & Li, G. Kinetics of Chromate Reduction by Ferrous Iron. *Environ. Sci. Technol.* **30,** 1614–1617 (1996).

30. Sedlak, D. L. & Chan, P. G. Reduction of hexavalent chromium by ferrous iron. *Geochim. Cosmochim. Acta* **61,** 2185–2192 (1997).

31. Doyle, M., Swedo, R. J. & Rocek, J. Effect of cerium (III) and cerium (IV) on chromic acid oxidations. Elimination of the chromium (IV)-alcohol oxidation. *J. Am. Chem. Soc.* **95,** 8352–8357 (1973).

32. Konovalova, V. V., Dmytrenko, G. M., Nigmatullin, R. R., Bryk, M. T. & Gvozdyak, P. I. Chromium(VI) reduction in a membrane bioreactor with immobilized Pseudomonas cells. *Enzyme Microb. Technol.* **33,** 899–907 (2003).

33. Ishibashi, Y., Cervantes, C. & Silver, S. Chromium reduction in Pseudomonas putida. *Appl. Environ. Microbiol.* **56,** 2268–2270 (1990).

34. Pratt, A. R., Blowes, D. W. & Ptacek, C. J. Products of Chromate Reduction on Proposed Subsurface Remediation Material. *Environ. Sci. Technol.* **31,** 2492–2498 (1997).

35. Wang, H. *et al.* Simultaneous Removal of Phenol and Cr(VI) by TiO2 Nanotube Array Photoelectrocatalysis: Simultaneous Removal of Phenol and Cr(VI) by TiO2 Nanotube Array Photoelectrocatalysis. *Chin. J. Catal. Chin. VERSION* **32,** 637–642 (2011).

36. Chen, S.-S., Cheng, C.-Y., Li, C.-W., Chai, P.-H. & Chang, Y.-M. Reduction of chromate from electroplating wastewater from pH 1 to 2 using fluidized zero valent iron process. *J. Hazard. Mater.* **142,** 362–367 (2007).

37. Chen, S.-S., Hsu, B.-C. & Hung, L.-W. Chromate reduction by waste iron from electroplating wastewater using plug flow reactor. *J. Hazard. Mater.* **152,** 1092–1097 (2008).

38. Chirwa, E. M. N. & Wang, Y.-T. Hexavalent Chromium Reduction by Bacillus sp. in a Packed-Bed Bioreactor. *Environ. Sci. Technol.* **31,** 1446–1451 (1997).

39. Wang, Y.-T. & Shen, H. Bacterial reduction of hexavalent chromium. *J. Ind. Microbiol.* **14,** 159–163 (1995).

40. Wang, Z., Bush, R. T., Sullivan, L. A. & Liu, J. Simultaneous Redox Conversion of Chromium(VI) and Arsenic(III) under Acidic Conditions. *Environ. Sci. Technol.* **47,** 6486–6492 (2013).

41. Hsu, H.-T., Chen, S.-S., Tang, Y.-F. & Hsi, H.-C. Enhanced photocatalytic activity of chromium(VI) reduction and EDTA oxidization by photoelectrocatalysis combining cationic exchange membrane processes. *J. Hazard. Mater.* **248-249,** 97–106 (2013).

42. Fiúza, A., Silva, A., Carvalho, G., la Fuente, A. V. de & Delerue-Matos, C. Heterogeneous kinetics of the reduction of chromium (VI) by elemental iron. *J. Hazard. Mater.* **175,** 1042–1047 (2010).

43. Gheju, M. & Iovi, A. Kinetics of hexavalent chromium reduction by scrap iron. *J. Hazard. Mater.* **135,** 66–73 (2006).

44. Gould, J. P. The kinetics of hexavalent chromium reduction by metallic iron. *Water Res.* **16,** 871–877 (1982).

45. Eary, L. E. & Rai, D. Chromate removal from aqueous wastes by reduction with ferrous ion. *Environ. Sci. Technol.* **22,** 972–977 (1988).

46. Apha, AWWA & Wef. *Standard Methods for the Examination of Water and Wastewater*. (Amer Water Works Assn, 2012).

47. Zhang, F., Wang, P., Koberstein, J., Khalid, S. & Chan, S.-W. Cerium oxidation state in ceria nanoparticles studied with X-ray photoelectron spectroscopy and absorption near edge spectroscopy. *Surf. Sci.* **563,** 74–82 (2004).

48. Michalowicz, J. & Duda, W. Phenols—sources and toxicity. *Pol. J. Environ. Stud.* **16,** 347–362 (2007).

49. US EPA, O. Phenol | Technology Transfer Network Air Toxics Web site | US EPA. at <http://www.epa.gov/airtoxics/hlthef/phenol.html>

50. Poyatos, J. M. *et al.* Advanced Oxidation Processes for Wastewater Treatment: State of the Art. *Water. Air. Soil Pollut.* **205,** 187–204 (2010).

51. Oller, I., Malato, S. & Sánchez-Pérez, J. A. Combination of Advanced Oxidation Processes and biological treatments for wastewater decontamination—A review. *Sci. Total Environ.* **409,** 4141–4166 (2011).

52. Andreozzi, R., Caprio, V., Insola, A. & Marotta, R. Advanced oxidation processes (AOP) for water purification and recovery. *Catal. Today* **53,** 51–59 (1999).

53. Feng, Y. J. & Li, X. Y. Electro-catalytic oxidation of phenol on several metal-oxide electrodes in aqueous solution. *Water Res.* **37,** 2399–2407 (2003).

54. Gattrell, M. & Kirk, D. W. A Study of the Oxidation of Phenol at Platinum and Preoxidized Platinum Surfaces. *J. Electrochem. Soc.* **140,** 1534–1540 (1993).

55. Li, X., Cui, Y., Feng, Y., Xie, Z. & Gu, J.-D. Reaction pathways and mechanisms of the electrochemical degradation of phenol on different electrodes. *Water Res.* **39,** 1972–1981 (2005).

56. Sharifian, H. & Kirk, D. W. Electrochemical Oxidation of Phenol. *J. Electrochem. Soc.* **133,** 921–924 (1986).

57. Tahar, N. B. & Savall, A. Mechanistic Aspects of Phenol Electrochemical Degradation by Oxidation on a Ta / PbO2 Anode. *J. Electrochem. Soc.* **145,** 3427–3434 (1998).

58. Long, M. *et al.* Efficient Photocatalytic Degradation of Phenol over Co3O4/BiVO4 Composite under Visible Light Irradiation. *J. Phys. Chem. B* **110,** 20211–20216 (2006).

59. Sclafani, A., Palmisano, L. & Schiavello, M. Influence of the preparation methods of titanium dioxide on the photocatalytic degradation of phenol in aqueous dispersion. *J. Phys. Chem.* **94,** 829–832 (1990).

60. Sun, B., Vorontsov, A. V. & Smirniotis, P. G. Role of Platinum Deposited on TiO2 in Phenol Photocatalytic Oxidation. *Langmuir* **19,** 3151–3156 (2003).

61. Tryba, B., Morawski, A. W. & Inagaki, M. Application of TiO2-mounted activated carbon to the removal of phenol from water. *Appl. Catal. B Environ.* **41,** 427–433 (2003).

62. Wang, W., Serp, P., Kalck, P. & Faria, J. L. Photocatalytic degradation of phenol on MWNT and titania composite catalysts prepared by a modified sol–gel method. *Appl. Catal. B Environ.* **56,** 305–312 (2005).

63. Wu, C., Liu, X., Wei, D., Fan, J. & Wang, L. Photosonochemical degradation of Phenol in water. *Water Res.* **35,** 3927–3933 (2001).

64. Kavitha, V. & Palanivelu, K. The role of ferrous ion in Fenton and photo-Fenton processes for the degradation of phenol. *Chemosphere* **55,** 1235–1243 (2004).

65. Zazo, J. A., Casas, J. A., Mohedano, A. F., Gilarranz, M. A. & Rodríguez, J. J. Chemical Pathway and Kinetics of Phenol Oxidation by Fenton's Reagent. *Environ. Sci. Technol.* **39,** 9295–9302 (2005).

66. Alnaizy, R. & Akgerman, A. Advanced oxidation of phenolic compounds. *Adv. Environ. Res.* **4,** 233–244 (2000).

67. Huang, C. P., Dong, C. & Tang, Z. Advanced chemical oxidation: Its present role and potential future in hazardous waste treatment. *Waste Manag.* **13,** 361–377 (1993).

68. Pignatello, J. J., Oliveros, E. & MacKay, A. Advanced Oxidation Processes for Organic Contaminant Destruction Based on the Fenton Reaction and Related Chemistry. *Crit. Rev. Environ. Sci. Technol.* **36,** 1–84 (2006).

69. Kang, Y. W. & Hwang, K.-Y. Effects of reaction conditions on the oxidation efficiency in the Fenton process. *Water Res.* **34,** 2786–2790 (2000).

70. Campos, J., Blanco, B. & Fierro, J. Hydrogen Peroxide Synthesis: An Outlook beyond the Anthraquinone Process. *Angew Chem.* 6962 – 6984 (2006).

71. Pashkova, A., Svajda, K. & Dittmeyer, R. Direct synthesis of hydrogen peroxide in a catalytic membrane contactor. *Chem. Eng. J.* 265–171 (2008).

72. Remias, J., Pavlosky, T. & Sen, A. Catalytic hydroxylation of benzene and cyclohexane using in situ generated hydrogen peroxide: new mechanistic insights and comparison with hydrogen peroxide added directly. *J. Mol. Catal. Chem.* 179–192 (2003).

73. Abate, S. *et al.* Preparation, performances and reaction mechanism for the synthesis of H2O2 from H2 and O2 based on palladium membranes. *Catal. Today* 323–328 (2005).

74. Pashkova, A., Dittmeyer, R., Kaltenborn, N. & Richter, H. Experimental study of porous tubular catalytic membranes for direct synthesis of hydrogen peroxide. *Chem. Eng. J.* 924–933 (2010).

75. Tomoya, I. *et al.* Direct production of hydrogen peroxide from oxygen and hydrogen applying membrane-permeation mechanism. *Chem. Eng. Sci.* 436–440 (2010).

76. Shi, L., Goldbach, A., Zeng, G. & Hengyong, X. Direct H2O2 synthesis over Pd membranes at elevated temperatures. *J. Membr. Sci.* 160–166 (2010).

77. Melada, S., Pinna, F., Strukul, G., Perathoner, S. & Centi, G. Palladium-modified catalytic membranes for the direct synthesis of H2O2: preparation and performance in aqueous solution. *J. Catal.* 241–248 (2005).

78. Han, Y. & Lunsford, J. Direct formation of H2O2 from H2 and O2 over a Pd/SiO2 catalyst: the roles of the acid and the liquid phase. *J. Catal.* 313–316 (2005).

79. Maehara, S., Taneda, M. & Kusakabe, K. Catalytic synthesis of Hydrogen Peroxide in a Capillary Microreactor. (2007).

80. Mori, K., Hanafusa, A., Che, M. & Yamashita, H. In Situ Generation of Active Pd Nanoparticles within a Macroreticular Acidic Resin: Efficient Catalyst for the Direct Synthesis of Hydrogen Peroxide. *J. Phys. Chem. Lett.* 1675–1678 (2010).

81. Ghedini, E. *et al.* Mesoporous silica as supports for Pd-catalyzed H2O2 direct synthesis: Effect of the textural properties of the support on the activity and selectivity. *J. Catal.* 266–273 (2010).

82. Wang, Y., Yao, J., Li, H., Su, D. & Antonietti, M. Highly Selective Hydrogenation of Phenol and Derivatives over a Pd@Carbon Nitride Catalyst in Aqueous Media. *J. Am. Chem. Soc.* **133,** 2362–2365 (2011).

83. Morales, J., Hutcheson, R., Noradoun, C. & Cheng, I. F. Hydrogenation of Phenol by the Pd/Mg and Pd/Fe Bimetallic Systems under Mild Reaction Conditions. *Ind. Eng. Chem. Res.* **41,** 3071–3074 (2002).

84. Zhu, J.-F. *et al.* Aqueous-phase selective hydrogenation of phenol to cyclohexanone over soluble Pd nanoparticles. *Green Chem.* **16,**

2664–2669 (2014).

85. Cheng, L., Dai, Q., Li, H. & Wang, X. Highly Selective Hydrogenation of Phenol and Derivates over Pd catalysts supported on SiO2 and γ-Al2O3 in aqueous media. *Catal. Commun.* **57,** 23–28 (2014).

86. Watanabe, S. & Arunajatesan, V. Influence of Acid Modification on Selective Phenol Hydrogenation Over Pd/Activated Carbon Catalysts. *Top. Catal.* **53,** 1150–1152 (2010).

87. Gonzalez-Velasco, J. R., Gonzalez-Marcos, M. P., Arnaiz, S., Gutierrez-Ortiz, J. I. & Gutierrez-Ortiz, M. A. Activity and Selectivity of Palladium Catalysts during the Liquid-Phase Hydrogenation of Phenol. Influence of Temperature and Pressure. *Ind. Eng. Chem. Res.* **34,** 1031–1036 (1995).

88. Itoh, N. & Xu, W.-C. Selective hydrogenation of phenol to cyclohexanone using palladium-based membranes as catalysts. *Appl. Catal. Gen.* **107,** 83–100 (1993).

89. Pérez, Y., Fajardo, M. & Corma, A. Highly selective palladium supported catalyst for hydrogenation of phenol in aqueous phase. *Catal. Commun.* **12,** 1071–1074 (2011).

90. Matos, J. & Corma, A. Selective phenol hydrogenation in aqueous phase on Pd-based catalysts supported on hybrid TiO2-carbon materials. *Appl. Catal. Gen.* **404,** 103–112 (2011).

91. Scirè, S., Minicò, S. & Crisafulli, C. Selective hydrogenation of phenol to cyclohexanone over supported Pd and Pd-Ca catalysts: an investigation on the influence of different supports and Pd precursors. *Appl. Catal. Gen.* **235,** 21–31 (2002).

92. Narayanan, S. & Krishna, K. Hydrotalcite-supported palladium catalysts: Part I: Preparation, characterization of hydrotalcites and palladium on uncalcined hydrotalcites for CO chemisorption and phenol hydrogenation. *Appl. Catal. Gen.* **174,** 221–229 (1998).

93. Narayanan, S. & Krishna, K. Hydrotalcite-supported palladium catalysts: Part II. Preparation, characterization of hydrotalcites and palladium hydrotalcites for CO chemisorption and phenol hydrogenation. *Appl. Catal. Gen.* **198,** 13–21 (2000).

94. Chen, Y. Z., Liaw, C. W. & Lee, L. I. Selective hydrogenation of phenol to cyclohexanone over palladium supported on calcined Mg/Al hydrotalcite. *Appl. Catal. Gen.* **177,** 1–8 (1999).

95. Liu, H., Jiang, T., Han, B., Liang, S. & Zhou, Y. Selective Phenol Hydrogenation to Cyclohexanone Over a Dual Supported Pd–Lewis Acid Catalyst. *Science* **326,** 1250–1252 (2009).

96. Liu, J., Li, H. & Li, H. Liquid-Phase Selective Hydrogenation of Phenol to Cyclohexanone over Pd-Ce-B/Hydrotalcite Catalyst. *Chin. J. Catal.* **28,** 312–316 (2007).

97. Maksimov, A. L., Kuklin, S. N., Kardasheva, Y. S. & Karakhanov, E. A. Hydrogenation of phenols in ionic liquids on rhodium nanoparticles. *Pet. Chem.* **53,** 157–163 (2013).

98. Mahata, N., Raghavan, K. V., Vishwanathan, V., Park, C. & Keane, M. A. Phenol hydrogenation over palladium supported on magnesia: Relationship between catalyst structure and performance. *Phys. Chem. Chem. Phys.* **3,** 2712–2719 (2001).

99. Mahata, N. & Vishwanathan, V. Gas phase hydrogenation of phenol over supported palladium catalysts. *Catal. Today* **49,** 65–69 (1999).

100. Mahata, N., Raghavan, K. V. & Vishwanathan, V. Influence of alkali promotion on phenol hydrogenation activity of palladium/alumina catalysts1. *Appl. Catal. Gen.* **182,** 183–187 (1999).

101. Mahata, N. & Vishwanathan, V. Kinetics of phenol hydrogenation over supported palladium catalyst. *J. Mol. Catal. Chem.* **120,** 267–270 (1997).

102. Sikhwivhilu, L. M., Coville, N. J., Naresh, D., Chary, K. V. R. & Vishwanathan, V. Nanotubular titanate supported palladium catalysts: The influence of structure and morphology on phenol hydrogenation activity. *Appl. Catal. Gen.* **324,** 52–61 (2007).

103. Park, C. & Keane, M. A. Catalyst support effects: gas-phase hydrogenation of phenol over palladium. *J. Colloid Interface Sci.* **266,** 183–194 (2003).

104. Claus, P. *et al.* Pd/MgO: Catalyst Characterization and Phenol Hydrogenation Activity. *J. Catal.* **192,** 88–97 (2000).

105. Chen, H., Sayari, A., Adnot, A. & Larachi, F. Composition–activity effects of Mn–Ce–O composites on phenol catalytic wet oxidation. *Appl. Catal. B Environ.* **32,** 195–204 (2001).

106. Bautista, P., Mohedano, A. F., Casas, J. A., Zazo, J. A. & Rodriguez, J. J. An overview of the application of Fenton oxidation to industrial wastewaters treatment. *J. Chem. Technol. Biotechnol.* **83,** 1323–1338 (2008).

107. Rome, K., McIntyre, A. & Macclesfield, A. Intelligent use of Relative Response Factors in Gas Chromatography-Flame Ionisation Detection. *Chromatogr. Today* 52–56 (2012).

108. Tew, M. W., Miller, J. T. & Van Bokhoven, J. A. Particle Size Effect of Hydride Formation and Surface Hydrogen Adsorption of Nanosized Palladium Catalysts: L3 Edge vs K Edge X-ray Absorption Spectroscopy. *J. Phys. Chem. C* **113,** 15140–15147 (2009).

109. Greenwood, N. N., Earnshaw, Alan & Earnshaw, A. *Chemistry of the elements*. (Butterworth-Heinemann, 1997).

110. Owen, E. A. & Jones, J. I. The effect of pressure and temperature on the occlusion of hydrogen by palladium. *Proc. Phys. Soc.* **49,** 587–602 (1937).

111. Jewell, L. L. & Davis, B. H. Review of absorption and adsorption in the hydrogen-palladium system. *Appl. Catal. -Gen.* **310,** 1–15 (2006).

112. Lewis, F. A. The Hydride of Palladium and Palladium Alloys. *Platin. Met. Rev* **4,** 132–137 (1960).

113. Fukai, Y. *The Metal-Hydrogen System: Basic Bulk Properties*. (Springer, 2006).

114. Owen, E. A. & Jones, J. I. The palladium-hydrogen system. *Proc. Phys. Soc.* **49,** 603–610 (1937).

115. Flanagan, T. B. & Oates, W. A. The palladium-hydrogen system. *Annu. Rev. Mater. Sci.* **21,** 4–1 – 4–11 (1991).

116. Kibria, A. K. M. F. & Sakamoto, Y. Hysteresis of pressure-composition and electrical resistance-composition relationships of palladium–hydrogen system. *Mater. Sci. Eng. B* **49,** 227–232 (1997).

117. Tamaki, M. *et al.* Visualization and analysis of forced diffusion of hydrogen in palladium by electrotransport. *Nucl. Instrum. Methods Phys. Res. Sect. Accel. Spectrometers Detect. Assoc. Equip.* **377,** 166–169 (1996).

118. Owen, E. A. & Williams, E. S. J. X- ray study of the hysteresis effect observed in the palladium-hydrogen system. *Proc. Phys. Soc.* **56,** 52–63 (1944).

119. Baranowski, B. High Presurre Research on Palladium-Hydrogen Systems. *Platin. Met. Rev* **16,** 10–15 (1972).

120. Cabrera, A. L. & Aguayo-Soto, R. Hydrogen absorption in palladium films sensed by changes in their resistivity. *Catal. Lett.* **45,** 79–83 (1997).

121. Everett, D. H. & Nordon, P. Hysteresis in the Palladium + Hydrogen System. *Proc. R. Soc. Lond. Ser. Math. Phys. Sci.* **259,** 341–360 (1960).

122. Kibria, A. K. M. F. & Sakamoto, Y. Pressure-composition and electrical resistance-composition isotherms of a palladium-hydrogen system. *Int. J. Hydrog. Energy* **23,** 475–481 (1998).

123. Johansson, M. *et al.* Hydrogen adsorption on palladium and palladium hydride at 1 bar. *Surf. Sci.* **604,** 718–729 (2010).

124. Narehood, D. G. *et al.* X-ray diffraction and H-storage in ultra-small palladium particles. *Int. J. Hydrog. Energy* **34,** 952–960 (2009).

125. Scholtus, N. A. & Hall, W. K. Hysteresis in the Palladium—Hydrogen System. *J. Chem. Phys.* **39,** 868–870 (1963).

126. Yamauchi, M., Ikeda, R., Kitagawa, H. & Takata, M. Nanosize Effects on Hydrogen Storage in Palladium. *J. Phys. Chem. C* **112,** 3294–3299 (2008).

127. Pundt, A. *et al.* Hydrogen and Pd-clusters. *Mater. Sci. Eng. B* **108,** 19–23 (2004).

128. Ingham, B. *et al.* Particle size effect of hydrogen-induced lattice expansion of palladium nanoclusters. *Phys. Rev. B* **78,** 245408 (2008).

129. Möbus, K., Grünewald, E., Wieland, S. D., Parker, S. F. & Albers, P. W. Palladium-catalyzed selective hydrogenation of nitroarenes: Influence of platinum and iron on activity, particle morphology and formation of β-palladium hydride. *J. Catal.* **311,** 153–160 (2014).

130. Sengar, S. K., Mehta, B. R., Kulriya, P. K. & Khan, S. A. Enhanced hydrogenation and reduced lattice distortion in size selected Pd-Ag and Pd-Cu alloy nanoparticles. *Appl. Phys. Lett.* **103,** 173107 (2013).

131. Sengar, S. K., Mehta, B. R. & Kulriya, P. K. Temperature, pressure, and size dependence of Pd-H interaction in size selected Pd-Ag and Pd-Cu alloy nanoparticles: In-situ X-ray diffraction studies. *J. Appl. Phys.* **115,** 114308 (2014).

Annexes

7.Annexes

7.1 TEM JEOL 1011: Palladium nanoparticles in corundum powder

7.1.1. TEM of the corundum powder

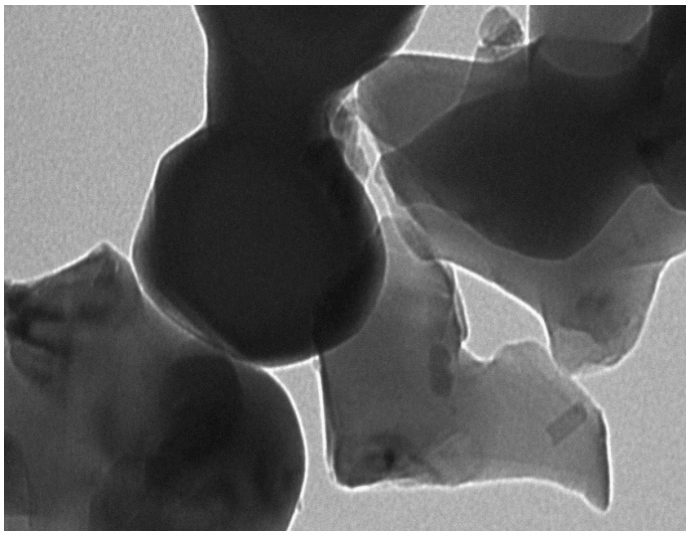

Figure 7.1: TEM image of corundum powder used as support of the different nanoparticles.

Figure 7.1 shows a typical image of corundum.

7.1.2. TEM of the nanoparticles by impregnation supported on corundum powder.

Figures 7.2 and 7.3 show respectively fresh and aged by TPD nanoparticles by impregnation.

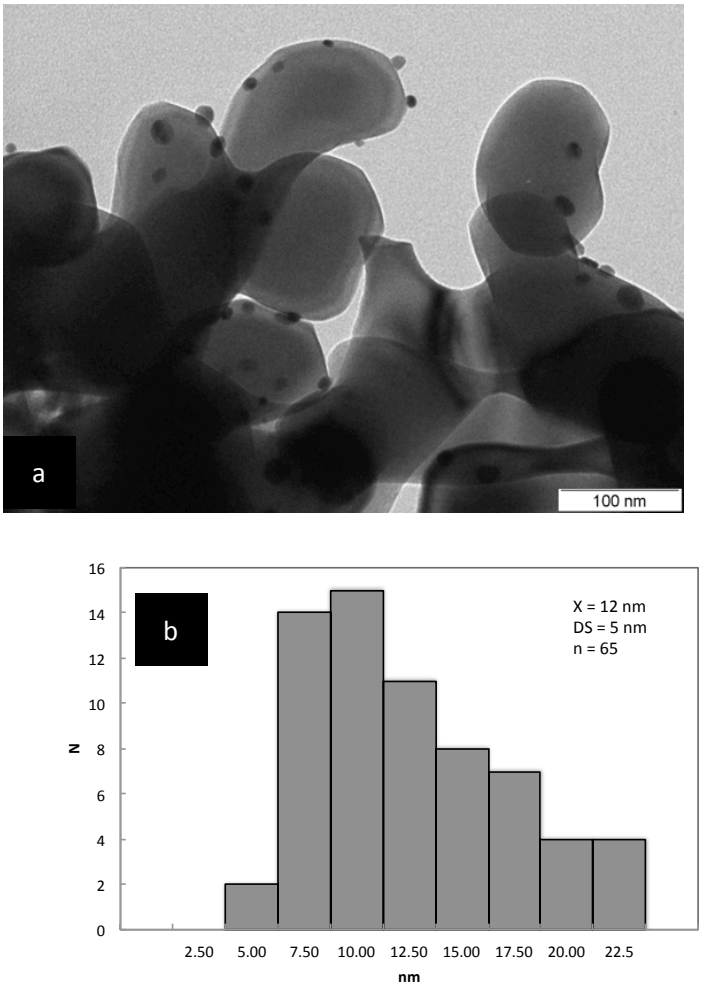

Figure 7.2: Representative TEM image of (a) fresh sample of palladium by impregnation and (b) histogram.

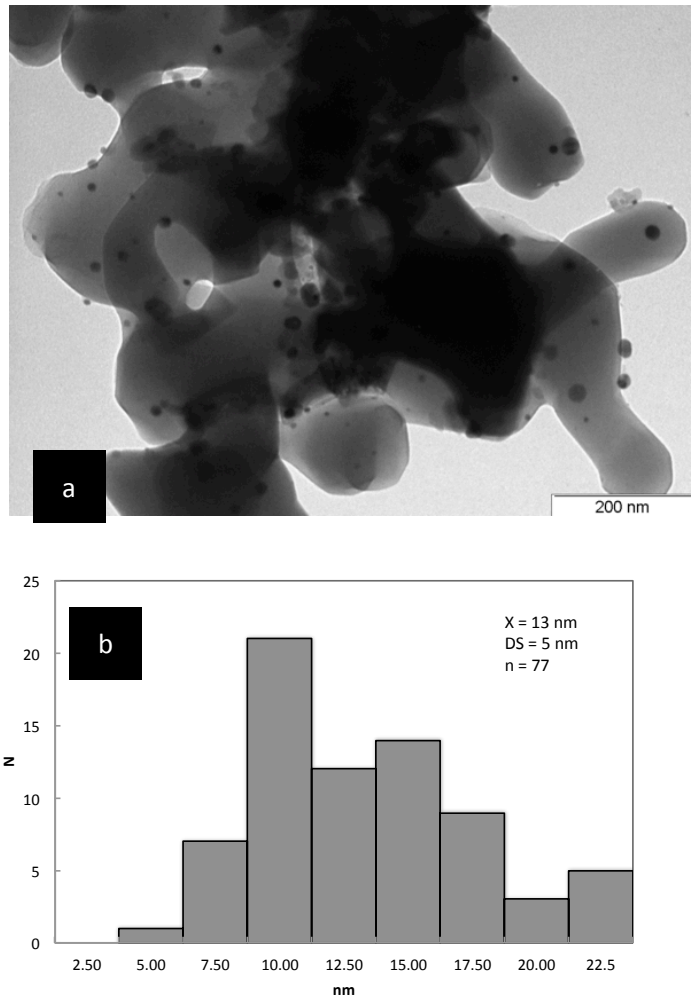

Figure 7.3: Representative TEM image of (a) sample of palladium by impregnation aged by three cycles of TPD and (b) histogram.

The figures show the palladium nanoparticles by impregnation ranging between 6 to 10 nm in size. In the figures well dispersed spherical dark gray palladium on corundum is observed. No interaction the between palladium and corundum was found.

No differences are detected between fresh and aged samples. The mean size of the nanoparticles by this technique is 12.5 nm. The samples have the same standard deviation.

7.1.3. TEM of the nanoparticles by sputtering supported on corundum powder.

In figures 7.4 – 7.8 the TEM images are shown for the palladium nanoparticles sputtered on corundum powder. For the different cases the sputtering time and the calcination temperature were varied

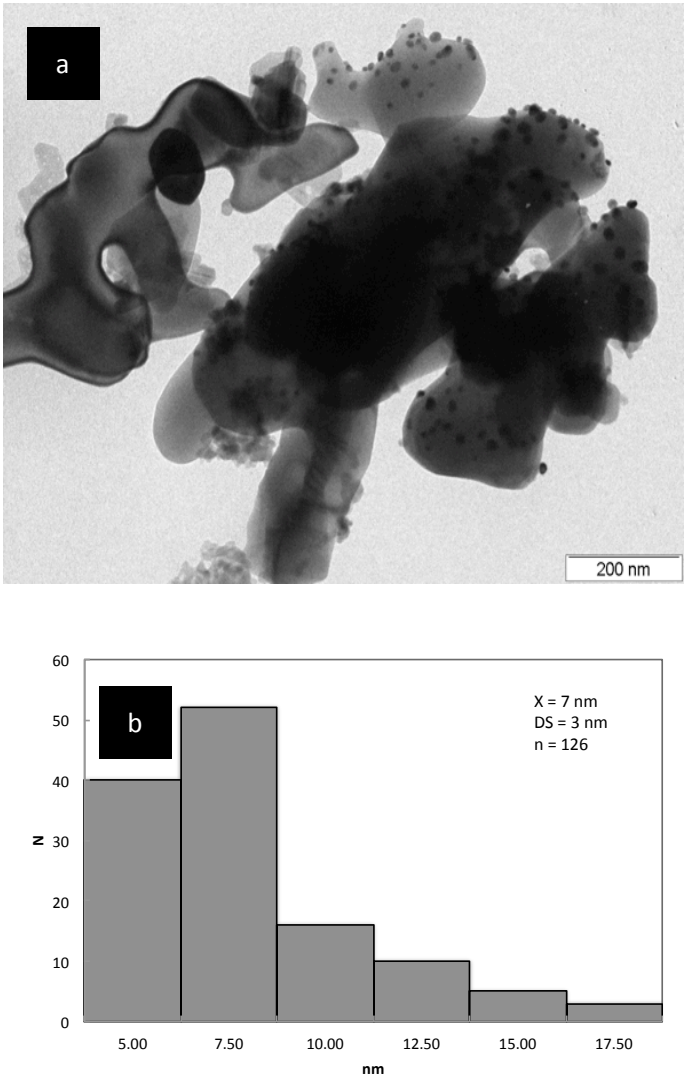

Figure 7.4: Representative TEM image of (a) Nanoparticles of palladium sputtered on corundum for 30" and calcined at 600 °C (b) histogram.

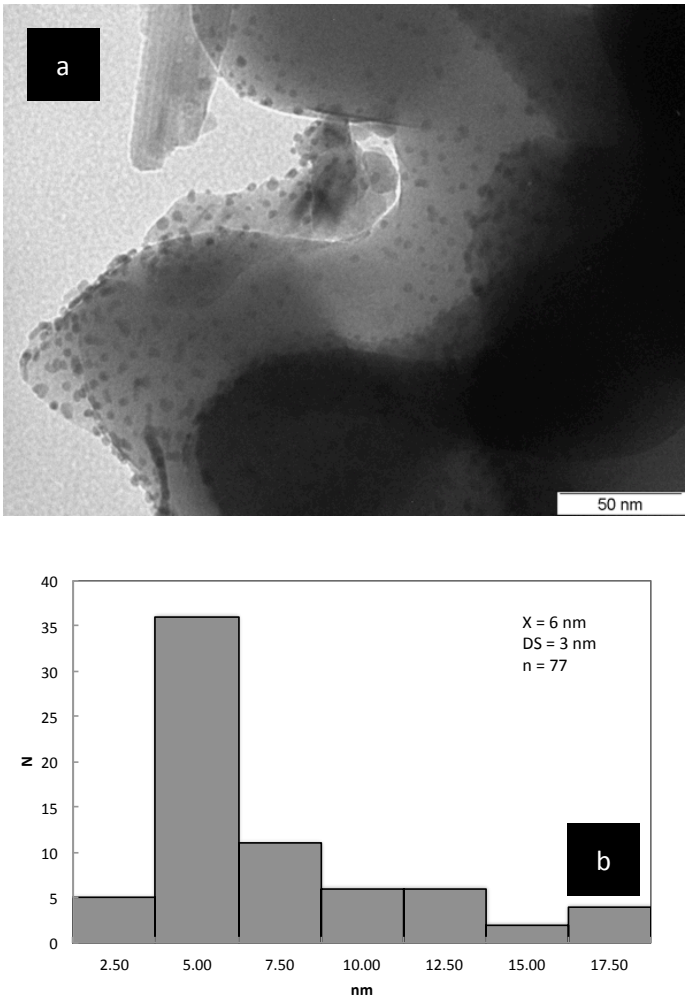

Figure 7.5: Representative TEM image of (a) Nanoparticles after Pd sputtering on corundum powder for 90" and calcined at 350 °C (b) histogram.

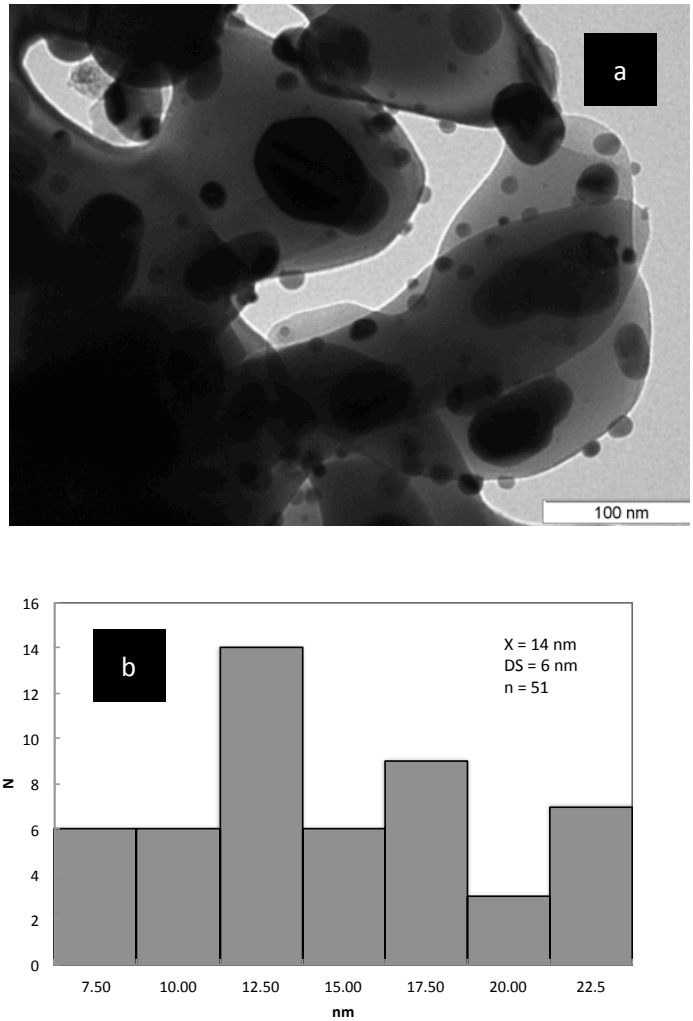

Figure 7.6: Representative TEM image of (a) Nanoparticles of Pd after sputtering for 90” on corundum and calcined at 600 °C (b) histogram.

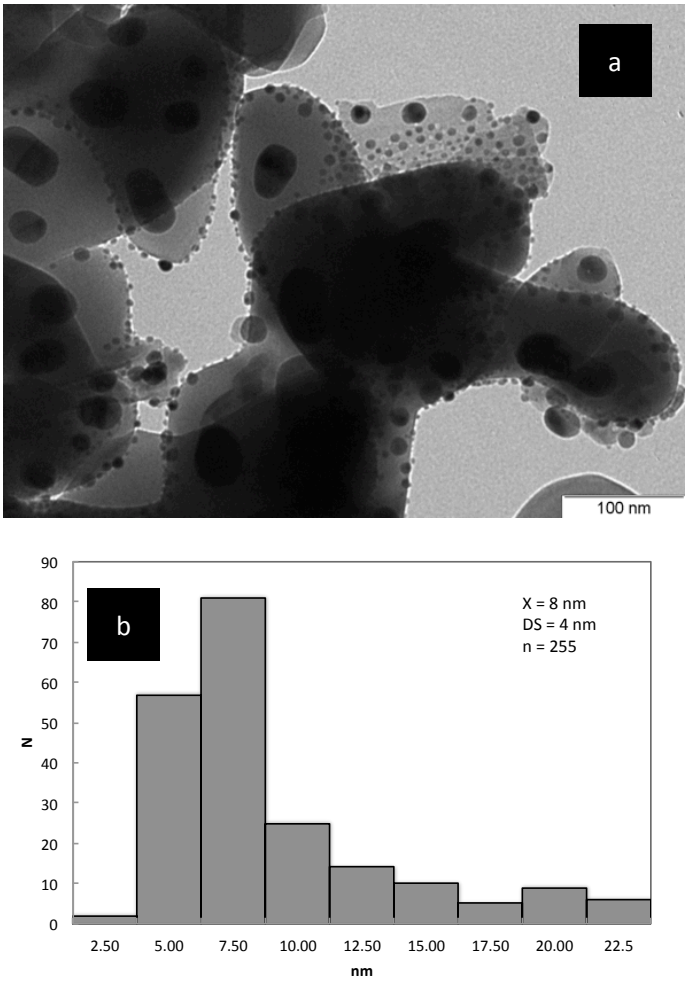

Figure 7.7: Representative TEM image of (a) Nanoparticles of Pd after sputtering for 150" and calcination at 350 °C (b) histogram.

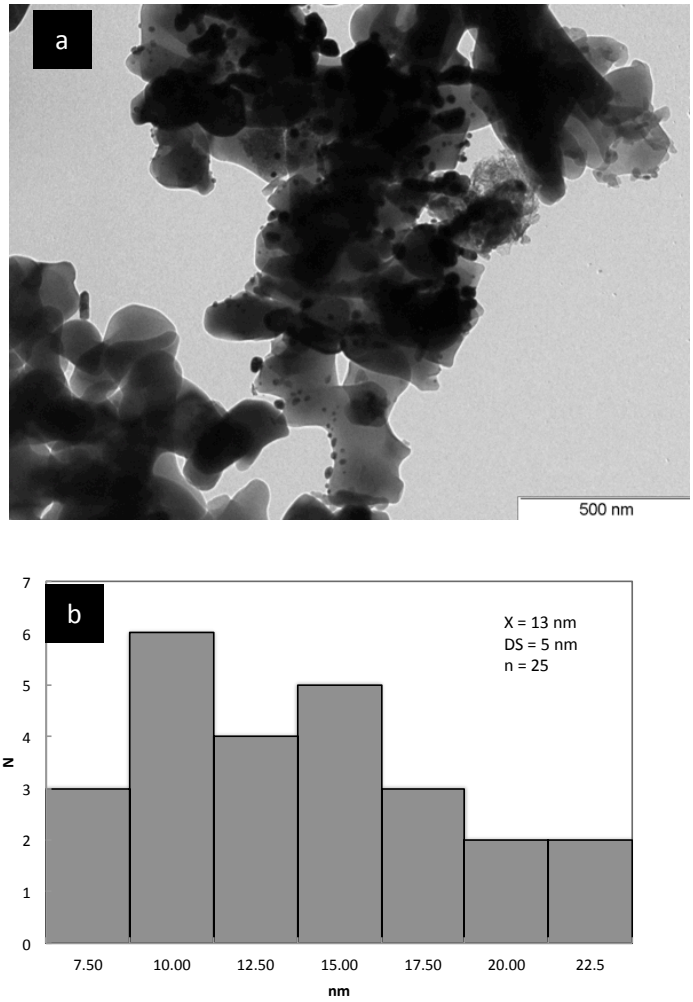

Figure 7.8: Representative TEM image of (a) Nanoparticles of Pd after sputtering for 150" on corundum and calcination at 600 °C (b) histogram.

In figures 7.4 to 7.8 well-dispersed spherical dark gray palladium on corundum is observed. No interaction between the palladium and corundum was found in any case. No differences in size were detected between nanoparticles calcined in the same temperature. Differences can be found among nanoparticles calcined at different temperatures. The palladium nanoparticles calcined at 600 ^{o}C overnight are almost double the size as that of the nanoparticles calcined at 350 ^{o}C. These results clearly indicate that Pd sintering occurs at 600 ^{o}C.

7.1.4 TEM of the nanoparticles by microemulsion supported on corundum powder.

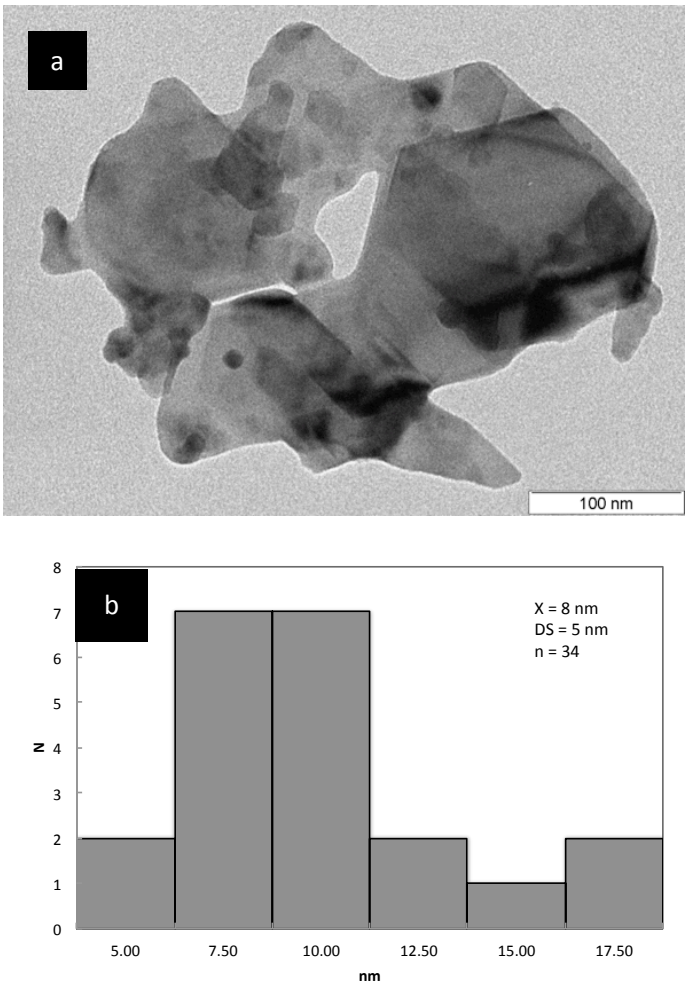

Figure 7.9: Representative TEM image of (a) TEM image of Pd nanoparticles obtained by microemulsion method loaded on corundum powder (b) histogram

In figure 7.9 well-dispersed spherical dark gray palladium by microemulsion on corundum is observed. No interaction between the palladium and corundum was found.

7.1.5. TEM of the nanoparticles by polyol route supported unsupported.

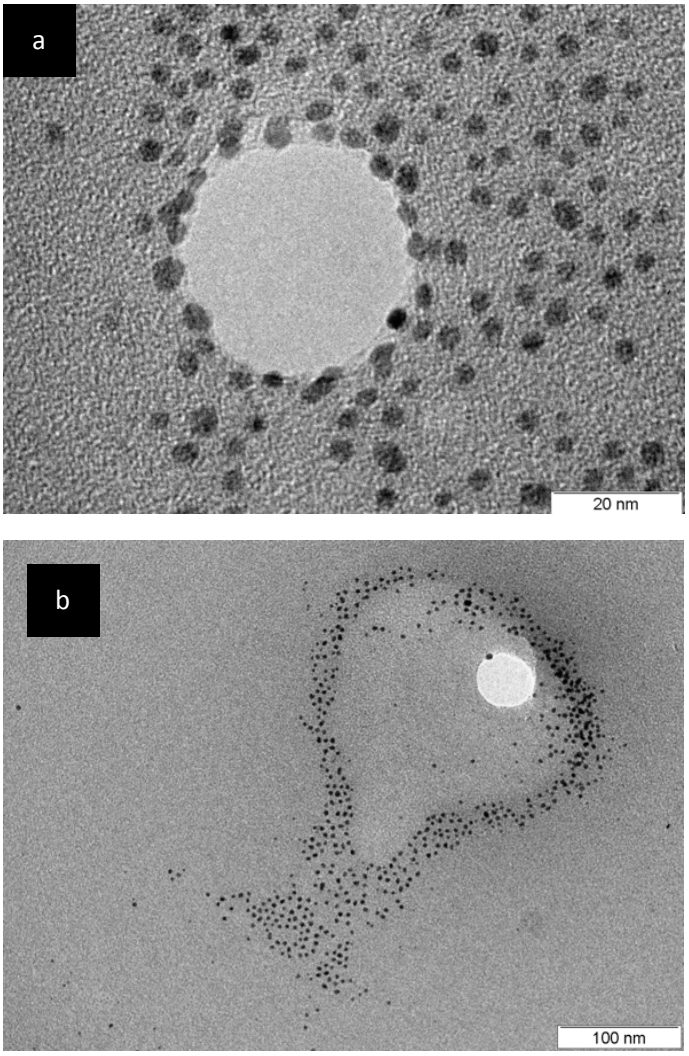

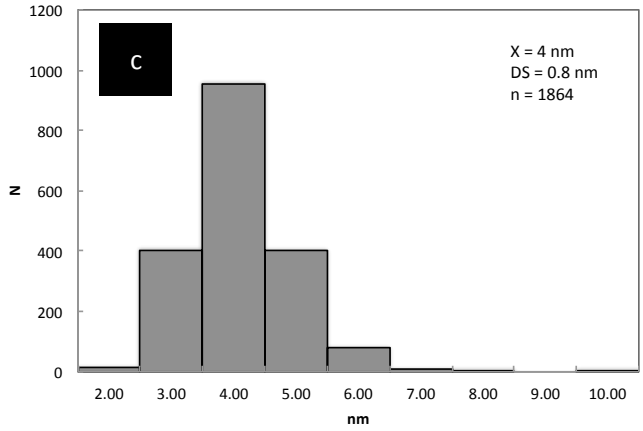

Figure 7.10: Representative TEM image of (a) and (b) TEM images of Pd_Cu nanoparticles obtained by Polyol route (c) Histogram.

In figure 7.10, unsupported well-dispersed spherical dark gray palladium is observed. The standard deviation is small, 0.8 nm. Very small (4 nm) and homogeneous nanoparticles can be seen with this technique.

7.2 XRD of the nanoparticles of palladium and copper palladium on corundum powder

In this section, a description is provided for the results obtained using the XRD technique for the palladium nanoparticles, and the nanoparticles of copper palladium supported on corundum powder.

7.2.1 diffractogram of the corundum powder

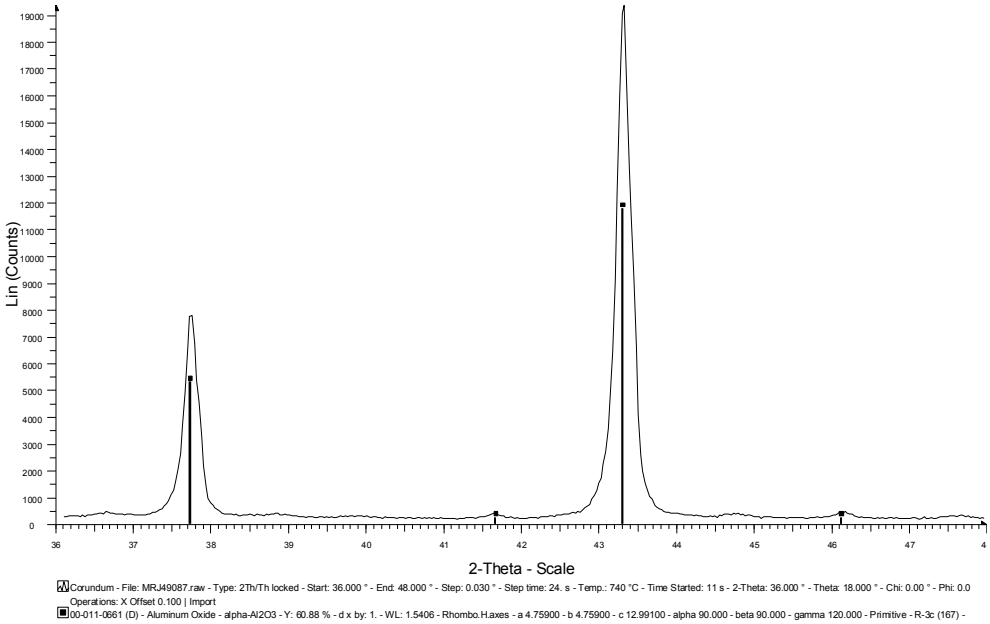

Figure 7.11: XRD diffractogram of corundum powder, blank.

The diffractogram 7.11 show low intensity peaks at 2θ of 37.7 and 43.3, both peaks are typical of the corundum.

7.2.2 XRD diffractogram of the nanoparticles of palladium obtained by impregnation supported on corundum

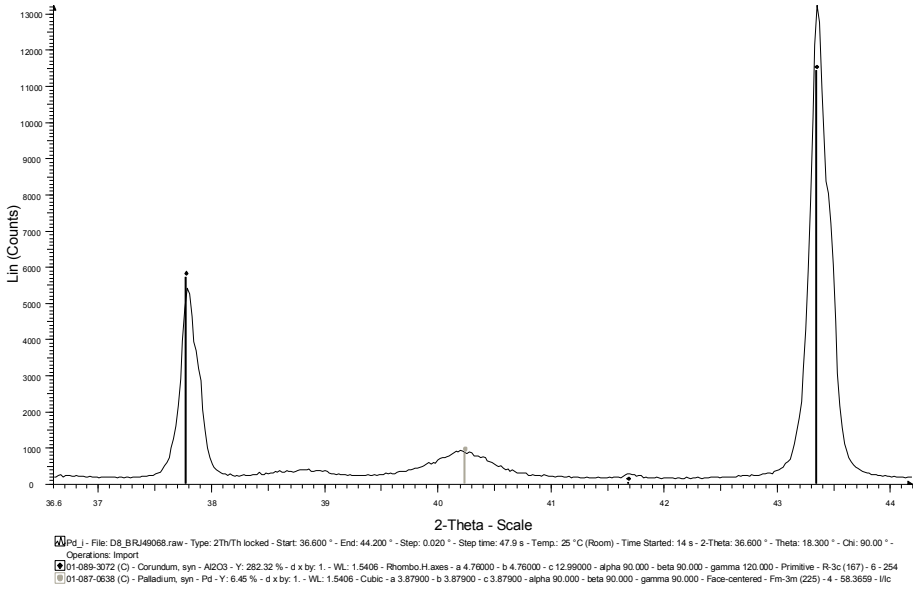

Figure 7.12: Diffractogram of palladium obtained by impregnation on corundum.

The diffractogram 7.12, shows a low intensity peak at 2θ = 40.2 corresponding to palladium as well as the two characteristic peaks of corundum at 2θ of 37.7 and 43.3 without disturbance. Pd is well dispersed on the support.

7.2.3 XRD diffractogram of the nanoparticles of palladium obtained by sputtering supported on corundum

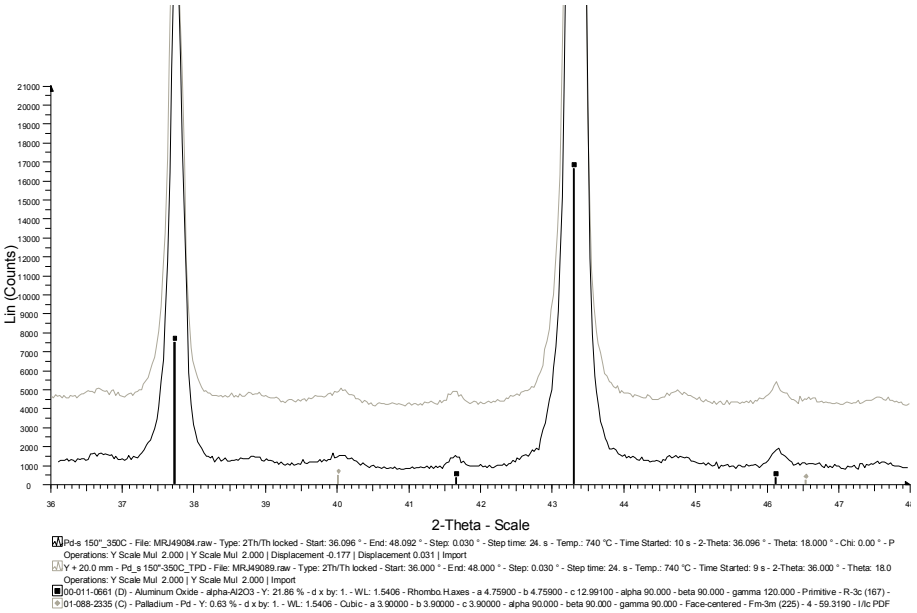

Figure 7.13: Diffractogram of palladium deposited by sputtering during 150 seconds and calcined at 350 ^{o}C fresh and aged for TPD.

In the diffractogram 7.13, in both cases, a low intensity peak at 2θ = 40.2 corresponding to palladium as well as the two characteristic peaks of corundum at 2θ of 37.7 and 43.3 without disturbance is observed. Pd is well dispersed on the support.

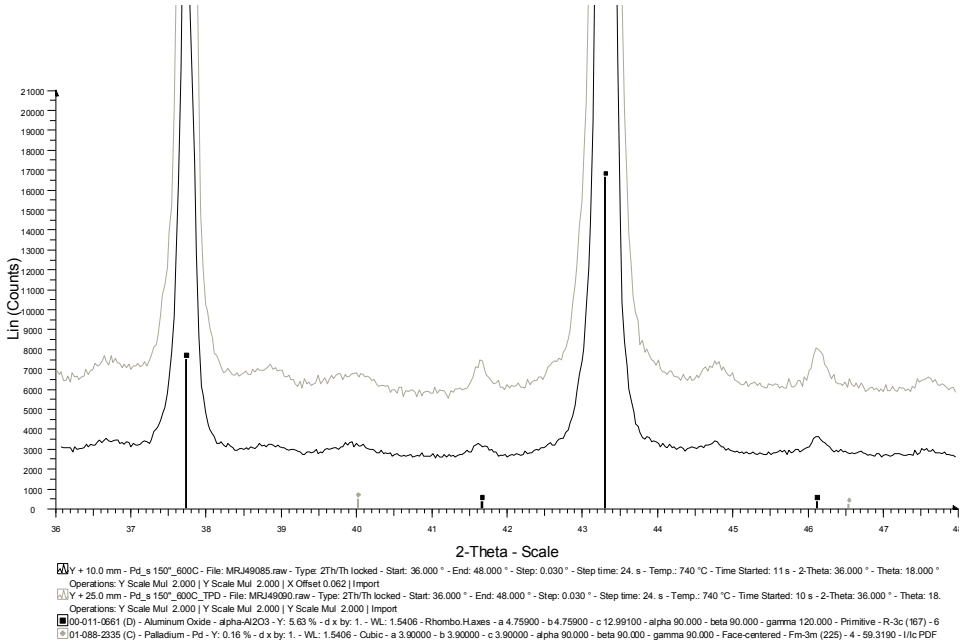

Figure 7.14: Diffractogram of palladium deposited by sputtering during 150 seconds and calcined at 600 ^{o}C fresh and aged for TPD

In the diffractogram 7.14, for nanoparticles calcined at 600 ^{o}C, in both cases, a low intensity peak at 2θ = 40.2 corresponding to palladium as well as the two characteristic peaks of corundum at 2θ of 37.7 and 43.3 without disturbance is observed. Pd is well dispersed on the support.

7.2.4 XRD diffractogram of the nanoparticles of palladium obtained by microemulsion supported on corundum

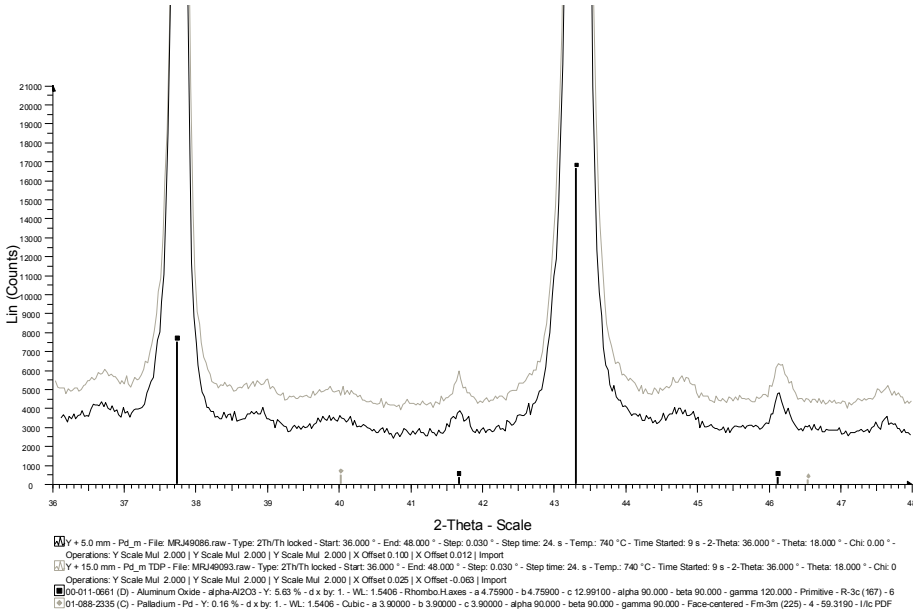

Figure 7.15: Diffractogram of palladium deposited by microemulsion fresh and aged for TPD.

The diffractogram 7.15 shows the results for the fresh and aged nanoparticles obtained by microemulsion. That is, the low intensity peaks at 2θ = 40.2 corresponding to palladium by microemulsion as well as the two characteristic peaks of corundum at 2θ of 37.7 and 43.3. Pd is well dispersed on the support. In both cases, no corundum modifications are observed.

7.2.5 XRD diffractogram of the nanoparticles of palladium obtained by polyol route supported on corundum

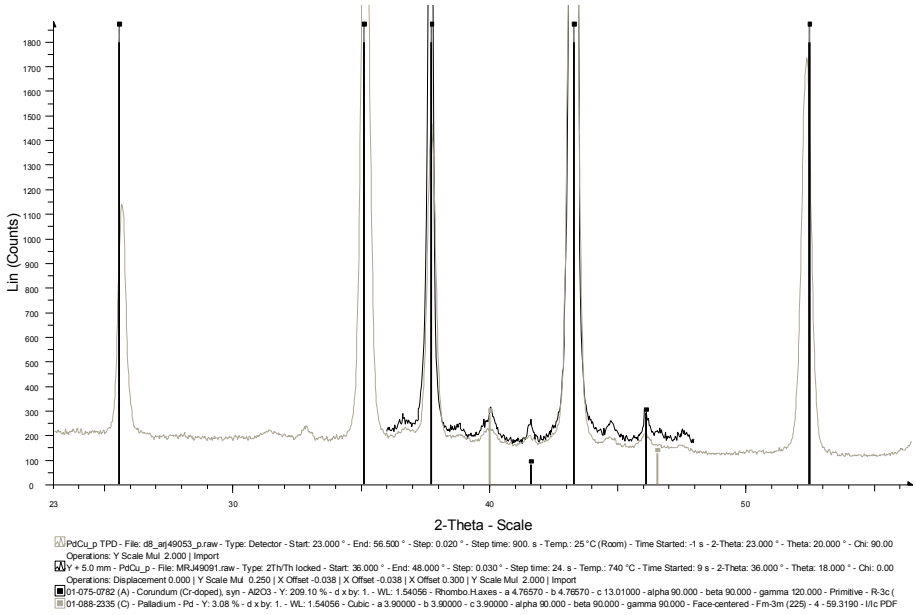

Figure 7.16: Diffractogram of fresh and aged by TPD palladium nanoparticles deposited by polyol route.

In the diffractogram 7.16 shows the results for the fresh and aged nanoparticles obtained by the polyol route. In both cases, a low intensity peak at 2θ = 40.2 corresponding to palladium by polyol and the two characteristic peaks of corundum at 2θ of 37.7 and 43.3 without disturbance are observed. Pd is well dispersed on the support.

7.3 TPD-MD: Palladium nanoparticles in corundum powder

7.3.1. TPD-MD results of the nanoparticles of palladium obtained by impregnation supported on corundum

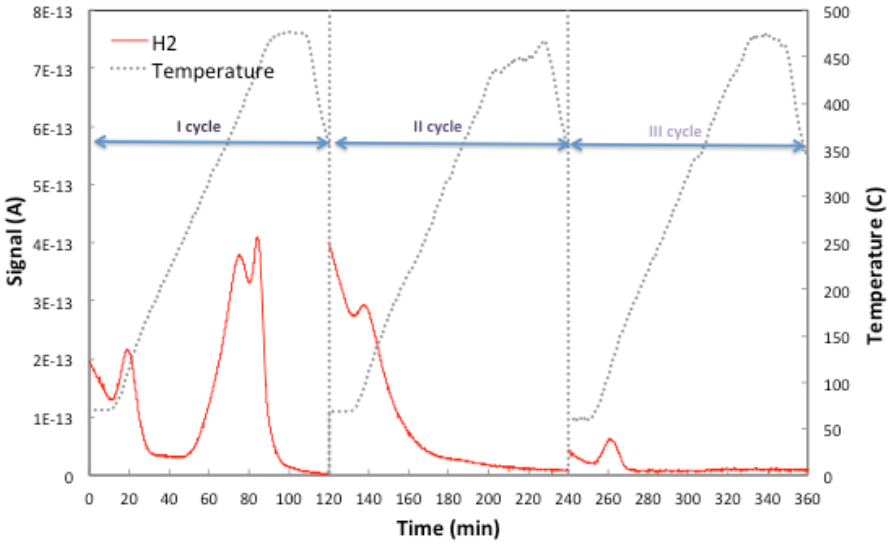

Figure 7.17: TPD-MD results for 1.67 % Pd/corundum sample obtained by impregnation.

Fig. 7.17 presents the results of the TPD experiments performed with Pd/corundum sample obtained by impregnation. The first peak with maximum intensity at 109 ^{o}C can be attributed to the desorption of the chemisorbed hydrogen. The second peak is observed with maximum intensity at 435 ^{o}C, so it correspond to the desorption of the absorbed hydrogen. Only the chemisorbed hydrogen was detected during the desorption step released around 100 ^{o}C in the following cycles.

7.3.2. TPD-MD results of the nanoparticles of palladium obtained by sputtering supported on corundum

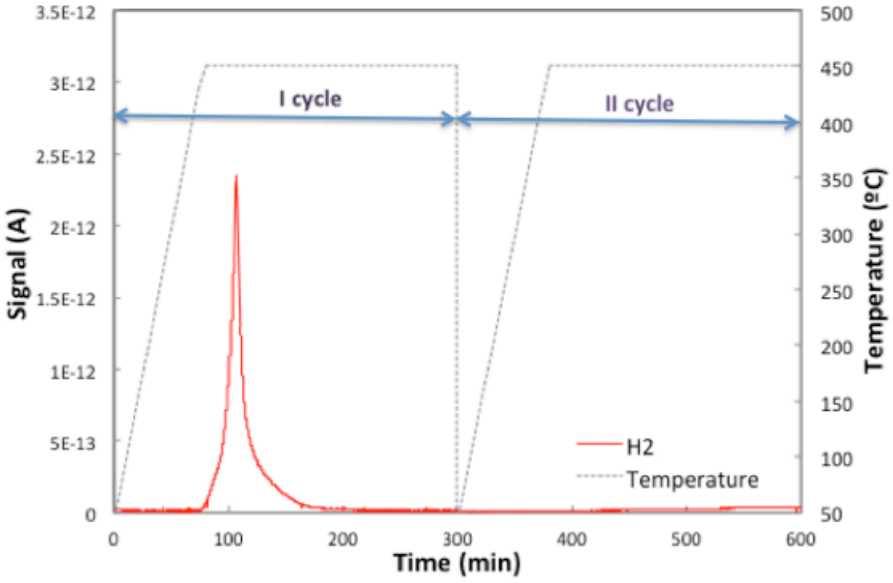

Figure 7.18: TPD-MD results for sputtered 0.004 % Pd/corundum sample; palladium sputtered for 30", sample calcined at 350 °C.

Fig. 7.18 presents the results for the TPD-MD measurements performed with 0.004 % w/w Pd on corundum powder obtained by metal sputtering for 30" and calcined at 350 °C. In this case, only the hydrogen released from the Pd lattice at about 400 °C was detected. No other peaks were detected.

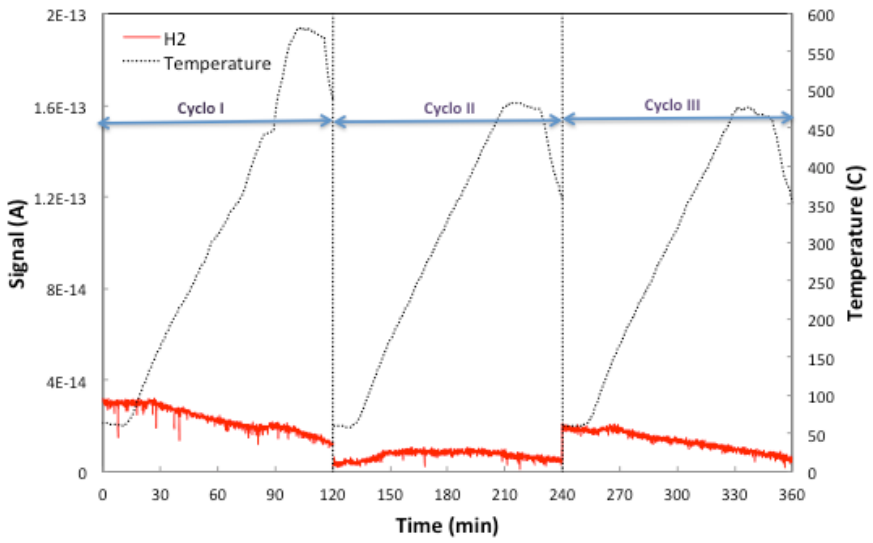

Figure 7.19: TPD-MD results for sputtered 0.004 % Pd/corundum sample; palladium sputtered for 30", sample calcined at 600 °C.

Figure 7.19 shows the response after the three TPD cycles of the sample 0.004 % of palladium by sputtering after the 30 seconds of exposure and calcined at 600 °C supported in corundum. This material did not present peaks in any cycle. This is due to the very low amount of palladium.

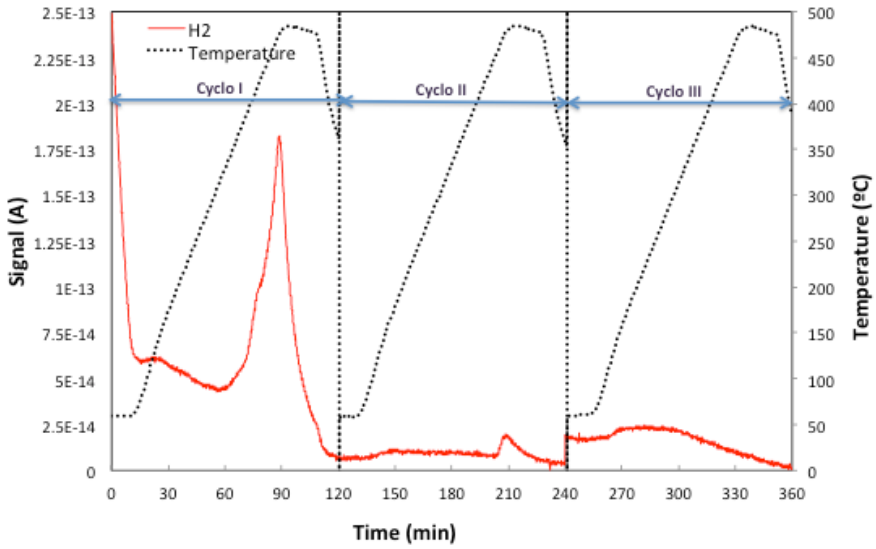

Figure 7.20: TPD-MD results for sputtered 0.012 % Pd/ corundum sample; palladium sputtered for 90", calcined at 350 °C.

In figure 7.20, the sample of 0.012 % Pd in α-Al_2O_3 by sputtering for 90 seconds, calcined at 350 °C present peaks at 450 °C in the first and in the second cycle. No peaks were detected in the third cycle. The peak size decreased cycle by cycle until it disappeared. The peaks appear at high temperature, thus both are due to the release of the absorbed hydrogen.

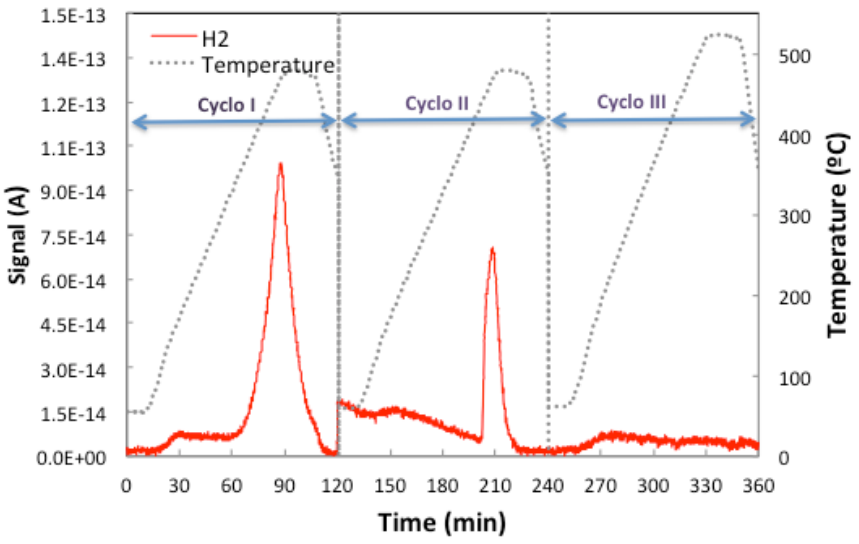

Figure 7.21: TPD-MD results for sputtered 0.012 % Pd/ corundum; palladium sputtered for 90", calcined at 600 °C.

In figure 7.21, the sample of 0.012 % of Pd by sputtering for 90 seconds, supported in alpha-Al_2O_3, calcined at 600 °C had the following results: This material present peaks at 450 °C in the first and the second cycle which may be due to desorption of the absorbed hydrogen in the palladium that formed beta palladium. Again, no peaks were detected in the third cycle. Once again, the peaks of hydrogen reduced their size each cycle until it disappeared in the third cycle. The peaks found in the sample calcined a lower temperature is higher than the present sample.

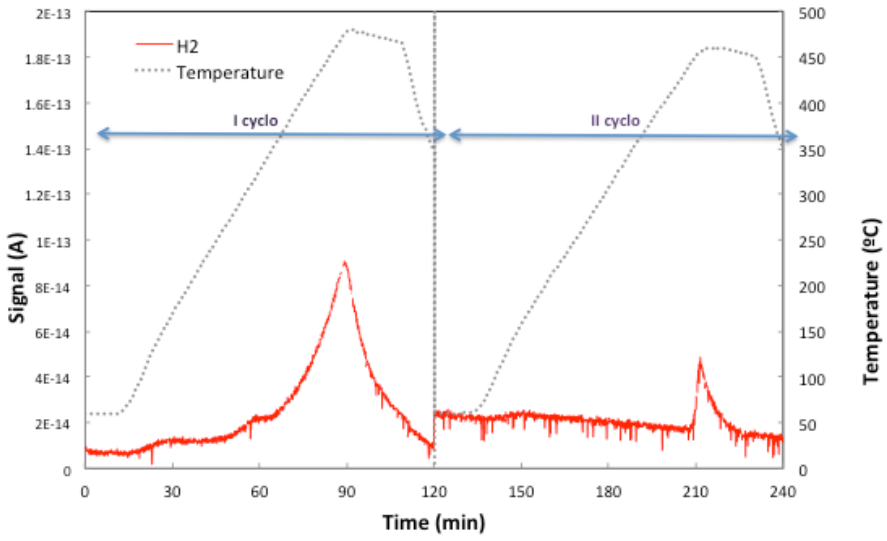

Figure 7.22: TPD-MD results for 0.02 % Pd/ corundum sample; Pd sputtered for 150", calcined at 350 ^{o}C.

In figure 7.22, the sample of 0.02 % of Pd by sputtering for 150 seconds, supported in alpha-Al_2O_3, calcined at 350 ^{o}C results in a first peak and a second peak at 450 ^{o}C. The size of the peak decreased cycle by cycle. One more time, the peaks appear at high temperature, thus, the peaks are due to desorption of the hydrogen absorbed in the palladium lattice.

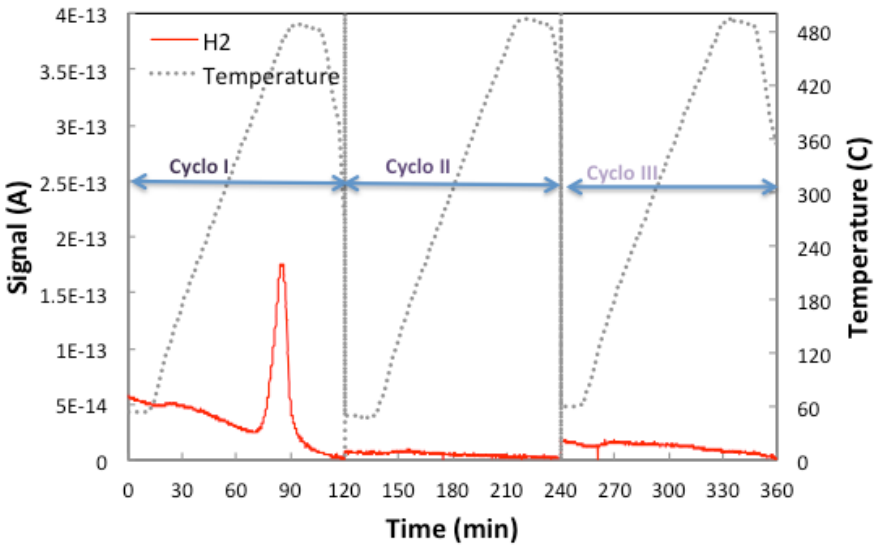

Figure 7.23: TPD-MD results for 0.02 % Pd/corundum sample; Pd sputtered for 150", calcined at 600 °C.

Figure 7.23 presents the sample of 0.02 % of Pd by sputtering, for 150 seconds, supported in alpha-Al_2O_3, calcined at 600 °C. Only one peak was found. This peak was found at 450 °C in the first cycle.

7.3.3. TPD-MD results of the nanoparticles of palladium obtained by microemulsion supported on corundum

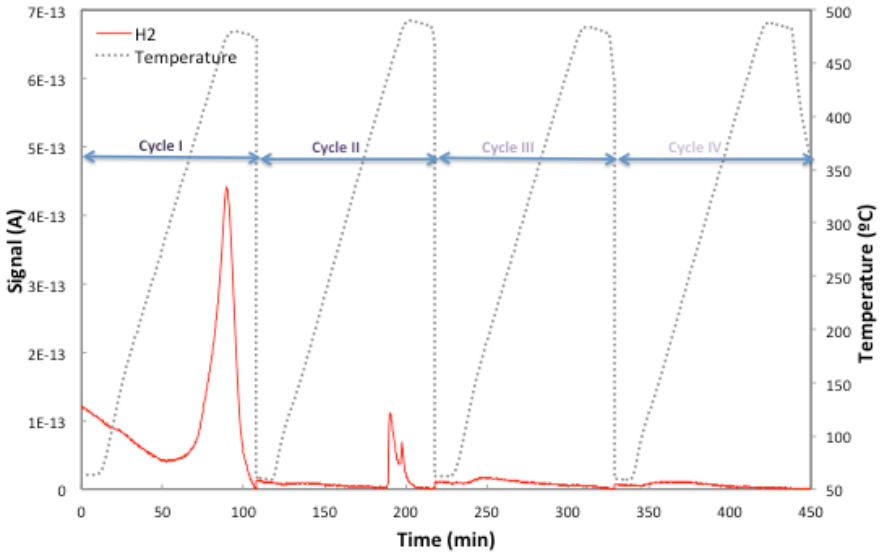

Figure 7.24: TPD-MD results for the 0.22 % Pd/corundum sample; Pd loaded from microemulsion.

In figure 7.24, the sample with 0.22 % of Pd in α-Al_2O_3 by microemulsion presented peaks at 450 ^{o}C in the first and the second cycle. No peaks were detected in the third and four the cycle. The size of the peaks of hydrogen decreased cycle by cycle until it disappeared. Only the peaks due to desorption of the absorbed hydrogen were found.

7.3.4. TPD-MD results of the nanoparticles of palladium copper alloy obtained by polyol route supported on corundum

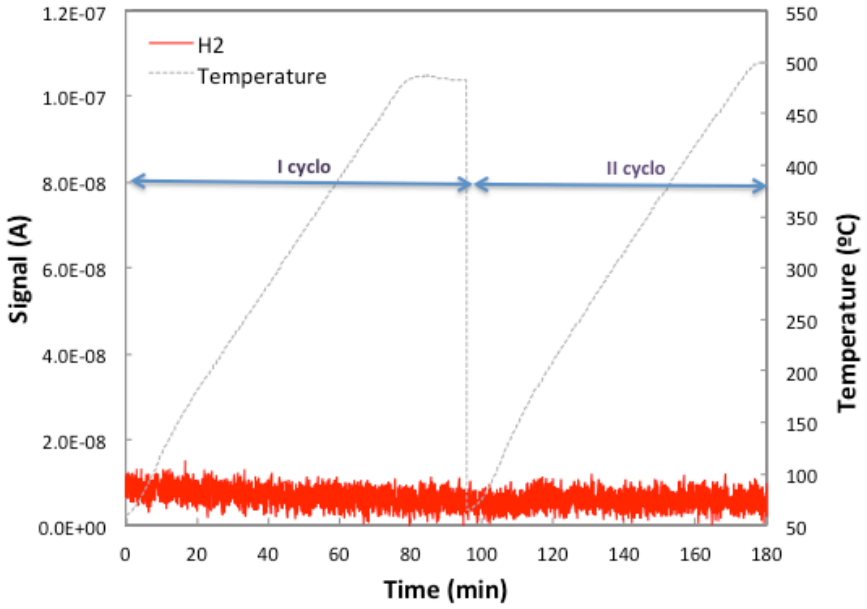

Figure 7.25: TPD-MD results for the 0.4 % of Pd and 0.1 % Cu/corundum sample; the PdCu nanoparticles were prepared using polyol route.

Figure 7.25 shows that no peaks were produced in the sample with 0.4 % Pd and 0.1 % Cu alloy obtained using the polyol route and supported in α-Al_2O_3.